AN APPLICATION OF NORMAL MODE THEORY TO THE RETRIEVAL OF STRUCTURAL PARAMETERS AND SOURCE MECHANISMS FROM SEISMIC SPECTRA

By F. GILBERT†
Institute of Geophysics and Planetary Physics, Scripps Institution of Oceanography, University of California, San Diego, La Jolla, California 92037

AND A. M. DZIEWONSKI
Hoffman Laboratory, Department of Geological Sciences, Harvard University, Cambridge, Massachusetts 02138

(*Communicated by Sir Edward Bullard, F.R.S. – Received* 10 *June* 1974)

CONTENTS

A cyclic process of refining models of the mechanical structure of the Earth and models of the mechanism of one or more earthquakes is developed. The theory of the elastic-gravitational free oscillations of the Earth is used to derive procedures for resolving nearly degenerate multiplets of normal modes. We show that a global network of seismographs (W.W.S.S.N.) permits resolution for angular orders $l \leqslant 76$ and for frequencies $\omega \leqslant 0.090\,\mathrm{s}^{-1}$. The peak or centre frequency of each nearly degenerate multiplet is interpreted to be a gross Earth datum. Together, the data are used to refine models of the mechanical structure of the Earth.

† Order of authors determined by lot.

The theory of free oscillations is used further to derive procedures for retrieving the mechanism, or moment tensor, of an earthquake point source. We show that a global network of seismographs permits retrieval for frequencies $0.0125\,s^{-1} \leqslant \omega \leqslant 0.0825\,s^{-1}$. We show that refined models of structure and mechanism lead to improved resolution and retrieval, and that an array of sources further complements the resolution of multiplets.

We present a 'standardized dataset' of 1064 distinct, observed eigenfrequencies of the elastic-gravitational free oscillations of the Earth. These gross-Earth data are compiled from 1461 modes reported in five studies: 2 modes reported by Derr (1969), 159 modes observed by Brune & Gilbert (1974), 240 modes observed by Mendiguren (1973), 248 modes observed by Dziewonski & Gilbert (1972, 1973) and 812 modes reported here. It is our opinion that the establishment of a standardized dataset should precede the establishment of a standardized model of the Earth.

Two new Earth models are presented that are compatible with the modal data. One is derived from model 508 (Gilbert & Dziewonski 1973) and the other from model B1 (Jordan & Anderson 1974). In the outer core and in the lower mantle, below a depth of about 950 km, the differences between the two models are negligibly small. In the inner core there are minor differences and in the upper mantle there are major differences in detail. The two models and the modal data are compatible with traditional ray data, provided that appropriate baseline corrections are made to the latter.

The source mechanisms, or moment tensors, of two deep earthquakes, Colombia (1970 July 31) and Peru–Bolivia (1963 August 15), have been retrieved from the seismic spectra. In both cases the moment tensor possesses a compressive (implosive) isotropic part. There is good evidence that isotropic stress release begins gradually, over 80 s before the origin time derived from the onset of short-period P and S waves. During the process of stress release the principal axes of the moment rate tensor migrate. The axis of compression is relatively stable, the compressive stress rate is dominant, and the other two axes rotate about the axis of compression.

We speculate that earthquakes, occurring deep within descending lithospheric plates, are not sudden shearing movements alone but do exhibit compressive changes in volume such as would be associated with a phase change. We further speculate that compressive changes in volume may occur without sudden shearing movements, that there may be 'silent earthquakes'.

1. Introduction

Note on units

In this paper traditional seismological units are used. The relation between these units and standard SI units is given in the following table.

unit	SI	this paper	
length	m	km	10^3 m
velocity	m s^{-1}	km s^{-1}	10^3 m s^{-1}
density	kg m^{-3}	g cm^{-3}	10^3 kg m^{-3}
moment	N m	dyn cm	10^{-7} N m
acceleration	m s^{-2}	cm s^{-2}	10^{-2} m s^{-2}
pressure	Pa (N m^{-2})	kbar	10^8 Pa

Also, frequencies are presented as radians per second. In terms of the standard unit, the hertz, $1\,\text{Hz} = 2\pi\,s^{-1}$.

In this report we continue our efforts to identify the normal modes of free oscillation of the Earth. Two important inverse problems depend for their data on observations of the normal modes. We have seen how the Earth's structure can be resolved from a knowledge of normal mode eigenfrequencies (Backus & Gilbert 1967, 1968, 1970) and we have reason to believe that the source mechanism of an earthquake can be found from a knowledge of normal mode amplitudes (Gilbert 1973*a*). The two problems are not independent but we strive to decouple them by developing a cyclic or iterative method of processing the observed data.

A seismogram may be regarded as a functional of the structure of the Earth, the mechanism of the earthquake, and the recording system. Enough is presumed to be known about the latter to remove its effects, and we disregard it hereafter. We wish to extract from the seismogram those factors that are both very strong functionals of the structure of the Earth and very weak functionals of the source mechanism, and vice versa. In this report we disregard the distinction between a functional and its observed values. It is our belief that the meaning is made clear by the context.

Classical seismology provides an illustrative example. The travel times of body pulses do not depend upon the source mechanism. They are functionals of structure alone. Solving the classical inverse problem for travel times has provided us with radially stratified Earth models that appear to be very good approximations to the real Earth (Jeffreys 1970). Calculations of ray paths based on a good model are, usually implicitly, considered to be very weakly dependent on the difference between the model and the Earth. This consideration is probably true except for critical phenomena, diffraction, tunnelling, etc. Tables of angles of incidence, which are used in first motion studies, are invariably assumed to belong to the real Earth, for all practical purposes. That is, the first motion of a body pulse is regarded to be a very strong functional of the source mechanism and a very weak one of structural differences between the real Earth and a radially stratified model of it. There are good reasons to believe that this is so. The remarkable geographical consistency of nodal plane solutions and their compatibility with other sets of tectonophysical data (Isacks & Molnar 1971) argue strongly in favour of the interpretation given. The effect of geographical variations in structure is certainly not negligible and recent improvements in nodal plane solutions and epicentral locations have been made by taking into account such variations (Davies & McKenzie 1969). However, especially for deep earthquakes and long horizontal wavelengths, a radially stratified model appears to be adequate.

The seismological application of normal mode theory parallels that of classical ray theory. First we extract from the observations those data that are functionals of Earth structure alone. These are the dispersion characteristics of travelling waves, the eigenfrequencies of normal modes, and the attenuation of both. In performing this extraction we use all that is currently known about Earth structure and source mechanisms. The newly augmented data set is inverted to obtain better models of the Earth.

The second stage is to return to the observations, and, by using the normal mode analogue of the tables of angles of incidence, to retrieve the source mechanism. It is clear that we have begun a cyclic or iterative process of successive refinements of structure and mechanism.

In this report we describe the results of an initial resolution of multiplets, the derivation of an improved model, the retrieval of the source mechanism for two earthquakes, a second resolution of multiplets, and the derivation of two Earth models compatible with the existing data.

This report stems directly from a number of recent developments in the application of normal mode theory to the inverse problems for the Earth's structure and for source mechanisms.

Dziewonski & Gilbert (1972, hereafter referred to as Alaska I) have identified some 60% of all possible spheroidal overtones with periods longer than 300 s. The normal mode data published in that report provided new constraints on the radial distribution of elastic parameters. Subsequently, the range of Earth models derived by using these constraints (cf. Jordan 1972;

Wang 1972), has been significantly narrowed in comparison to some earlier studies. Dziewonski & Gilbert (1973*b*, hereafter referred to as Alaska II) published a list of 86 additional overtone data.

Results of an inversion study based upon the normal mode data from Alaska I and II, toroidal overtone data of Brune & Gilbert (1974) and a selected set of 122 travel times have been presented by Gilbert, Dziewonski & Brune (1973). This study has shown that the travel time data and normal mode data are compatible if one makes base-line corrections to the travel times and that the normal mode data contain nearly all of the information provided by the teleseismic travel time data. A parallel study, incorporating the data of Alaska I, has been made by Jordan & Anderson (1974).

These efforts are important in the context of the present report because they have provided the initial data for constructing realistic Earth models, and, in more general terms, proved that much more information can be retrieved from seismic recordings than had previously been thought possible.

Gilbert (1971*a*) presented a method for calculating the excitation of normal modes due to a source represented by an arbitrary moment tensor. Previously published methods considered only special cases of a moment tensor such as, for example, a double couple (Saito 1967). Section 2.1 contains the algebraical details required for using equation (23) of Gilbert (1971*a*) in actual calculations.

A novel method for identifying normal modes is due to Mendiguren (1972, 1973). Knowing the fault plane solution for a given earthquake and using equations derived by Saito (1967) he was able to calculate, for a particular normal mode, the sign and amplitude of the initial displacement at any point on the surface of the Earth. Mendiguren developed a phase equalization procedure in which spectra from many stations were added with the appropriate sign to reinforce the amplitude of the mode of interest and to reduce the effect of other modes. Mendiguren (1973) published a list of eigenperiods of 240 normal modes derived from spectra of the W.W.S.S.N. recordings of the Colombian earthquake of 1970 July 31.

Dziewonski & Gilbert (1973*a*) have proposed some improvements in the phase equalization approach. Section 2.2 provides the theoretical background of the phase equalization method applied in this study. It is worth while to note that the phase equalization methods may represent the best possible approach to the problem of resolving the fine structure of the Earth's eigenspectrum.

Gilbert (1973*a*) pointed out that the excitation equations in the form proposed by Gilbert (1971*a*) leads directly to the formulation of a linear inverse problem for the six independent elements of the moment tensor of the source. Dziewonski & Gilbert (1974) have extended the theory of Gilbert (1971*a*, 1973*a*) to sources of finite duration and applied it to the analysis of the source mechanism of two deep earthquakes. The theory related to this method is presented in § 2.3.

The approach to the source mechanism problem first described by Dziewonski & Gilbert (1974) and explained in a more detailed way in the present report avoids the reliance on *a priori* assumptions made in most of the published analyses.

The balanced 'double-couple' system of equivalent forces has been virtually universally adopted in studies of the source mechanism of earthquakes. Representing a stress tensor by such a system involves two assumptions: (i) the stress is deviatoric; and (ii) one of the principal stresses is zero. This means that the six linear equations for the elements of a moment tensor are supplemented by two constraint equations: one linear, requiring that the trace of the tensor be zero, and the other non-linear, equivalent to the condition that one of the roots of the secular equation be zero. If an earthquake should have, for example, a partly isotropic moment tensor, then studies of its source mechanism based upon the *a priori* assumption of a system of double couples must fail to reveal the isotropic part, even though the least-squares condition is satisfied. It is clear that a procedure in which the elements of a moment tensor can be determined directly from the seismic data is preferable to one that imposes *a priori* restrictions.

Another assumption commonly made in published reports is that the orientation of the principal axes of stress remains constant during the stress release process. On the basis of this assumption the fault plane solutions obtained from observations of P-waves with periods of the order of 1 s were used in studies of the excitation of surface waves or normal modes with periods greater by two or three orders of magnitude. The method described in this report yields the moment tensor at each frequency of interest.

The generality of the method would be of only academic interest if the results of its application were to show that the commonly adopted *a priori* assumptions are principally correct. But our analysis of the source mechanism of two deep earthquakes has shown, among other findings, that the stress drop tensors associated with these events possess a statistically significant isotropic component and that the orientation of the principal axes of stress may change significantly during the event.

In § 3 we apply the methods described in § 2 to processing the seismic data and present the results of analyses for the source mechanism and eigenfrequencies of normal modes. The final list of normal modes identified by simultaneously processing 211 seismograms of two deep earthquakes contains data for 812 modes.

Section 4 is devoted to a discussion and interpretation of our results. We concentrate our attention on the subject of systematic differences between the eigenfrequencies determined from the analysis of the Alaskan data (Alaska I and II) and those obtained by application of the phase equalization methods from the set of seismograms from two South American sources. The differences are generally less than 0.1 %, with the exception of the fundamental toroidal modes where, on average, they are close to 0.3 %.

Inverting the data shows that the effect of these differences on the derived Earth model is very small. Yet, the existence of bias; undoubtedly related to multiplet splitting on a rotating, ellipsoidal and laterally heterogeneous Earth, indicates that, by using the present approach of phase equalization for multiplets, it will be difficult to improve the precision of our gross Earth data.

Dziewonski & Gilbert (Alaska II) stated that a further increase in the resolving power of the gross Earth data set is more likely to be assured by improving the quality rather than by increasing the quantity of the data. Such an improvement in the quality is most likely to be achieved by attacking the problem of 'super-resolution' (Gilbert 1971 *b*); that is, to attempt to measure eigenfrequencies of the singlets. Also, one can combine the eigenfrequencies of the singlets to obtain the splitting parameters which are new gross Earth data. That such data are desirable is obvious when one remembers that, for example, the splitting parameters for ellipticity depend upon the radial derivatives of the density and elastic parameters (Dahlen 1968).

Also in § 4, we discuss the temporal variation of the moment rate tensor. Our findings support an interpretation made by Isacks, Oliver & Sykes (1968) for deep earthquakes to explain the tendency for the compressive principal axis of stress release to be more stable in position than the other two. We find the compressive principal stress rate to be dominant with an axis that varies little in time. The other two principal axes rotate about it, in a systematic way, as stress release occurs. For the Peru–Bolivian earthquake the rotation amounts to 70°. The dominance of the compressive principal stress rate supports the isotropic stress rate being compressive. By applying the minimum phase criterion (Bode 1945) to the observed spectra of the moment rate tensor, we are able to show that isotropic stress release begins gradually, over 80 s before the 'main shock'. There is some evidence that deviatoric stress release is precursive but it is marginal. The implications of there being a precursive release of isotropic stress are discussed at the close of § 4.

2. Modal excitation and the retrieval of spectra

In §§ 2.1–2.3 we collect the theoretical results and computational methods necessary for our purposes. The final procedures are quite simple and involve nothing more than the application of successive linear processes. The most difficult task is the construction of the generalized inverse of a symmetric matrix. Inasmuch as the decomposition of a symmetric matrix is a well-understood problem, both theoretically and numerically (Wilkinson & Reinsch 1971), we are left with very stable computational procedures.

We discuss the excitation of normal modes in § 2.1. The basic results are classical (Rayleigh 1877) and quite general. Gilbert (1971 *a*) showed how to use them to express the excitation of normal modes by a point force or point dislocation (moment tensor). A thorough discussion of dislocation sources in a spherical Earth model has been given by Dahlen (1972, 1973) and by Phinney & Burridge (1973). Several special cases, including a double-couple have been considered by Saito (1967) and Ben-Menahem & Singh (1972). We have gone into considerable detail in § 2.1 because it forms the basis for subsequent derivations and applications.

Our method for resolving normal mode multiplets is presented in § 2.2. Basically, a vector spherical harmonic expansion is made of vector (displacement) seismic spectra from a global network (W.W.S.S.N.). Because of the mean-square approximating property of spherical harmonics, our method turns out to be another version of the method of least squares. Knowledge of the source mechanism is used to equalize the phase in the expansion.

Still another version of the method of least squares is used in § 2.3 to retrieve the moment tensor (Gilbert 1973 *a*). In principle, the effect of dissipation can be removed from the observed spectra by averaging; in practice, for truncated records, corrections for dissipation have to be made.

2.1. *Excitation of normal modes by point sources*

The normal modes of oscillation of the non-rotating, spherically symmetric Earth (the terrestrial monopole) are of two kinds, the poloidal (spheroidal) and the toroidal (torsional) oscillations, respectively written

$$ {}_n\boldsymbol{\sigma}_l^m(\boldsymbol{r})\exp(\mathrm{i}\,{}_n\omega_l^m t) \quad \text{and} \quad {}_n\boldsymbol{\tau}_l^m(\boldsymbol{r})\exp(\mathrm{i}\,{}_n\acute{\omega}_l^m t)$$

with

$$\left.\begin{aligned} {}_n\boldsymbol{\sigma}_l^m(\boldsymbol{r}) &= \hat{\boldsymbol{r}}\,{}_nU_l(r)\,Y_l^m(\vartheta,\varphi) + {}_nV_l(r)\,\boldsymbol{\nabla}_1 Y_l^m(\vartheta,\varphi), \\ {}_n\boldsymbol{\tau}_l^m(\boldsymbol{r}) &= -{}_nW_l(r)\,\hat{\boldsymbol{r}}\times\boldsymbol{\nabla}_1 Y_l^m(\theta,\varphi). \end{aligned}\right\} \tag{1}$$

In (1) ϑ is co-latitude, φ is longitude and $Y_l^m(\vartheta,\varphi)$ is a normalized surface harmonic

$$Y_l^m(\vartheta,\varphi) = X_l^m(\vartheta)\,\mathrm{e}^{\mathrm{i}m\varphi} = (-)^m\left(\frac{2l+1}{4\pi}\frac{(l-m)!}{(l+m)!}\right)^{\frac{1}{2}} P_l^m(\cos\vartheta)\,\mathrm{e}^{\mathrm{i}m\varphi}. \tag{2}$$

All of the $2l+1$ poloidal oscillations ${}_n\sigma_l^m(r)$ with fixed angular order l and radial order n, and with $-l \leqslant m \leqslant l$ have the same frequency ${}_n\omega_l$; together they form a multiplet, denoted ${}_nS_l$. All of the $2l+1$ toroidal oscillations ${}_n\tau_l^m(r)$ with fixed l and n, and $-l \leqslant m \leqslant l$, have the same frequency ${}_n\acute{\omega}_l$; together they form a multiplet, denoted ${}_nT_l$.

Perturbations, such as rotation, ellipticity of figure and geographical features, remove the $(2l+1)$-fold degeneracy of a multiplet; the multiplet is said to be split. Although splitting has been observed, and more observations are desirable, in this paper we shall confine our attention to multiplets and we shall ignore splitting.

To simplify notation let s_k denote either ${}_n\sigma_l^m$ or ${}_n\tau_l^m$ as is required. The normalization

$$\omega_k^2 \int \mathrm{d}V \rho(r)\, s_j(\boldsymbol{r}) \cdot \bar{s}_k(\boldsymbol{r}) = \delta_{jk} \tag{3}$$

is used.

Some classical results, due to Rayleigh and Routh, have been used to express the excitation of normal modes caused by an external force $\boldsymbol{f}(\boldsymbol{r},t)$ for the case where $\boldsymbol{f}(\boldsymbol{r},t) = \boldsymbol{f}(\boldsymbol{r})\,H(t)$. The response $\boldsymbol{u}(\boldsymbol{r},t)$ is

$$\boldsymbol{u}(\boldsymbol{r},t) = \sum_k s_k(\boldsymbol{r})\,\psi_k(\cos\omega_k t - 1)\,H(t), \tag{4}$$

$$\psi_k = -\int \mathrm{d}V \boldsymbol{f}(\boldsymbol{r}) \cdot s_k(\boldsymbol{r}). \tag{5}$$

For earthquakes the external force is regarded as the divergence of the moment density tensor $\mathscr{M}(\boldsymbol{r},t)$ (using the definition of Gilbert (1971*a*), the moment tensor is the negative of the action tensor). We have found it convenient to use the moment density rate tensor

$$\boldsymbol{M}(\boldsymbol{r},t) = \mathrm{d}\mathscr{M}(\boldsymbol{r},t)/\mathrm{d}t.$$

For the case where $\mathscr{M}(\boldsymbol{r},t) = \mathscr{M}(\boldsymbol{r})\,H(t)$ we have $\boldsymbol{M}(\boldsymbol{r},t) = \mathscr{M}(\boldsymbol{r})\,\delta(t)$. With $\boldsymbol{f}(\boldsymbol{r}) = \nabla\cdot\mathscr{M}(\boldsymbol{r})$ (5) becomes

$$\left.\begin{aligned} \psi_k &= \int \mathrm{d}V \mathscr{M}(\boldsymbol{r}) : \bar{\boldsymbol{E}}_k(\boldsymbol{r}), \\ \boldsymbol{E}_k &= \tfrac{1}{2}(\nabla s_k + s_k \nabla). \end{aligned}\right\} \tag{6}$$

When the temporal behaviour of the moment density tensor is not a step function we replace (6) by

$$\psi_k = \int \mathrm{d}V \boldsymbol{M}(\boldsymbol{r},t) : \bar{\boldsymbol{E}}_k(\boldsymbol{r}) = \psi_k(t) \tag{7}$$

and (4) becomes

$$\boldsymbol{u}(\boldsymbol{r},t) = \sum_k s_k(\boldsymbol{r})\,\psi_k(t) * [(\cos\omega_k t - 1)\,H(t)]. \tag{8}$$

In this paper we shall confine our attention to point sources

$$\boldsymbol{M}(\boldsymbol{r},t) = \boldsymbol{M}(t)\,\delta(\boldsymbol{r}-\boldsymbol{r}_0) \tag{9}$$

and (7) is simplified to

$$\psi_k(t) = \boldsymbol{M}(t) : \bar{\boldsymbol{E}}_k(\boldsymbol{r}_0). \tag{10}$$

To account for dissipation, assumed small, we introduce $\alpha_k = \omega_k/2Q_k$ with Q being the quality factor

$$\boldsymbol{u}(\boldsymbol{r},t) = \sum_k s_k(\boldsymbol{r})\,\psi_k(t) * [(\cos\omega_k t\,\mathrm{e}^{-\alpha_k t} - 1)\,H(t)]. \tag{11}$$

We shall use (11) for two numerical experiments. Assuming s and ψ to be known we shall first try to extract ω_k. Let

$$C_k(t) = (\cos\omega_k t\,\mathrm{e}^{-\alpha_k t} - 1)\,H(t) \tag{12}$$

and

$$\boldsymbol{a}_k(\boldsymbol{r},t) = s_k(\boldsymbol{t})\,\psi_k(t), \tag{13}$$

and rewrite (11) as
$$\boldsymbol{u}(\boldsymbol{r},t) = \sum_k \boldsymbol{a}_k(\boldsymbol{r},t) * C_k(t). \tag{14}$$

Having good approximations to $\boldsymbol{a}$ and numerous observations $\boldsymbol{u}$, our first experiment is to extract C_k whose spectral peak occurs at ω_k.

Let
$$\mathscr{E}_k(\boldsymbol{r},\boldsymbol{r}_0,t) = \boldsymbol{s}_k(\boldsymbol{r})\, C_k(t)\, \overline{\boldsymbol{E}}_k(\boldsymbol{r}_0), \tag{15}$$
and rewrite (11) as
$$\boldsymbol{u}(\boldsymbol{r},t) = \sum_k \mathscr{E}_k : * \boldsymbol{M}(t). \tag{16}$$

Having good approximations to $\mathscr{E}$ and numerous $\boldsymbol{u}$, our second experiment is to extract the moment rate tensor $\boldsymbol{M}(t)$. The moment tensor $\mathscr{M}(t)$ is then found by integration.

It is convenient to write the elements of the moment rate tensor $\boldsymbol{M}(t)$ and the strain tensor $\boldsymbol{E}$ as linear arrays.
$$\left.\begin{aligned} &f_1 = M_{rr}, \quad f_2 = M_{\theta\theta}, \quad f_3 = M_{\phi\phi},\\ &f_4 = M_{r\theta}, \quad f_5 = M_{r\phi}, \quad f_6 = M_{\theta\phi},\\ &\epsilon_1 = E_{rr}, \quad \epsilon_2 = E_{\theta\theta}, \quad \epsilon_3 = E_{\phi\phi},\\ &\epsilon_4 = 2E_{r\theta}, \quad \epsilon_5 = 2E_{r\phi}, \quad \epsilon_6 = 2E_{\theta\phi},\end{aligned}\right\} \tag{17}$$
and to write
$$\overline{\boldsymbol{E}}_k : \boldsymbol{M}(t) = \bar{\boldsymbol{\varepsilon}}_k \cdot \boldsymbol{f}(t), \tag{18}$$
where the six elements of $\boldsymbol{\varepsilon}_k$, for a fixed modal index k, are given explicitly in (17).

Using the standard expressions for $\boldsymbol{E}$ (Sokolnikoff 1956, p. 184) we find $\boldsymbol{\varepsilon}$ for a fixed l, m, n (fixed k) for poloidal (spheroidal) modes
$$\left.\begin{aligned} &\epsilon_1 = U'Y, \quad \epsilon_2 = r^{-1}[UY - V(\cot\vartheta Y' - m^2 \operatorname{cosec}^2\vartheta Y + l(l+1)\,Y)],\\ &\epsilon_3 = r^{-1}[UY + V(\cot\theta Y' - m^2\operatorname{cosec}^2\vartheta Y)],\\ &E_s = V' + r^{-1}(U-V), \quad \epsilon_4 = E_s Y', \quad \epsilon_5 = \mathrm{i}E_s m \operatorname{cosec}\vartheta Y,\\ &\epsilon_6 = \mathrm{i}\,2mr^{-1}V\operatorname{cosec}\vartheta(Y' - \cot\vartheta Y),\end{aligned}\right\} \tag{19}$$
and for toroidal (torsional) modes
$$\left.\begin{aligned} &\epsilon_1 = 0, \quad \epsilon_2 = \mathrm{i}mr^{-1}W\operatorname{cosec}\vartheta(Y' - \cot\vartheta Y),\\ &\epsilon_3 = -\epsilon_2, \quad E_T = W' - r^{-1}W, \quad \epsilon_4 = \mathrm{i}\,m\operatorname{cosec}\vartheta Y E_T,\\ &\epsilon_5 = -Y'E_T, \quad \epsilon_6 = r^{-1}W(2\cot\vartheta Y' - 2m^2\operatorname{cosec}^2\vartheta Y + l(l+1)\,Y).\end{aligned}\right\} \tag{20}$$

In (19) and (20) U, V, W and Y denote the scalars in (1) and (2). A prime denotes differentiation with respect to either r or ϑ and is made explicit by the context.

Thus the terms in (10) and (11) are easily evaluated, and the displacement $\boldsymbol{u}$ is simply represented as the superposition of normal modes. In geographical coordinates, where $\vartheta = 0$ at one of the Earth's poles, the normal modes (1) remain, to zero order in the perturbations, normal modes in the presence of rotation and ellipticity of figure (Dahlen 1968). Since these are the dominant perturbations for small l, n (1) can be used in a super-resolution scheme to extract singlets from seismic spectra.

In epicentral coordinates, where $\vartheta = 0$ at the epicentre, the azimuthal order m is restricted for a point dislocation; $|m| \leqslant \min(2,l)$. Our attention in this paper is confined to nearly degenerate multiplets, so it is useful and economical to use epicentral coordinates. We seek $\lim_{\vartheta\to 0}\epsilon(\vartheta)$. Expanding Y about $\vartheta = 0$ and using the definition, for fixed l, n
$$b_j = \frac{(-)^j}{2^j j!}\left(\frac{2l+1}{4\pi}\frac{(l+j)!}{(l-j)!}\right)^{\frac{1}{2}} \quad (0 \leqslant j \leqslant l), \tag{21}$$

we find respectively for (19) and (20) for poloidal (spheroidal) multiplets

$$
\left.\begin{array}{llll}
 & m=0 & m=\pm 1 & m=\pm 2 \\
\epsilon_1 = & U'b_0 & 0 & 0 \\
\epsilon_2 = & r^{-1}\left(U-\tfrac{1}{2}l(l+1)\,V\right)b_0 & 0 & 2r^{-1}Vb_2 \\
\epsilon_3 = & \epsilon_2 & 0 & -\epsilon_2 \\
\epsilon_4 = & 0 & E_s b_1 & 0 \\
\epsilon_5 = & 0 & \mathrm{i}mE_s b_1 & 0 \\
\epsilon_6 = & 0 & 0 & \mathrm{i}m\,2r^{-1}Vb_2
\end{array}\right\} \tag{22}
$$

and for toroidal (torsional) multiplets

$$
\left.\begin{array}{llll}
 & m=0 & m=\pm 1 & m=\pm 2 \\
\epsilon_1 = & 0 & 0 & 0 \\
\epsilon_2 = & 0 & 0 & \mathrm{i}mr^{-1}Wb_2 \\
\epsilon_3 = & 0 & 0 & -\epsilon_2 \\
\epsilon_4 = & 0 & \mathrm{i}mE_T b_1 & 0 \\
\epsilon_5 = & 0 & -E_T b_1 & 0 \\
\epsilon_6 = & 0 & 0 & -4r^{-1}Wb_2
\end{array}\right\} \tag{23}
$$

It is convenient to work in the frequency domain where temporal convolutions are replaced by multiplications. In the foregoing equations we replace all functions of time by their Fourier transforms, and the argument t is replaced by ω.

It is also convenient to factor the response $\boldsymbol{u}$ into three terms: the source, represented by the moment rate tensor $\boldsymbol{M}(\omega)$ or $\boldsymbol{f}(\omega)$, the multiplet spectrum $C_k(\omega)$, and the state function or transfer function $\boldsymbol{A}_k(\boldsymbol{r})$.

$$\boldsymbol{u}(\boldsymbol{r},\omega) = \sum_k \boldsymbol{A}_k(\boldsymbol{r})\cdot\boldsymbol{f}(\omega)\,C_k(\omega). \tag{24}$$

Thus, in (13)

$$\boldsymbol{a}_k(\boldsymbol{r},\omega) = \boldsymbol{A}_k(\boldsymbol{r})\cdot\boldsymbol{f}(\omega) \tag{25}$$

and in (15)

$$\mathscr{E}_k(\boldsymbol{r},\omega) = \boldsymbol{A}_k(\boldsymbol{r})\,C_k(\omega). \tag{26}$$

Therefore $\boldsymbol{A}_k(\boldsymbol{r})$ is given by

$$\boldsymbol{A}_k(\boldsymbol{r}) = \boldsymbol{s}_k(\boldsymbol{r})\,\bar{\boldsymbol{\epsilon}}_k(\boldsymbol{r}_0). \tag{27}$$

Henceforward we confine our attention to multiplets and use epicentral coordinates.

Each term in the sum in (24) is still a normal mode of the unperturbed earth, but is not a zero order normal mode of the rotating, elliptical Earth, because we are using epicentral coordinates. However, our interest lies in nearly degenerate multiplets, and they remain zero order multiplets in the presence of all perturbations unless quasi-degeneracy between multiplets becomes important. It has been shown by Luh (1973, 1974) that quasi-degeneracy is rarely important.

Therefore, we perform the sum over azimuthal order $m(|m| \leqslant \min(2,l))$ and absorb it into the definition of $\boldsymbol{A}(\boldsymbol{r})$ in (27) while k is redefined to be the common index for angular order l and radial order n

$$\boldsymbol{A}_k(\boldsymbol{r}) = \sum_m \boldsymbol{s}_k^m(\boldsymbol{r})\,\bar{\boldsymbol{\epsilon}}_k^m(\boldsymbol{r}_0). \tag{28}$$

Before presenting the expressions for $\boldsymbol{A}_k(\boldsymbol{r})$ in (28) we write the elements of the moment rate tensor in terms of its principal values. In the conventional coordinate system, adopted here, for the source mechanism, the pole is the epicentre, the r-axis increases radially, the ϑ-axis southerly, and the ϕ-axis easterly. (When we come to consider the principal axes of the moment tensor in the lower hemisphere of the focal sphere we use a coordinate system that preserves symmetry with respect to inversion through the hypocentre.)

In terms of the principal values of the moment tensor, τ_i; $i = 1, 2, 3$, their azimuths ζ_i, measured with respect to North, and plunges η_i the components of $\boldsymbol{f}$ are

$$\left.\begin{array}{ll} f_1 = \tau_i \sin^2 \eta_i, & f_2 = \tau_i \cos^2 \eta_i \cos^2 \zeta_i, \\ f_3 = \tau_i \cos^2 \eta_i \sin^2 \zeta_i, & f_4 = \tfrac{1}{2}\tau_i \sin 2\eta_i \cos \zeta_i, \\ f_5 = -\tfrac{1}{2}\tau_i \sin 2\eta_i \sin \zeta_i, & f_6 = -\tfrac{1}{2}\tau_i \cos^2 \eta_i \sin 2\zeta_i, \end{array}\right\} \tag{29}$$

where summation over $i = 1, 2, 3$ is implied.

With the source coordinates adopted, the epicentral coordinates of a receiver at azimuth ζ from the source are colatitude (epicentral distance) ϑ and epicentral longitude $\varphi = \pi - \zeta$.

For poloidal (spheroidal) multiplets we use (1), (2) and (22) to evaluate (28)

$$\boldsymbol{A}_j(\boldsymbol{r}) = \hat{\boldsymbol{r}} U(r)\, A_{1j} + \hat{\boldsymbol{\vartheta}} V(r)\, A_{2j} + \hat{\boldsymbol{\varphi}} \operatorname{cosec} \vartheta V(r)\, A_{3j}:$$

$$\left.\begin{array}{llll} j & A_{1j} & A_{2j} & A_{3j} \\ 1 & \epsilon_1^0 X_l^0 & \epsilon_1^0 X_l'^0 & 0 \\ 2 & \epsilon_2^0 X_l^0 + 2\epsilon_2^2 X_l^2 \cos 2\varphi & \epsilon_2^0 X_l'^0 + 2\epsilon_2^2 X_l'^2 \cos 2\varphi & -4\epsilon_2^2 X_l^2 \sin 2\varphi \\ 3 & \epsilon_2^0 X_l^0 - 2\epsilon_2^2 X_l^2 \cos 2\varphi & \epsilon_2^0 X_l'^0 - 2\epsilon_2^2 X_l'^2 \cos 2\varphi & 4\epsilon_2^2 X_l^2 \sin 2\varphi \\ 4 & 2\epsilon_4^1 X_l^1 \cos \varphi & 2\epsilon_4^1 X_l'^1 \cos \varphi & -2\epsilon_4^1 X_l^1 \sin \varphi \\ 5 & 2\epsilon_4^1 X_l^1 \sin \varphi & 2\epsilon_4^1 X_l'^1 \sin \varphi & 2\epsilon_4^1 X_l^1 \cos \varphi \\ 6 & 4\epsilon_2^2 X_l^2 \sin 2\varphi & 4\epsilon_2^2 X_l'^2 \sin 2\varphi & 8\epsilon_2^2 X_l^2 \cos 2\varphi \end{array}\right\} \tag{30}$$

In (30) we see that $A_{2j} = \partial_\theta A_{1j}$ and $A_{3j} = \partial_\phi A_{1j}$. This is a consequence of the representation (1) for poloidal modes.

For toroidal (torsional) multiplets we use (1), (2) and (23) to evaluate (28)

$$\boldsymbol{A}_j(\boldsymbol{r}) = \hat{\boldsymbol{\theta}} \operatorname{cosec} \vartheta W(r)\, A_{2j} + \hat{\boldsymbol{\varphi}} W(r)\, A_{3j}:$$

$$\left.\begin{array}{lll} j & A_{2j} & A_{3j} \\ 1 & 0 & 0 \\ 2 & -2\epsilon_6^2 X_l^2 \cos 2\varphi & \epsilon_6^2 X_l'^2 \sin 2\varphi \\ 3 & 2\epsilon_6^2 X_l^2 \cos 2\varphi & -\epsilon_6^2 X_l'^2 \sin 2\varphi \\ 4 & -2\epsilon_5^1 X_l^1 \cos \varphi & 2\epsilon_5^1 X_l'^1 \sin \varphi \\ 5 & -2\epsilon_5^1 X_l^1 \sin \varphi & -2\epsilon_5^1 X_l'^1 \cos \varphi \\ 6 & -4\epsilon_6^2 X_l^2 \sin 2\varphi & 2\epsilon_6^2 X_l'^2 \cos 2\varphi \end{array}\right\} \tag{31}$$

and there is no A_{1j}.

In (31) we see that A_{2j} and A_{3j} can be derived from a single scalar by differentiation as a consequence of the representation (1) for toroidal modes.

We now have $\boldsymbol{A}_k(\boldsymbol{r})$ in epicentral coordinates. Since the W.W.S.S.N. stations record the positive directions as (up, north, east) we rotate $\boldsymbol{A}_k$ accordingly.

$$\left.\begin{array}{l} A_{Nj} = -A_{2j} \cos \xi - A_{3j} \sin \xi, \\ A_{Ej} = -A_{2j} \sin \xi + A_{3j} \cos \xi, \end{array}\right\} \tag{32}$$

where ξ is now the azimuth of the source from the station.

If it is necessary or desirable to consider the excitation of normal modes by more than one point source, the extension of the theory is relatively simple. If we have earthquakes (point sources) in different locations $\boldsymbol{r}_1, \boldsymbol{r}_2, \ldots,$ we can calculate $\boldsymbol{A}_k(\boldsymbol{r})$ in (27) for each one

$$\boldsymbol{A}_k(\boldsymbol{r}, \boldsymbol{r}_i) = \boldsymbol{A}_k^{(i)}(\boldsymbol{r}) = \boldsymbol{s}_k(\boldsymbol{r})\, \bar{\boldsymbol{\varepsilon}}_k(\boldsymbol{r}_i) \quad (i = 1, 2, \ldots). \tag{33}$$

Using (33) we extend the definition of $\boldsymbol{a}_k(\boldsymbol{r}, \omega)$ in (25)

$$\boldsymbol{a}_k(\boldsymbol{r}, \omega) = \sum_i \boldsymbol{A}_k^{(i)}(\boldsymbol{r}) \cdot \boldsymbol{f}^{(i)}(\omega), \tag{34}$$

where $\boldsymbol{f}^{(i)}(\omega)$ represents the ith source mechanism. For multiplets we use (28) and sum (33) over m for each multiplet.

2.2. *Resolution of multiplets*

We begin with (2.1.24) and (2.1.25)

$$\boldsymbol{u}(\boldsymbol{r}, \omega) = \sum_k \boldsymbol{a}_k(\boldsymbol{r}, \omega)\, C_k(\omega), \tag{1}$$

$$\boldsymbol{a}_k(\boldsymbol{r}, \omega) = \boldsymbol{A}_k(\boldsymbol{r}) \cdot \boldsymbol{f}(\omega). \tag{2.1.25}$$

For a particular source mechanism $\boldsymbol{f}(\omega)$, $\boldsymbol{a}_k(\boldsymbol{r}, \omega)$ is the geographical shape of the kth (degenerate) multiplet. The spherical harmonics are orthonormal over the unit sphere and that is sufficient to suggest a method to retrieve $C_k(\omega)$ from (1). Let ${}_n\boldsymbol{a}_l^q$ denote $\boldsymbol{a}_k$ for a particular multiplet of radial order n, angular order l and type q ($q = 1$ for toroidal and $q = 2$ for spheroidal, for example). Then from the orthogonality of the spherical harmonics

$$\int \mathrm{d}\Omega\, {}_{n'}\bar{\boldsymbol{a}}_{l'}^{q'} \cdot {}_n\boldsymbol{a}_l^q = \int \mathrm{d}\Omega\, {}_{n'}\bar{\boldsymbol{a}}_l^q \cdot {}_n\boldsymbol{a}_l^q\, \delta_{l'l}\, \delta_{q'q}. \tag{2}$$

Multiplets of different type or different l are orthogonal over the unit sphere regardless of n, but multiplets of the same type and the same l but different n are not necessarily orthogonal.

Consequently the hermitean inner product matrix $\mathscr{A}$

$$\mathscr{A}_{jk} = \int \mathrm{d}\Omega\, \bar{\boldsymbol{a}}_j \cdot \boldsymbol{a}_k \tag{3}$$

is block diagonal. All multiplets of the same type and the same l belong to one block, called the overtone block. For example, the T_l overtone block refers to toroidal multiplets of angular order l.

Suppose now that the $\boldsymbol{a}_k(\boldsymbol{r}, \omega)$ are known and that $\boldsymbol{u}(\boldsymbol{r}, \omega)$ are observed. Define

$$v_j(\omega) = \int \mathrm{d}\Omega\, \bar{\boldsymbol{a}}_j(\boldsymbol{r}, \omega) \cdot \boldsymbol{u}(\boldsymbol{r}, \omega). \tag{4}$$

From (1), (3), and (4) we have

$$v_j(\omega) = \sum_k \mathscr{A}_{jk} C_k(\omega). \tag{5}$$

Since $\mathscr{A}$ is block diagonal each $v_j(\omega)$ is a linear combination of $C_k(\omega)$ that are overtones of either S_l or T_l type. The overtones, for fixed l, are well separated in frequency with very rare exceptions. Therefore, there is no difficulty in identifying the spectral peaks in $v_j(\omega)$ as the overtones belonging to a particular block of $\mathscr{A}$. If we do not use those $\boldsymbol{a}_k$ that are zero then each block of $\mathscr{A}$ is a positive definite, hermitean inner product matrix. Thus each block in (5)

$$\boldsymbol{v}(\omega) = \mathscr{A} \cdot \boldsymbol{C}(\omega), \tag{6}$$

can be inverted and $\boldsymbol{C}(\omega)$ can be found

$$\boldsymbol{C}(\omega) = \mathscr{A}^{-1} \cdot \boldsymbol{v}(\omega). \tag{7}$$

Even if those $\boldsymbol{a}_k$ that are zero are included, the resulting zero eigenvalues of $\mathscr{A}$ can be suppressed by constructing the generalized inverse of $\mathscr{A}$ for use in (7).

We can think of (4) as a phase equalization process in which each component of $\boldsymbol{u}$ is equalized for a particular (jth) multiplet and then summed or stacked to enhance that multiplet. Thus $v_j(\omega)$ is termed the spectral stack for the jth multiplet and the process yielding $v_j(\omega)$ is termed *stacking*.

By inverting the blocks of $\mathscr{A}$ to extract $\boldsymbol{C}(\omega)$ in (7) we use each row of $\mathscr{A}^{-1}$ to strip a single overtone multiplet from the overtone stacks $\boldsymbol{v}(\omega)$. For this reason, the process (7) is termed *stripping*.

Mendiguren (1973) was the first to apply the stacking process for a global network of stations. He assumed the moment tensor to be a step function which makes $\boldsymbol{f}$ in (2.1.25) real and independent of frequency. Thus $\boldsymbol{a}_k(\boldsymbol{r})$ is real. In (4) Mendiguren used sgn $\boldsymbol{a}_j(\boldsymbol{r})$ in place of $\bar{\boldsymbol{a}}_j(\boldsymbol{r}, \omega)$ to construct his stacks. As he showed, this process works very well; he retrieved 240 multiplets, 160 of which had never before been reported. However, Mendiguren's method of stacking does not lend itself easily to stripping.

In a practical application of (4)–(7) several factors must be considered. We must take into account the network of stations, the degrading effect of limited dynamic range in the recording system, the absence of some components from some stations, the extent to which the real multiplets are sufficiently degenerate to yield good stacks, and the error caused by using values of $\boldsymbol{a}_k(\boldsymbol{r}, \omega)$ calculated for some model of the Earth and the source.

The individual seismograms are Fourier transformed and ordered, $u_p(\omega)$ $(p = 1, 2, \ldots, P)$. The calculated $\boldsymbol{a}_k(\boldsymbol{r}, \omega)$ are ordered similarly, $a_{pk}(\boldsymbol{r}, \omega)$. It is assumed that the spectra $\boldsymbol{f}(\omega)$ vary very smoothly and $a_{pk}(\boldsymbol{r})$ is taken to be independent of ω in any frequency band of interest; i.e. $\boldsymbol{f}(\omega)$ is replaced by its frequency averaged value.

The data come from the W.W.S.S.N. The recordings are in analog form and must be digitized, a boring, time-consuming task. Large signals can be off-scale, especially shortly after the earthquake. Such signals are simply lost and the recordings are unfortunately truncated. Small signals may be obscured by background noise in a different frequency range or may be masked by the width of the trace being digitized and this leads to another unfortunate loss. For example, for the Colombian earthquake, 1970 July 31, Dratler, Farrell, Block & Gilbert (1971) report useful signal levels 80 h after the event (signal/noise ratio of 20 dB after 50 h for some multiplets). They used digital recording systems and very sensitive instruments and their results demonstrate vividly what could be achieved with a global network of digitally recording instruments.

However, for the present, we must face the problems caused by truncated records wherein both large and small signals are lost. We choose our origin-time to be that assigned to the earthquake from a study of the onset of high-frequency P waves. Suppose that digitization begins at time T. Then we replace $C_k(\omega)$ in (1) by $\gamma_k(\omega)$

$$\gamma_k(\omega) = \pi^{-1} \int_{-\infty}^{\infty} C_k(\lambda) \frac{\sin(\lambda - \omega)\, T}{\lambda - \omega} \,\mathrm{d}\lambda, \tag{8}$$

and (8) represents the convolution of C_k with the familiar sinc function or 'boxcar transform'. If our main goal is to find the spectral peak of a multiplet we can use γ_k as well as C_k because their peaks are coincident. In principle we can use (4)–(7) for truncated records, while realizing that stripping will give γ_k rather than C_k.

If it is desirable to have C_k, or a better approximation to it than γ_k, we approximate (8) for $|\omega - \omega_k| \ll \omega_k$ (for convenience we consider only $\omega > 0$).

$$\gamma_k(\omega) = C_k(\omega)\, \mathrm{e}^{\mathrm{i}(\omega_k - \omega) T - \alpha_k T}. \tag{9}$$

In (9) we have neglected the spectrum of $-H(t)$ (which is i/ω) in (2.1.12) because

$$C_k(\omega_k) = 1/2\alpha_k + \mathrm{i}/\omega_k,$$

and for $\alpha_k \ll \omega_k$, the second term is negligible. Replacing C_k by γ_k in (1) and using (9) gives

$$\left.\begin{aligned} \boldsymbol{u}(\boldsymbol{r},\omega) &= \sum_k \boldsymbol{a}_k(\boldsymbol{r},\omega)\, d_k(\omega)\, C_k(\omega), \\ d_k(\omega) &= \mathrm{e}^{\mathrm{i}(\omega_k-\omega)T-\alpha_k T}. \end{aligned}\right\} \tag{10}$$

We must approximate d_k further because neither ω_k nor α_k is presumed to be known at this stage. Since the peak of $C_k(\omega)$ is defined to occur at ω_k we can use only the value of $d_k(\omega_k)$ in (10)

$$d_k = \mathrm{e}^{-\alpha_k T} \tag{11}$$

and we need only have α_k. As we have already mentioned, it is perfectly reasonable to extract γ_k and to take its peak frequency to be ω_k. However, observed values of Q ($\alpha_k = \omega_k/2Q_k$) vary from a low of about 100 for short period ${}_0\mathrm{T}_l$ modes to about 1000 for some of the high-Q overtones to as much as perhaps 10 000 for ${}_0\mathrm{S}_0$.

When low-Q and high-Q modes are nearly coincident in frequency, it seems to us that it is desirable to use (10) as a basis for stacking and stripping. Although observations of Q are scanty and of inferior quality, and although our understanding of the dissipative mechanism is poor, almost any rough choice of α_k in (11) represents a favourable correction.

Accordingly, we have adopted the following Q model. Dissipation is independent of frequency (an impossibility, but, hopefully, an acceptable approximation), isotropic strain is not dissipative ($Q_\kappa^{-1}(r) = 0$), $Q_\mu(r) = 1000$ in the inner core, $Q_\mu(r) = 400$ in the mantle below a depth of 650 km and $Q_\mu(r) = 115$ in the mantle above a depth of 650 km. Using this model and the relation between Q_k^{-1} for the kth eigenfrequency and $Q_\mu^{-1}(r)$ (Anderson & Archambeau 1964; Backus & Gilbert 1968) we make the following comparison between observed and computed values of Q in the form: mode (observed, computed):

${}_0\mathrm{S}_0$	(2000–10000, 7500);	${}_4\mathrm{S}_0$	(1160, 1240);
${}_0\mathrm{S}_{10}$	(280, 360);	${}_0\mathrm{S}_{12}$	(275, 330);
${}_0\mathrm{S}_{25}$	(195, 175);	${}_0\mathrm{S}_{57}$	(130, 130);
${}_0\mathrm{T}_{23}$	(135, 123);	${}_0\mathrm{T}_{39}$	(131, 116).

Considering that uncertainties in the observed values may, in some cases, be as large as 50 %, perhaps more, it appears that our computed values, which fit the observations with an r.m.s. error of 20 %, are as good as one should reasonably expect. We do *not* pretend that our adopted model of $Q_\mu(r)$ should be accepted for any purpose other than estimating α_k in (11).

If it is considered important to consider both the effect of starting digitization at T_{1p} and stopping at T_{2p} we replace (11) by (p is the ordering index for the seismograms)

$$d_{pk} = \mathrm{e}^{-\alpha_k T_{1p}} - \mathrm{e}^{-\alpha_k T_{2p}}. \tag{12}$$

We now combine (10) and (11) or (12) for our ordered array $u_p(\omega)$ of spectra

$$u_p(\omega) = \sum_k a_{pk} d_{pk} C_k(\omega). \tag{13}$$

Stacking is performed

$$v_j(\omega) = \sum_p \bar{a}_{pj} d_{pj} u_p(\omega), \tag{14}$$

the hermitean inner product matrix is formed

$$\mathscr{A}_{jk} = \sum_{p} \bar{a}_{pj} d_{pj} a_{pk} d_{pk} \tag{15}$$

and stripping is done, usually with a generalized inverse,

$$C(\omega) = \mathscr{A}^{-1} \cdot \boldsymbol{v}(\omega), \tag{16}$$

to retrieve multiplets whose peak frequencies are interpreted to be the eigenfrequencies ω_k. Notice that we could have used d_k as defined in (10) and we could have used $\boldsymbol{f}(\omega)$ rather than its average value. Then $\mathscr{A}$ is a function of frequency and the equivalent of constructing $\mathscr{A}^{-1}$ must be done for each value of ω. While this does not lead to a preposterous amount of computing, the improvement over using (11) or (12) is thought to be slight.

Using a real global network W.W.S.S.N., with some components absent or rejected and with incomplete geographical coverage, destroys the theoretical block diagonal character of $\mathscr{A}$ in (15). Multiplets of different angular order, or different type, or both, interfere in the stacks. In addition imperfect spherical symmetry in the real Earth contributes to the interference. Interference between multiplets widely separated in frequency is certainly slight and this fact is exploited to form $\mathscr{A}^{-1}$.

Arranging the multiplets in order of increasing frequency, computed for some model, we neglect those elements of $\mathscr{A}$ that are sufficiently far from the main diagonal that they represent the interference of multiplets widely separated in frequency. Effectively, $\mathscr{A}$ is reduced to banded form.

The width of the frequency band to be stripped for a particular multiplet is chosen to have end points at the theoretical -10 dB levels for that multiplet. All multiplets whose computed eigenfrequencies lie in the band, and that were therefore used to compute $\boldsymbol{v}$, are used to construct $\mathscr{A}^{-1}$. Thus, stripping is done one multiplet at a time in practice. When core modes (Alaska II) are not included some reduction in the order of $\mathscr{A}$ can be realized.

If seismic spectra from two or more events are to be processed we use (2.1.34) in place of (2.1.25) for $\boldsymbol{a}_k(\boldsymbol{r}, \omega)$. In this way we can treat multiple events, foreshocks and aftershocks, as well as events widely separated in time and space.

In summary, stacking and stripping are methods for recovering the spectrum of a nearly degenerate multiplet from seismograms recorded by a global network of stations.

Stacking is a method of phase equalization. If one has a good model of the Earth and of the mechanisms of the events being studied, then one can calculate the amplitude and phase spectra for a particular multiplet at any element of the global network of stations. By element is meant any one component of acceleration, strain, tilt, etc. If the models are sufficiently good, the difference between the calculated spectra and observed spectra should be negligibly small. Therefore, one can use the calculated spectra to equalize the observed spectra to have (nearly) zero phase at each element. The equalized observed spectra are then amplitude weighted and summed. The multiplet being sought should be maximally reinforced while others, without zero phase, should tend to cancel. The truth of the foregoing remark has been proved for a uniformly distributed global network, in which case stacking amounts to vector spherical harmonic analysis. For a real network of non-uniformly distributed stations, experimentation must be done to assess the value of the method of stacking.

Stripping is also a method of phase equalization and is a more refined method than stacking. It enables one to suppress the unwanted influence of interfering multiplets. For a real network stacking cannot yield perfect results. Each stack is a linear combination of a wanted multiplet and its unwanted neighbours. By computing the coefficients in the linear combination one can derive a set of linear equations relating the (imperfect) stacks to the multiplets. Inverting the system of equations should yield the multiplets. Each multiplet is said to be stripped from the stacks. With perfect coverage, the coefficient matrix is diagonal and stripping becomes a redundant operation. The method of stripping works well when the coefficient matrix is diagonally dominant, but is often useful even when stacking is not an obvious success.

2.3. *Retrieving the moment spectrum*

We begin with (2.1.24) and (2.1.26)

$$\boldsymbol{u}(\boldsymbol{r},\omega) = \sum_k \boldsymbol{\mathscr{E}}_k(\boldsymbol{r},\omega)\cdot\boldsymbol{f}(\omega), \tag{1}$$

$$\boldsymbol{\mathscr{E}}_k(\boldsymbol{r},\omega) = \boldsymbol{A}_k(\boldsymbol{r})\,C_k(\omega). \tag{2.1.26}$$

We assume that the peak frequency of $C_k(\omega)$ is known or can be accurately estimated. For example, an approximation to $\boldsymbol{f}$, determined from studies of the first motion of P waves, could be used to resolve $C_k(\omega)$ as discussed in § 2.2.

Again we use the orthogonality of the spherical harmonics to derive

$$\int \mathrm{d}\Omega\, {}_{n'}\boldsymbol{A}_{l'}^{q'\mathrm{T}}\cdot{}_n^q\boldsymbol{A}_l = \int \mathrm{d}\Omega\, {}_{n'}\boldsymbol{A}_l^{q\mathrm{T}}\cdot{}_n\boldsymbol{A}_l^q\,\delta_{ll'}\,\delta_{qq'}, \tag{2}$$

where ${}_r\boldsymbol{A}_l^q$ denotes $\boldsymbol{A}_k$ for radial order n, angular order l, and type q. Transposition is denoted by the superscript T.

A slightly different form of stacking is performed

$$\boldsymbol{v}_j(\omega) = \int \mathrm{d}\Omega\,\boldsymbol{A}_j^{\mathrm{T}}(\boldsymbol{r})\cdot\boldsymbol{u}(\boldsymbol{r},\omega), \tag{3}$$

and a symmetric matrix is formed (a symmetric array of symmetric dyadics)

$$\mathscr{S}_{jk} = \int \mathrm{d}\Omega\,\boldsymbol{A}_j^{\mathrm{T}}(\boldsymbol{r})\cdot\boldsymbol{A}_k(\boldsymbol{r}) \tag{4}$$

and the (six) vector stack for the jth multiplet becomes

$$\boldsymbol{v}_j(\omega) = \sum_k (\mathscr{S}_{jk}\cdot\boldsymbol{f}(\omega))\,C_k(\omega). \tag{5}$$

We use the fact that the multiplet $C_k(\omega)$ has a very narrow peak at ω_k and that

$$\int_{\omega_k-\mathrm{w}}^{\omega_k+\mathrm{w}} C_k(\omega)\,\mathrm{d}\omega = \arctan(\mathrm{w}/\alpha_k) + \mathrm{i}2\mathrm{w}/\omega_k \tag{6}$$

for $\mathrm{w} \ll \omega_k$. The arctangent in (6) represents the contribution from the spectrum of the cosine term in (2.1.11) and the second term comes from the spectrum of $-H(t)$. For $\mathrm{w} \ll \omega_k$ but $\mathrm{w} > \alpha_k$ the integral approaches $\frac{1}{2}\pi$ and the second term is negligibly small. Thus, we can remove the effect of dissipation by integrating across the resonance curve. We have found that an acceptable value of $N = \mathrm{w}/\alpha_k$ to use is $N = 3$; arctan (3) = 1.25. Since the values of α are computed from our simple model (section 2.2) the actual ratio $N = \mathrm{w}/\alpha_k$ might differ from 3. However, since arctan (2.4) = 1.18 and arctan (3.6) = 1.30 we see that an error in α of about 20 % causes an error in (6) of less than 6 %. This is the main virtue of using (6) to remove the effect of dissipation. Let us define

$$I[C_k(\omega)] = \int_{\omega_k-\mathrm{w}}^{\omega_k+\mathrm{w}} C_k(\omega)\,\mathrm{d}\omega = \beta_k = 1.25 \quad \text{for} \quad \mathrm{w} = 3\alpha_k. \tag{7}$$

In (5) $\mathscr{S}_{jk}$ is zero (see (2)) unless both j and k belong to the same angular order and the same type. The radial orders can be different, but overtones for fixed angular order and type are almost invariably well separated in frequency. That is, the interval between successive overtones is almost always very much greater than α. Therefore, if we apply (7) to (5) we force j and k to be equal for the overwhelming majority of multiplets. We have

$$I[\boldsymbol{v}_j(\omega)] = \mathscr{S}_{jj}\cdot\boldsymbol{f}(\omega)\,\beta_j. \tag{8}$$

Let

$$\boldsymbol{w}_j = \beta_j^{-1}I[\boldsymbol{v}_j(\omega)] = \mathscr{S}_{jj}\cdot\boldsymbol{f}(\omega). \tag{9}$$

It is our expectation that $\boldsymbol{f}(\omega)$ is a very smooth function of ω for the frequencies of interest in this report. We choose to regard $\boldsymbol{f}(\omega)$ as constant in any given frequency band and to sum (9) for all multiplets in that band. We define

$$\boldsymbol{h} = \sum_j \boldsymbol{w}_j, \quad \boldsymbol{F} = \sum_j \mathscr{S}_{jj}, \quad \boldsymbol{h} = \boldsymbol{F}\cdot\boldsymbol{f}, \tag{10}$$

and if there are more than six multiplets in the given frequency band $\boldsymbol{F}$ is positive definite. Thus

$$\boldsymbol{f} = \boldsymbol{F}^{-1}\cdot\boldsymbol{h}, \tag{11}$$

and we have retrieved the spectrum of the moment rate tensor (Gilbert 1973*a*).

In applying this theoretical method to real data we face the same problems here as in §2.2. Because of the use of (6) and (7) we use $d_k(\omega)$ in (2.2.10) and also include the effect of terminating the record at time T_2

$$d_{pk}(\omega) = \mathrm{e}^{\mathrm{i}(\omega_k-\omega)T_{1p}-\alpha_k T_{1p}} - \mathrm{e}^{\mathrm{i}(\omega_k-\omega)T_{2p}-\alpha_k T_{2p}}, \tag{12}$$

where T_{1p} is now the time when digitization begins.

For most multiplets with periods greater than 64 s, T_{2p} is so large, usually 24 h, that its effect in (12) is negligible. This is especially true for short period, low-Q multiplets. At the other extreme, for long period, high-Q multiplets, such as all radial modes (${}_nS_0$ singlets), ${}_3S_1$, ${}_3S_2$, ${}_6S_1$, etc., the effect of T_{2p} can be more important than that of T_{1p}. Therefore, we factor (12) into the product of two terms

$$\left.\begin{aligned} d_{pk}(\omega) &= g_{pk}\psi_{pk}(\omega),\\ g_{pk} &= \mathrm{e}^{-\alpha_k T_{1p}} - \mathrm{e}^{-\alpha_k T_{2p}},\\ \psi_{pk}(\omega) &= \frac{(\mathrm{e}^{\mathrm{i}(\omega_k-\omega)T_{1p}} - \mathrm{e}^{\mathrm{i}(\omega_k-\omega)T_{2p}-\alpha_k(T_{2p}-T_{1p})})}{(1-\mathrm{e}^{-\alpha_k(T_{2p}-T_{1p})})},\end{aligned}\right\} \tag{13}$$

and perform the actual calculations as follows.

The observed, ordered spectra $u_p(\omega)$ are corrected for truncation

$$U_{pk}(\omega) = u_p(\omega)\,\psi_{pk}^{-1}(\omega), \tag{14}$$

for each multiplet, $k = 1, 2, \ldots$. Before applying (7) to (14) we observe that (1) has become

$$U_{pk}(\omega) = \sum_j \mathscr{E}_{pj}(\omega)\cdot\boldsymbol{f}(\omega)\,d_{pj}(\omega)\,\psi_{pk}^{-1}(\omega). \tag{15}$$

The eigenfrequencies are assumed to be known very accurately from resolution of hundreds of multiplets. This has been achieved through successful stacking and stripping. Therefore, we reverse the order of forming (3) and (9) by applying (7) to (14) and (15) before stacking. Furthermore, we are justified in dropping the sum in (15). The application of (7) eliminates most of the multiplets $j \neq k$. Stacking eliminates the remainder. From (7) and (15) we have, neglecting the sum over j (setting $j = k$)

$$I[U_{pk}(\omega)] = \beta_k \mathbf{A}_{pk} \cdot \mathbf{f}(\omega)\, g_{pk}, \tag{16}$$

where the $\mathbf{A}_{pk}$ are the $\mathbf{A}_k(\mathbf{r})$ ordered similarly to the $u_p(\omega)$.

The next step is to stack (16) over the network of stations

$$\nu_k(\omega) = \sum_p \mathbf{A}_{pk}^{\mathrm{T}} g_{pk} I[U_{pk}(\omega)], \tag{17}$$

and to form the matrix

$$\mathscr{S}_{kk} = \sum_p \mathbf{A}_{pk}^{\mathrm{T}} \mathbf{A}_{pk} g_{pk}^2, \tag{18}$$

which leads to our approximation to (9)

$$\mathbf{w}_k = \mathscr{S}_{kk} \cdot \mathbf{f}. \tag{19}$$

We now follow (10) and (11) to find $\mathbf{f}$ in successive frequency bands.

The sequence of steps leading from the observed seismograms to the spectrum of the moment rate tensor represents the application of successive linear operations. Consequently, the order in which these operations is applied is, in principle, unimportant. While the order (3)–(9) followed by (10) and (11) is appealing for its theoretical insight, the order actually used, (14)–(19), followed by (10) and (11) is preferable from a computational point of view.

It should be clear from the foregoing presentation that there is no difficulty, in principle, to retrieve, simultaneously, the source spectra of multiple or interfering events. We simply use (2.1.33) in place of (2.1.27), for singlets, or (2.1.28), for multiplets. In each frequency band the order of $\mathbf{F}$ in (10) and (11) is $6I$, where I is the number of point sources being retrieved. For the applications in this report $I = 1$.

3. Numerical applications and results

We approach the problems of resolving multiplets and retrieving source mechanisms by attempting to factor the observed data into two categories. In the first category are the source-independent factors and in the second are the structure-independent factors. A successful factorization depends on there being a 'sufficiently good' Earth model, and, as we shall see, there is.

After describing the sources of our data in § 3.1 we discuss our initial attempt to resolve multiplets in § 3.2. Both stacking and stripping are used. The latter appears to be more sensitive to the details of correcting the data for the effects of truncation, but yields a superior signal/noise ratio in the majority of cases where it can be applied. In our initial attempt some 500 multiplets are resolved. Their eigenfrequencies are combined with those of Alaska I and II to derive a new Earth model.

The spectra of the moment rate tensor for two deep earthquakes are presented in § 3.3. A statistically very significant isotropic (compressive) component is detected in both cases. It is quite evident that the stress release is not instantaneous.

A second resolution experiment, using the Earth model of § 3.2 and the source mechanisms of § 3.3, is discussed in § 3.4. Stacking and stripping have yielded 812 multiplets.

3.1. *Sources of data and the studies of others*

The Colombian earthquake of 1970 July 31 is one of the largest events in the depth range from 500 to 700 km since the beginning of the World-Wide Standard Seismograph Network

(W.W.S.S.N.). The hypocentral parameters of this earthquake determined by the National Oceanic and Atmospheric Administration are: origin time 17:08:05.4 G.M.T., latitude 1.5° S, longitude 72.6° W, depth 651 km, magnitude 7.1 (m_b).

Dratler *et al.* (1971) have found from the analysis of gravimeter recordings that the spectra were rich in overtones with a large content of compressional potential energy. As an isotropic source excites compressional normal modes much more efficiently than a deviatoric source (Gilbert 1973 *b*) it occurred to us that a detailed study of the mechanism of this earthquake could provide a definitive answer to the problem of the existence of an isotropic component in the released stress.

Mendiguren (1972, 1973) obtained a high quality nodal plane solution for this earthquake with both nodal planes being well constrained. His P-wave data excluded the possibility that an implosive component could be superimposed upon a double couple source (Mendiguren 1972). It should be pointed out, however, that this conclusion is valid only for the high frequency part of the spectrum of the source. The validity of extrapolating the results obtained from short period body wave studies to periods greater by two orders of magnitude has never been properly tested. The fact that Mendiguren was successful in improving the signal/noise ratio by applying his phase equalization procedure with the source parameters determined from the nodal plane solutions does not prove that the extrapolation is valid. If the strain tensor at the source (equations (2.1.22) and (2.1.23)) is such that excitation for a particular m, for example $m = \pm 1$, is much greater than that for the other m values (in this case $m = 0$ and $m = \pm 2$) then the success of the phase equalization procedure does not depend on the source mechanism. A vector spherical harmonic expansion of the displacements suffices. Even if excitation for different m is balanced, the fact that applying the phase equalization procedure is successful in improving the signal-to-noise ratio means only that the adopted source mechanism is not grossly wrong, but it does not prove that the optimum in the signal/noise ratio has been reached.

In view of the potential importance of the information contained in the recordings of this earthquake we decided to undertake the time consuming operation of converting the analog W.W.S.S.N. recordings into digital form.

All of the available W.W.S.S.N. long period seismograms covering the period from the origin time until two days after the earthquake were examined for technical quality and 202 recordings were selected for digitization. Digitization was performed on a semi-automatic digitizer (CALMA Graphic-III) which has a nominal resolution of 0.025 mm; the actual digitization errors probably exceed this value by an order of magnitude, but they may be expected to be random.

The sampling interval was 2 s per sample or 4 s per sample, depending on the level of the microseism noise. The digitized recordings were low passed with a zero phase shift filter with a cut-off frequency of 0.0505 Hz and the sampling rate was reduced to 8 s per sample. These time series were subsequently Fourier transformed with a time basis of 2^{17} s; the equivalent frequency increment is 7.62939×10^{-6} Hz.

The amplitude spectra of the Fourier transforms of the digitized records were examined and the records with a poor signal-to-noise ratio were rejected; nearly all of these were records from the second day after the earthquake. Table 1 contains parameters related to 165 seismograms retained for further analysis. Figure 1 shows the world-wide distribution of the stations from which at least one recording is used; the lack of uniform coverage is obvious.

The Fourier spectra were corrected for instrumental response (reduction to ground motion; Hagiwara 1958) and the phase shift resulting from the delay in beginning of digitization with respect to the origin time. Deconvolution of the instrumental response was performed using the nominal parameters of W.W.S.S.N. seismograph–galvanometer system: $T_0 = 15\,\text{s}$, $T_g = 100\,\text{s}$, $h_0 = 1$, $h_g = 1$; the coupling constant σ^2 was set to 0.05 (Mitchell & Landisman 1969) and the peak magnification was assumed to correspond to that indicated on a seismogram. The errors resulting from the differences between the actual and nominal parameters of the system should be insignificant for our purpose if the differences are not greater than 10% (see, for example, table 3 in Mitchell & Landisman 1969). An *ad hoc* inspection of the calibration pulses revealed that this condition is satisfied.

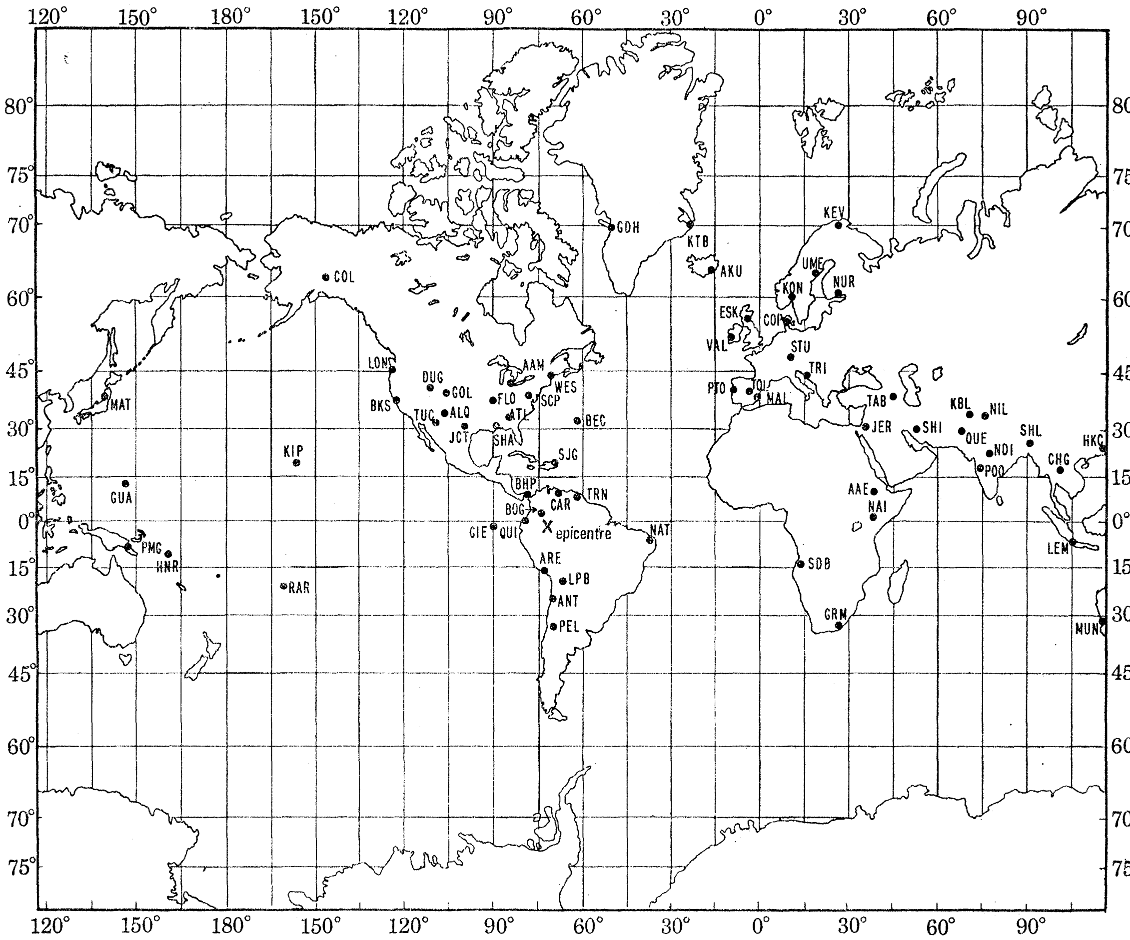

FIGURE 1. Distribution of W.W.S.S.N. stations which provided the recordings of the Colombian earthquake used in this study.

The set of the Fourier spectra of 165 seismograms corrected as described above represents the basic input data for further analysis.

The second event considered in our study is the earthquake on the Peru–Bolivia border of 1963 August 15. The hypocentral data reported by the U.S.C.G.S. are: origin time 17:25:27.9 G.M.T., latitude 13.8° S, longitude 69.3° W, depth 543 km. The estimates of its magnitude vary widely: 6 (U.S.C.G.S.), 7.75 (Pasadena), 7.9 (Berkeley).

Alsop & Brune (1965) analysed a long-period recording of this event and reported a series of the fundamental and higher spheroidal modes of free oscillations in the period range from 100–500 s.

TABLE 1. STATIONS AND PARAMETERS OF DIGITIZATION OF RECORDINGS OF THE COLUMBIAN EARTHQUAKE OF 1970, JULY 31, USED IN THIS STUDY

record no.	code	lat. deg.	long. deg.	distance deg.	azimuth at epicentre	azimuth at station	comp.	start H:M	length H:M
1	AAE	9.03 N	38.77 E	111.3	80.9	271.9	up	14:17	22:45
2	AAM	42.30 N	83.66 W	44.7	348.3	164.2	up	1:20	20:20
3	—	—	—	—	—	—	NS	1: 4	20:45
4	AKU	65.69 N	18.11 W	77.5	20.2	236.5	up	1:53	23:59
5	ALQ	34.94 N	106.46 W	48.2	322.1	131.6	up	1:52	18:50
6	—	—	—	—	—	—	NS	1:52	18:50
7	ANT	23.70 S	70.42 W	22.2	174.7	354.2	up	4:52	16:30
8	—	—	—	—	—	—	NS	5:22	15:59
9	—	—	—	—	—	—	EW	4:10	17:11
10	ARE	16.46 S	71.49 W	14.9	175.9	355.7	up	7: 0	23:39
11	—	—	—	—	—	—	NS	7: 0	23:39
12	ATL	33.43 N	84.34 W	36.5	343.4	160.0	up	3: 2	21:34
13	—	—	—	—	—	—	NS	2:13	22:24
14	—	—	—	—	—	—	EW	2:32	22: 4
15	BEC	32.28 N	64.68 W	34.4	11.9	194.1	up	1: 4	22:12
16	—	—	—	—	—	—	NS	1: 4	20:45
17	—	—	—	—	—	—	EW	1:32	15: 0
18	BHP	8.96 N	79.56 W	12.5	326.4	145.9	up	1: 3	18:49
19	BKS	37.88 N	122.24 W	60.2	316.0	118.7	up	2:14	21:17
20	—	—	—	—	—	—	NS	2:15	21:17
21	—	—	—	—	—	—	EW	2: 4	21:28
22	—	—	—	—	—	—	up	24: 8	23:56
23	BOG	4.62 N	74.07 W	6.3	346.4	166.4	up	2:31	17:21
24	CAR	10.50 N	66.93 W	13.2	25.2	205.7	up	2: 4	14:22
25	—	—	—	—	—	—	NS	2: 8	14:18
26	—	—	—	—	—	—	EW	2:11	14:15
27	—	—	—	—	—	—	up	18:59	20:48
28	CHG	18.79 N	98.98 E	160.9	25.1	333.4	up	8:58	23:15
29	—	—	—	—	—	—	EW	9: 4	23: 0
30	COL	64.90 N	147.79 W	85.1	335.6	104.1	up	3:20	20:34
31	—	—	—	—	—	—	NS	0:59	22:55
32	—	—	—	—	—	—	EW	2:25	21:29
33	COP	55.48 N	12.43 E	88.4	34.6	265.1	up	1: 1	14: 0
34	—	—	—	—	—	—	NS	1: 1	14: 0
35	DUG	40.20 N	112.81 W	55.4	323.1	128.4	NS	6: 3	23:28
36	—	—	—	—	—	—	EW	6: 3	23:28
37	ESK	55.32 N	3.20 W	79.6	32.9	252.0	up	1:27	13:31
38	—	—	—	—	—	—	NS	1:27	13:31
39	—	—	—	—	—	—	EW	1:38	13:20
40	FLO	38.50 N	90.37 W	43.0	339.5	153.4	up	1:52	17: 0
41	—	—	—	—	—	—	NS	1:52	16:58
43	GDH	69.25 N	53.53 W	71.8	7.0	200.1	up	1:37	18: 0
44	—	—	—	—	—	—	NS	1:37	18: 0
45	—	—	—	—	—	—	EW	1:37	18: 0
46	—	—	—	—	—	—	up	19:56	24:47
47	GIE	0.73 S	90.30 W	17.7	272.3	92.6	up	5:44	19: 2
48	GOL	39.70 N	105.37 W	50.8	327.4	135.7	up	2:34	18:10
49	—	—	—	—	—	—	NS	2:15	18:29
50	—	—	—	—	—	—	up	21:52	23:33
51	GRM	33.31 S	26.57 E	96.8	123.6	263.7	up	1:44	19: 8
52	GUA	13.54 N	144.91 E	141.0	289.7	75.3	up	3: 0	25:11
53	—	—	—	—	—	—	NS	3: 0	25:10
54	—	—	—	—	—	—	EW	3: 0	25:10
55	HKC	22.30 N	114.17 E	158.3	342.8	18.6	up	9:26	23:44
56	HNR	9.43 S	159.95 E	126.5	257.2	98.9	up	7:12	23:52
57	JCT	30.48 N	99.80 W	41.0	323.0	135.9	up	1:18	16:57
58	—	—	—	—	—	—	NS	2:13	16: 2
59	—	—	—	—	—	—	EW	1:52	16:23
60	JER	31.77 N	35.20 E	105.9	57.5	278.2	up	2:37	13:15
61	—	—	—	—	—	—	NS	2:24	13:28
62	—	—	—	—	—	—	EW	2:25	12:27
63	—	—	—	—	—	—	up	16:29	21: 9
64	KBL	34.50 N	69.17 E	131.5	43.1	304.3	up	2:43	8:27
65	—	—	—	—	—	—	NS	2:43	8:27
66	—	—	—	—	—	—	EW	2:43	5:40
67	—	—	—	—	—	—	NS	12:30	20:22
68	—	—	—	—	—	—	EW	12:30	20:22
69	KEV	69.76 N	27.01 E	94.7	20.1	278.5	up	1:32	14: 0
70	—	—	—	—	—	—	NS	1:27	14: 5
71	—	—	—	—	—	—	EW	1:27	14: 5
72	—	—	—	—	—	—	up	16: 2	24:20
73	KIP	21.42 N	158.90 W	87.1	291.4	92.7	up	1:52	24:58
74	—	—	—	—	—	—	NS	1:52	24:58
75	—	—	—	—	—	—	EW	1:52	24:58
76	KON	59.65 N	9.63 E	87.3	30.2	262.5	up	2:23	22: 7
77	—	—	—	—	—	—	NS	2:23	21:17
78	—	—	—	—	—	—	EW	2:30	22: 0
79	KTG	70.42 N	21.98 W	79.1	15.4	231.9	up	0:52	16:32
80	—	—	—	—	—	—	NS	1:48	16:36
81	—	—	—	—	—	—	EW	0:48	16:36
82	LEM	6.83 S	107.62 E	171.7	181.5	178.5	up	8:15	22:42
83	LON	46.75 N	121.81 W	64.5	324.8	123.0	NS	0:48	21:19

TABLE 1 (*cont.*)

record no.	code	lat. deg.	long. deg.	distance deg.	azimuth at epicentre	azimuth at station	comp.	start H:M	length H:M
85	LPB	16.53 S	68.10 W	15.6	163.7	343.0	up	3:23	21:29
86	—	—	—	—	—	—	NS	2:39	22:13
87	—	—	—	—	—	—	EW	3: 9	21:43
88	MAL	36.73 N	4.41 W	73.6	51.0	255.4	up	1:28	13:24
89	—	—	—	—	—	—	NS	1:23	13:29
90	—	—	—	—	—	—	EW	1:23	10:29
91	MAT	36.54 N	138.21 E	135.0	324.3	46.4	up	7:39	23:29
92	—	—	—	—	—	—	NS	7:38	23:43
93	—	—	—	—	—	—	EW	7:38	23:43
94	MUN	31.98 S	116.21 E	145.7	193.3	164.2	EW	0:42	7:55
95	NAI	1.27 S	36.80 E	109.4	91.9	268.0	up	1:35	10:21
96	—	—	—	—	—	—	EW	1:33	10:23
97	—	—	—	—	—	—	up	12:10	23:42
98	NAT	5.12 S	35.03 W	37.7	96.4	274.2	up	1:57	17:16
99	—	—	—	—	—	—	NS	1:42	14:10
100	—	—	—	—	—	—	EW	2: 8	13:44
101	NDI	26.68 N	77.20 E	141.7	46.6	305.8	up	1:38	7:22
102	—	—	—	—	—	—	up	9:33	22:58
103	NIL	33.65 N	73.25 E	134.8	41.3	307.8	up	9:20	23:36
104	—	—	—	—	—	—	NS	9:20	23:36
105	—	—	—	—	—	—	EW	9:20	23:36
106	NUR	60.51 N	24.65 E	94.9	29.5	275.6	up	1:32	10:37
107	—	—	—	—	—	—	NS	1:52	10:25
108	—	—	—	—	—	—	EW	1:27	10:50
109	—	—	—	—	—	—	up	12:33	23:57
110	PEL	33.14 S	70.69 W	31.5	176.9	356.3	up	1:38	18:14
111	—	—	—	—	—	—	NS	2: 6	17:46
112	—	—	—	—	—	—	EW	1:37	18:15
113	PMG	9.41 S	147.15 E	139.0	253.9	103.2	up	0:47	6:15
114	—	—	—	—	—	—	NS	0:17	6:45
115	—	—	—	—	—	—	EW	0:47	6:15
116	POO	18.53 N	73.85 E	143.0	60.6	293.3	up	1:36	7:19
117	PTO	41.14 N	8.60 W	71.7	45.6	251.1	up	1:26	14:39
118	—	—	—	—	—	—	NS	0:52	15:10
119	—	—	—	—	—	—	EW	1:34	14:18
120	QUE	30.14 N	66.95 E	132.2	49.4	298.9	up	9:38	23:13
121	—	—	—	—	—	—	NS	9:38	23:14
122	—	—	—	—	—	—	EW	9:38	23:14
123	QUI	0.20 S	78.50 W	6.0	282.3	102.4	up	3:14	18:57
124	—	—	—	—	—	—	NS	2: 0	18: 7
125	—	—	—	—	—	—	EW	2: 1	17:51

record no.	code	lat. deg.	long. deg.	distance deg.	azimuth at epicentre	azimuth at station	comp.	start H:M	length H:M
126	RAR	21.21 S	159.77 W	86.8	249.0	89.6	NS	1:59	26:31
127	SCP	40.81 N	77.87 W	42.4	354.1	172.2	NS	0:53	18:40
128	—	—	—	—	—	—	EW	0:53	18:39
129	SDB	14.93 S	13.57 E	85.9	104.8	269.5	NS	1:29	12:32
130	SHA	30.69 N	88.14 W	35.3	336.4	152.4	up	4:49	23:29
131	SHI	29.63 N	52.50 E	120.9	56.1	287.6	up	1:43	9:28
132	—	—	—	—	—	—	NS	1:43	9:28
133	—	—	—	—	—	—	EW	1:46	9:25
134	—	—	—	—	—	—	NS	11:47	23: 5
135	SHL	25.57 N	91.58 E	151.6	31.2	325.0	up	2: 3	6:23
136	—	—	—	—	—	—	up	9:37	22:50
137	SJG	18.11 N	66.15 W	20.5	17.8	198.7	up	0:52	18:17
138	—	—	—	—	—	—	NS	0:52	18:17
139	—	—	—	—	—	—	EW	0:52	18:17
140	STU	48.77 N	9.28 E	85.8	41.1	262.9	up	1: 7	14:36
141	—	—	—	—	—	—	NS	0:40	15: 3
142	TAB	38.07 N	46.33 E	113.4	48.8	287.5	up	1:22	9:29
143	—	—	—	—	—	—	up	11: 9	21:43
144	TOL	39.88 N	4.05 W	74.7	48.0	254.8	up	1:28	11:19
145	—	—	—	—	—	—	NS	1:24	11:28
146	—	—	—	—	—	—	EW	1:33	11:19
147	—	—	—	—	—	—	up	13:21	19:31
148	TRI	45.64 N	13.75 E	88.5	44.5	266.4	NS	1:37	11: 7
149	—	—	—	—	—	—	EW	1:37	11: 7
150	—	—	—	—	—	—	NS	13:52	19: 0
151	—	—	—	—	—	—	EW	13:52	19: 0
152	TRN	10.65 N	61.40 W	16.4	42.5	223.4	up	1:52	14:25
153	—	—	—	—	—	—	EW	1:52	15:25
154	TUC	32.31 N	110.78 W	49.3	316.4	125.5	up	1:32	21:55
155	—	—	—	—	—	—	EW	1:39	21:48
156	UME	63.82 N	20.24 E	92.6	26.3	271.9	up	2:24	13:17
157	—	—	—	—	—	—	NS	2:19	13:22
158	—	—	—	—	—	—	EW	3:16	12:25
159	VAL	51.93 N	10.25 W	74.5	34.7	246.8	up	1:30	14:22
160	—	—	—	—	—	—	NS	1:23	14:29
161	—	—	—	—	—	—	EW	1:24	14:28
162	—	—	—	—	—	—	up	16:15	16:37
163	WES	42.38 N	71.32 W	43.7	1.4	181.9	up	1:48	22:33
164	—	—	—	—	—	—	NS	1:42	22:39
165	—	—	—	—	—	—	EW	1:41	22:40

TABLE 2. STATIONS AND PARAMETERS OF DIGITIZATION OF RECORDINGS OF THE PERU–BOLIVIA BORDER EARTHQUAKE OF 1963, AUGUST 15, USED IN THIS STUDY

record no.	code	lat. deg.	long. deg.	distance deg.	azimuth at epicentre	azimuth at station	comp.	start H:M	length H:M
1	AAE	9.02 N	38.77 E	109.5	85.2	258.5	up	0:12	12:02
2	ADE	34.37 S	138.71 E	124.7	208.0	146.3	up	0:13	6:44
3	AFI	13.91 S	171.78 W	98.5	253.4	106.5	up	0:11	7:35
4	ALQ	34.94 N	106.46 W	59.9	325.0	137.3	up	0:58	20:19
5	ANP	25.18 N	121.52 E	164.8	319.6	44.0	up	0:19	6:17
6	AQU	42.35 N	13.40 E	93.9	47.5	255.0	up	0:59	11:48
7	—	—	—	—	—	—	up	13:35	21:48
8	ATL	33.43 N	84.34 W	49.1	343.3	160.5	up	2:20	12:48
9	ATU	37.97 N	23.72 E	100.7	53.4	260.9	up	0:10	12:37
10	—	—	—	—	—	—	NS	0:13	8:06
11	BAG	16.41 N	120.58 E	170.1	286.5	76.1	up	0:52	6:08
12	BEC	32.38 N	64.68 W	46.1	5.4	186.2	up	1:50	11:45
13	BKS	37.88 N	122.24 W	71.4	318.2	125.1	up	0:46	8:30
14	—	—	—	—	—	—	up	9:29	11:47
15	BLA	37.21 N	80.42 W	51.8	348.7	166.2	EW	2:10	13:01
16	CAR	10.51 N	66.93 W	24.3	5.7	185.6	up	0:53	15:55
17	—	—	—	—	—	—	NS	0:52	9:55
18	COP	55.68 N	12.43 E	96.7	34.4	255.5	up	0:12	10:38
19	FLO	38.80 N	90.37 W	55.9	340.2	155.1	up	0:36	18:59
20	GDH	69.25 N	53.53 W	83.6	5.6	195.4	up	0:45	16:55
21	GOL	39.70 N	105.37 W	62.9	329.3	140.0	up	0:44	22:05
22	GSC	35.30 N	116.80 W	66.4	318.8	128.6	up	0:43	21:57
23	HNR	9.43 S	159.94 E	126.0	247.4	114.6	up	0:14	6:13
24	IST	41.04 N	28.98 E	105.1	50.8	264.8	up	0:12	11:29
25	KON	59.65 N	9.60 E	96.3	30.1	253.5	up	0:54	20:15
26	LPA	34.91 S	57.93 W	23.4	155.9	331.2	up	0:29	5:28
27	LUB	33.58 N	101.87 W	56.4	327.4	141.1	up	0:33	21:40
28	MAL	36.73 N	4.41 W	79.0	47.8	243.6	up	0:49	12:26
29	MUN	31.98 S	116.21 E	134.2	186.5	172.5	up	0:14	7:55
30	—	—	—	—	—	—	EW	0:13	7:57
31	NDI	28.68 N	77.22 E	145.6	59.1	288.4	up	0:14	8:39
32	—	—	—	—	—	—	up	10:08	22:46
33	NNA	11.99 S	76.84 W	7.6	282.9	104.6	up	0:54	5:13
34	—	—	—	—	—	—	up	7:08	15:54
35	NUR	60.51 N	24.65 E	103.8	30.6	266.5	up	0:58	11:02
36	—	—	—	—	—	—	NS	0:11	11:30
37	RAB	4.19 S	152.17 E	135.1	249.4	114.2	up	0:16	6:42
38	RIV	33.83 S	151.16 E	118.9	218.1	133.9	up	0:08	5:44
39	SBA	77.85 S	166.76 E	83.3	190.2	125.8	up	0:10	5:52
40	SCP	40.81 N	77.87 W	54.9	352.1	169.8	up	0:36	10:18
41	SHA	30.69 N	88.14 W	47.8	337.9	154.9	up	0:39	7:39
42	SHL	25.57 N	91.88 E	158.8	53.7	300.0	up	1:27	6:26
43	TOL	39.88 N	4.05 W	80.7	45.1	243.4	up	0:09	9:00
44	TUC	32.31 N	110.78 W	60.6	319.9	132.4	up	0:36	22:15
45	UME	63.82 N	20.24 E	102.1	27.0	263.4	up	0:12	14:41
46	—	—	—	—	—	—	NS	0:11	9:55

Chandra (1970) analysed the recordings of this event and found multiple P-phases indicating that the rupture propagation occurred in a series of jerks and he located one of the secondary events. He has also found a nodal plane solution from the analysis of amplitudes of P-waves; his solution differs from either of the two alternative solutions obtained from S-wave data by Stauder & Bollinger (1966). The nodal plane solution of Chandra is not nearly as well constrained as that of Mendiguren: 36 out of 39 P-wave first motion data covered an azimuthal range of only 95°; only two first motions are of compressive character; the direction of the inferred tension axis is significantly different from that for all the other events in this depth range in the Peru–Chile region, as compiled by Isacks & Molnar (1971). It may be that these apparent discrepancies in the nodal plane solutions are related to the temporal variations in the stress release pattern as determined from the results of our analysis described in §4.3.

Dziewonski (1971) used digitized recordings of 35 vertical component seismograms of this earthquake in his analysis of the regional variations in dispersion of mantle Rayleigh waves. For the purpose of this study we have augmented the digitization interval for a number of recordings and eight new recordings were added, some of them for horizontal components. Table 2 is a list of parameters related to 46 seismograms of the Peru–Bolivia earthquake used in further analysis. The initial data processing procedure are identical to those described for the Colombian data set except that in 1963 the standard seismograph period T_0 was 30 s.

3.2. *Initial resolution of multiplets*

The 165 spectra of the Colombian earthquake (table 1, §3.1) and the source mechanism of Mendiguren (1973) are used to apply the theoretical and computational methods of §§2.1 and 2.2.

The parameters of the principal axes (2.1.29) are $\tau_1 = -1$ (compression), $\zeta_1 = 32°$, $\eta_1 = 75°$; $\tau_2 = 1$, $\zeta_2 = 244°$, $\eta_2 = 12°$; $\tau_3 = 0$. The elements of $\boldsymbol{f}$, independent of frequency, are

$$\left.\begin{array}{lll} f_1 = -0.890, & f_2 = 0.136, & f_3 = 0.754, \\ f_4 = -0.301, & f_5 = 0.315, & f_6 = -0.347. \end{array}\right\} \tag{1}$$

Those parameters that depend on Earth structure in §§2.1 and 2.2 were computed for model UTD124A′ (Alaska I).

In the upper part of figure 2 we show examples of 'stacking' for modes ${}_0S_{25}$–${}_0S_{28}$. The effect of incomplete coverage is expressed by the presence of side lobes with maxima at frequencies corresponding to the eigenfrequencies of ${}_0S_{l-1}$ and ${}_0S_{l+1}$. The amplitude of side lobes for the example shown is approximately one third of the amplitude of the main peak. The periods T in the figure correspond to the frequency at which the main peak reaches its maximum (spline fitting). They are interpreted as the eigenperiods of the appropriate modes.

In the lower part of figure 2 we show the result of stripping, by using (2.2.12)–(2.2.16). Note that we recover not $C_k(\omega)$ but $C_k(\omega)\ \psi_k(\omega)$ (2.3.13). The matrix $\mathscr{A}$ (2.2.15) was constructed to include all multiplets within the frequency range of each of the diagrams in figure 2.

The process of stripping resulted in a nearly complete removal of the side-lobes present in the stacked spectra and in a general improvement of the signal : noise ratio. We note, however, that the eigenfrequencies inferred from both processes are nearly identical; the largest difference is observed for ${}_0S_{28}$ and it amounts to 0.05 s or less than 0.02 %. Thus, we infer that when the signal : noise ratio in the immediate vicinity of the maximum of the main peak is good, equally reliable estimates of eigenfrequencies can be made from the stacked as from the stripped spectra.

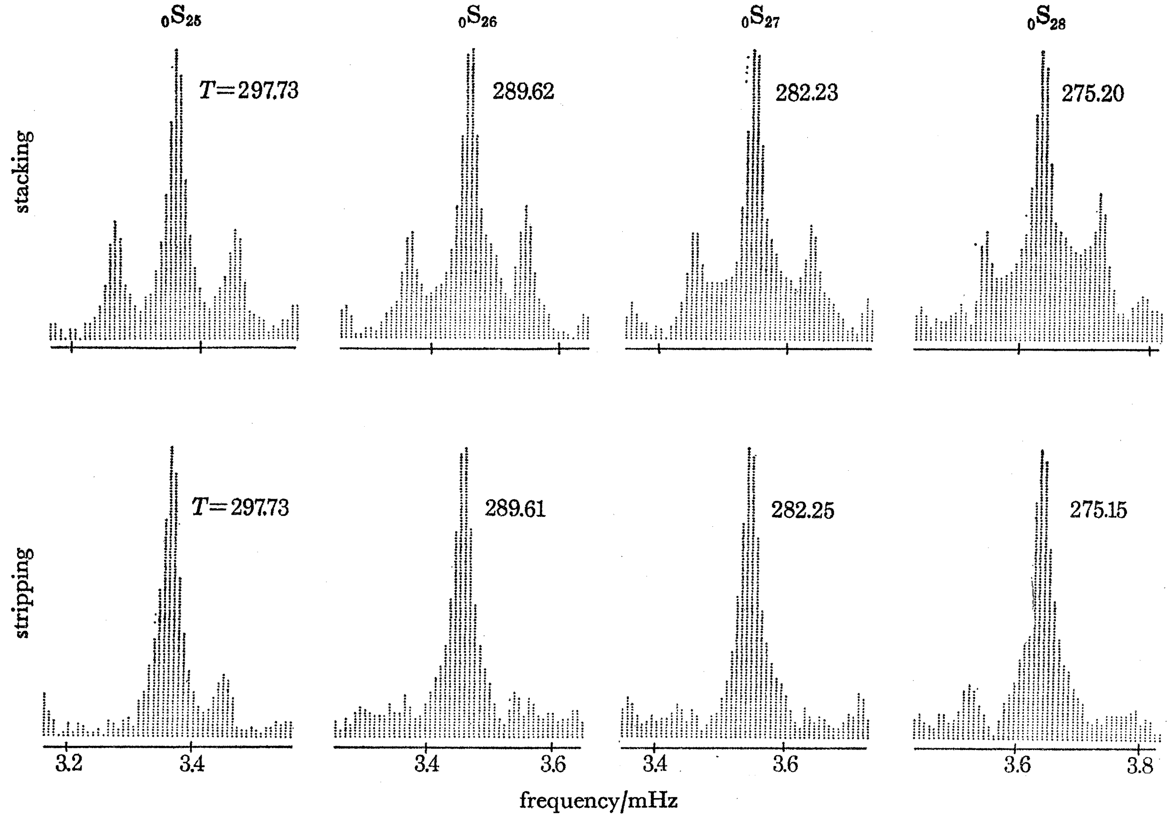

FIGURE 2. Comparison of the results of 'stacking' and 'stripping' 165 spectra (Colombian earthquake) for the modes $_0S_{25}$–$_0S_{28}$.

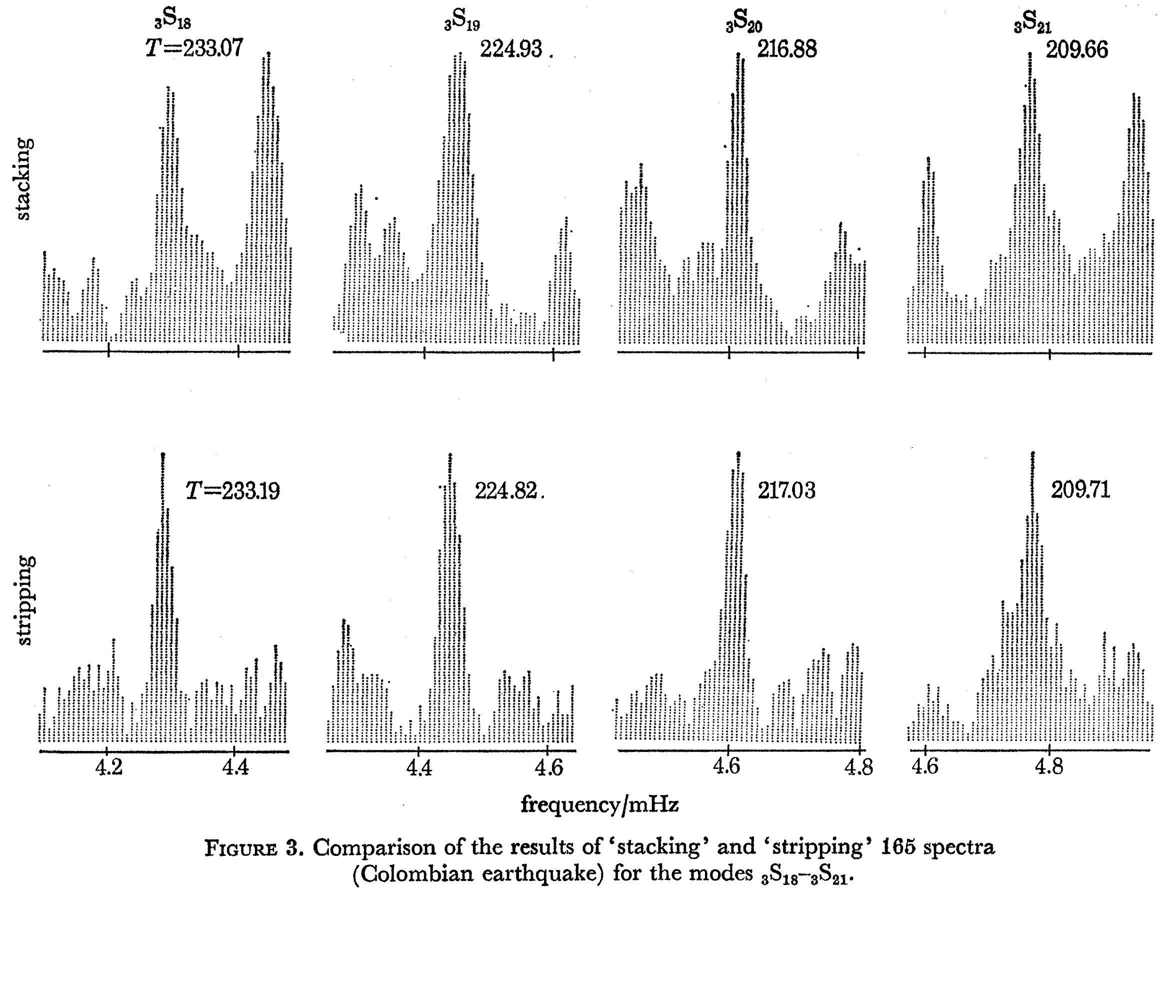

FIGURE 3. Comparison of the results of 'stacking' and 'stripping' 165 spectra (Colombian earthquake) for the modes $_3S_{18}$–$_3S_{21}$.

The improvement brought about by the stripping process is much more significant for the modes shown in figure 3. In the stack for ${}_3S_{18}$ the amplitude of the side lobe due to, most likely, ${}_3S_{19}$ exceeds that of the main peak; this side lobe is nearly entirely eliminated in the spectrum stripped for ${}_3S_{18}$. The central peak in the stack for ${}_3S_{19}$ is broader than that in the stripped stack; the most probable reason for this difference is that the stack is contaminated by several other modes which have eigenfrequencies very close to that of ${}_3S_{19}$. The improvement due to the stripping process is also clearly visible for ${}_3S_{20}$ and ${}_3S_{21}$.

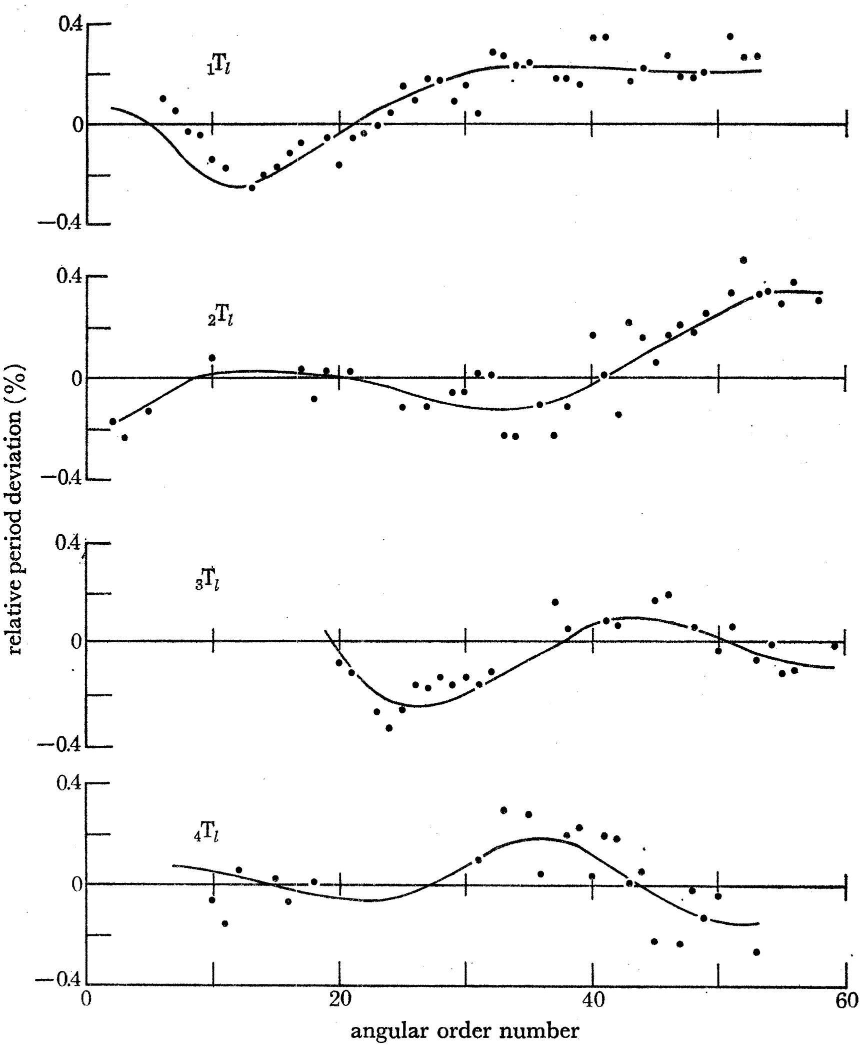

FIGURE 4. Relative deviations of the observed eigenperiods of the first four toroidal overtones from the periods computed for model UTD124A′ are shown as dots. The solid line represents relative differences between theoretical eigenperiods for models 508 and UTD124A′.

Approximating the effect of truncation by (2.2.12) is apparently insufficient for very low and very high frequencies. The scatter in the total length of digitized recordings (table 1) is the cause of failure of the stripping procedure for periods greater than 450–500 s, while at periods shorter than 150–130 s differences between the time of beginning of digitization of individual recordings causes the failure. However, in the period range from 150 to 450 s the stripped spectra have, in

TABLE 3. PARAMETERS OF MODEL 508

level	radius km	ρ g cm^{-3}	V_p km s^{-1}	V_s km s^{-1}	level	radius km	ρ g cm^{-3}	V_p km s^{-1}	V_s km s^{-1}	level	radius km	ρ g cm^{-3}	V_p km s^{-1}	V_s km s^{-1}
1	0.0	13.300	11.386	3.629	57	2200.0	11.575	9.644	0.000	113	4360.0	5.085	12.747	6.918
2	80.0	13.291	11.382	3.629	58	2240.0	11.529	9.606	0.000	114	4400.0	5.059	12.715	6.901
3	120.0	13.287	11.378	3.628	59	2280.0	11.482	9.568	0.000	115	4440.0	5.033	12.685	6.884
4	160.0	13.284	11.371	3.628	60	2320.0	11.434	9.530	0.000	116	4480.0	5.009	12.656	6.866
5	200.0	13.280	11.363	3.627	61	2360.0	11.385	9.494	0.000	117	4520.0	4.986	12.627	6.848
6	240.0	13.277	11.353	3.626	62	2400.0	11.335	9.458	0.000	118	4560.0	4.965	12.598	6.830
7	280.0	13.274	11.342	3.624	63	2440.0	11.285	9.423	0.000	119	4600.0	4.945	12.567	6.812
8	320.0	13.270	11.328	3.623	64	2480.0	11.235	9.388	0.000	120	4640.0	4.925	12.533	6.793
9	360.0	13.265	11.314	3.621	65	2520.0	11.184	9.353	0.000	121	4680.0	4.907	12.495	6.774
10	400.0	13.259	11.297	3.619	66	2560.0	11.131	9.318	0.000	122	4720.0	4.889	12.453	6.754
11	440.0	13.252	11.280	3.616	67	2600.0	11.078	9.281	0.000	123	4760.0	4.872	12.404	6.733
12	480.0	13.244	11.261	3.614	68	2640.0	11.024	9.242	0.000	124	4800.0	4.855	12.348	6.712
13	520.0	13.236	11.241	3.611	69	2680.0	10.970	9.202	0.000	125	4840.0	4.839	12.287	6.689
14	560.0	13.228	11.221	3.607	70	2720.0	10.916	9.160	0.000	126	4880.0	4.822	12.220	6.667
15	600.0	13.220	11.200	3.603	71	2760.0	10.863	9.117	0.000	127	4920.0	4.806	12.151	6.644
16	640.0	13.213	11.178	3.599	72	2800.0	10.812	9.074	0.000	128	4960.0	4.789	12.079	6.622
17	680.0	13.206	11.156	3.594	73	2840.0	10.762	9.029	0.000	129	5000.0	4.772	12.007	6.601
18	720.0	13.200	11.134	3.589	74	2880.0	10.713	8.983	0.000	130	5040.0	4.754	11.936	6.580
19	760.0	13.195	11.111	3.584	75	2920.0	10.664	8.934	0.000	131	5080.0	4.735	11.863	6.558
20	800.0	13.190	11.089	3.578	76	2960.0	10.615	8.882	0.000	132	5120.0	4.714	11.788	6.533
21	840.0	13.186	11.066	3.572	77	3000.0	10.566	8.828	0.000	133	5160.0	4.692	11.709	6.506
22	880.0	13.182	11.044	3.566	78	3040.0	10.515	8.770	0.000	134	5200.0	4.666	11.625	6.473
23	920.0	13.179	11.022	3.559	79	3080.0	10.464	8.710	0.000	135	5240.0	4.640	11.539	6.437
24	960.0	13.176	10.999	3.552	80	3120.0	10.413	8.647	0.000	136	5280.0	4.614	11.459	6.400
25	1000.0	13.174	10.977	3.545	81	3160.0	10.362	8.582	0.000	137	5320.0	4.590	11.390	6.366
26	1040.0	13.172	10.955	3.538	82	3200.0	10.311	8.515	0.000	138	5360.0	4.571	11.337	6.337
27	1080.0	13.170	10.932	3.531	83	3240.0	10.260	8.447	0.000	139	5400.0	4.558	11.309	6.317
28	1120.0	13.169	10.910	3.523	84	3280.0	10.209	8.379	0.000	140	5440.0	4.551	11.301	6.306
29	1160.0	13.167	10.888	3.516	85	3320.0	10.159	8.312	0.000	141	5480.0	4.549	11.306	6.301
30	1200.0	13.166	10.866	3.508	86	3360.0	10.109	8.247	0.000	142	5520.0	4.551	11.320	6.303
31	1228.9	13.169	10.852	3.504	87	3400.0	10.062	8.186	0.000	143	5560.0	4.526	11.268	6.263
32	1228.9	12.094	10.474	0.000	88	3430.0	10.010	8.126	0.000	144	5600.0	4.474	11.143	6.180
33	1240.0	12.089	10.461	0.000	89	3460.0	9.969	8.084	0.000	145	5640.0	4.394	10.944	6.052
34	1280.0	12.077	10.423	0.000	90	3483.6	9.940	8.049	0.000	146	5680.0	4.285	10.670	5.877
35	1320.0	12.066	10.385	0.000	91	3483.6	5.502	13.786	7.194	147	5720.0	4.146	10.322	5.656
36	1360.0	12.055	10.348	0.000	92	3520.0	5.492	13.771	7.187	148	5760.0	4.035	10.038	5.476
37	1400.0	12.043	10.311	0.000	93	3560.0	5.480	13.750	7.177	149	5800.0	3.950	9.818	5.337
38	1440.0	12.032	10.274	0.000	94	3600.0	5.469	13.710	7.168	150	5840.0	3.875	9.631	5.215
39	1480.0	12.021	10.239	0.000	95	3640.0	5.458	13.661	7.158	151	5880.0	3.810	9.476	5.112
40	1520.0	12.009	10.204	0.000	96	3680.0	5.447	13.614	7.148	152	5920.0	3.754	9.355	5.028
41	1560.0	11.997	10.170	0.000	97	3720.0	5.435	13.565	7.138	153	5960.0	3.680	9.200	4.920
42	1600.0	11.985	10.135	0.000	98	3760.0	5.423	13.513	7.127	154	6000.0	3.588	9.012	4.791
43	1640.0	11.972	10.100	0.000	99	3800.0	5.411	13.457	7.116	155	6040.0	3.513	8.825	4.669
44	1680.0	11.958	10.066	0.000	100	3840.0	5.398	13.398	7.103	156	6080.0	3.454	8.639	4.555
45	1720.0	11.942	10.031	0.000	101	3880.0	5.383	13.338	7.091	157	6120.0	3.413	8.454	4.471
46	1760.0	11.924	9.996	0.000	102	3920.0	5.367	13.277	7.078	158	6160.0	3.389	8.271	4.417
47	1800.0	11.903	9.962	0.000	103	3960.0	5.349	13.217	7.064	159	6200.0	3.382	8.088	4.391
48	1840.0	11.880	9.929	0.000	104	4000.0	5.328	13.158	7.050	160	6240.0	3.376	7.937	4.407
49	1880.0	11.854	9.898	0.000	105	4040.0	5.305	13.101	7.036	161	6270.0	3.372	7.824	4.462
50	1920.0	11.826	9.867	0.000	106	4080.0	5.281	13.047	7.022	162	6300.0	3.368	7.741	4.514
51	1960.0	11.796	9.838	0.000	107	4120.0	5.255	12.995	7.007	163	6320.0	3.365	7.696	4.563
52	2000.0	11.764	9.809	0.000	108	4160.0	5.227	12.946	6.993	164	6340.0	3.363	7.682	4.609
53	2040.0	11.731	9.779	0.000	109	4200.0	5.199	12.900	6.978	165	6350.0	3.361	7.675	4.632
54	2080.0	11.695	9.749	0.000	110	4240.0	5.170	12.857	6.964	166	6360.0	3.360	7.668	4.635
55	2120.0	11.658	9.716	0.000	111	4280.0	5.142	12.818	6.949	167	6361.0	2.169	4.702	2.581
56	2160.0	11.617	9.681	0.000	112	4320.0	5.113	12.781	6.934	168	6371.0	2.168	4.698	2.582

general, much better signal-to-noise ratio than the corresponding spectral stacks. Outside that range spectral stacking gives more reliable results.

Using our models of the Earth and the source, and the techniques of stacking and stripping, we were able to identify and measure eigenfrequencies of some 500 multiplets in a period range from 83 to 540 s and overtone range from 0 to 4 for toroidal modes and from 0 to 30 for the spheroidal modes (Dziewonski & Gilbert 1973*a*).

We have selected the most reliable data from the data set above and the sets published in Alaska I and II to form a set of 506 normal modes plus the Earth's mass and moment of inertia. This set of data was inverted, with model C 196 (Alaska II) as a starting model, to yield model 508 (Gilbert & Dziewsonski 1973, and table 3).

Figure 4 shows, for the first four toroidal overtones, the relative differences between the measured eigenperiods and those predicted by the model UTD124A′ (Alaska I). The continuous line represents the corresponding relative differences for the eigenperiods predicted by model 508.

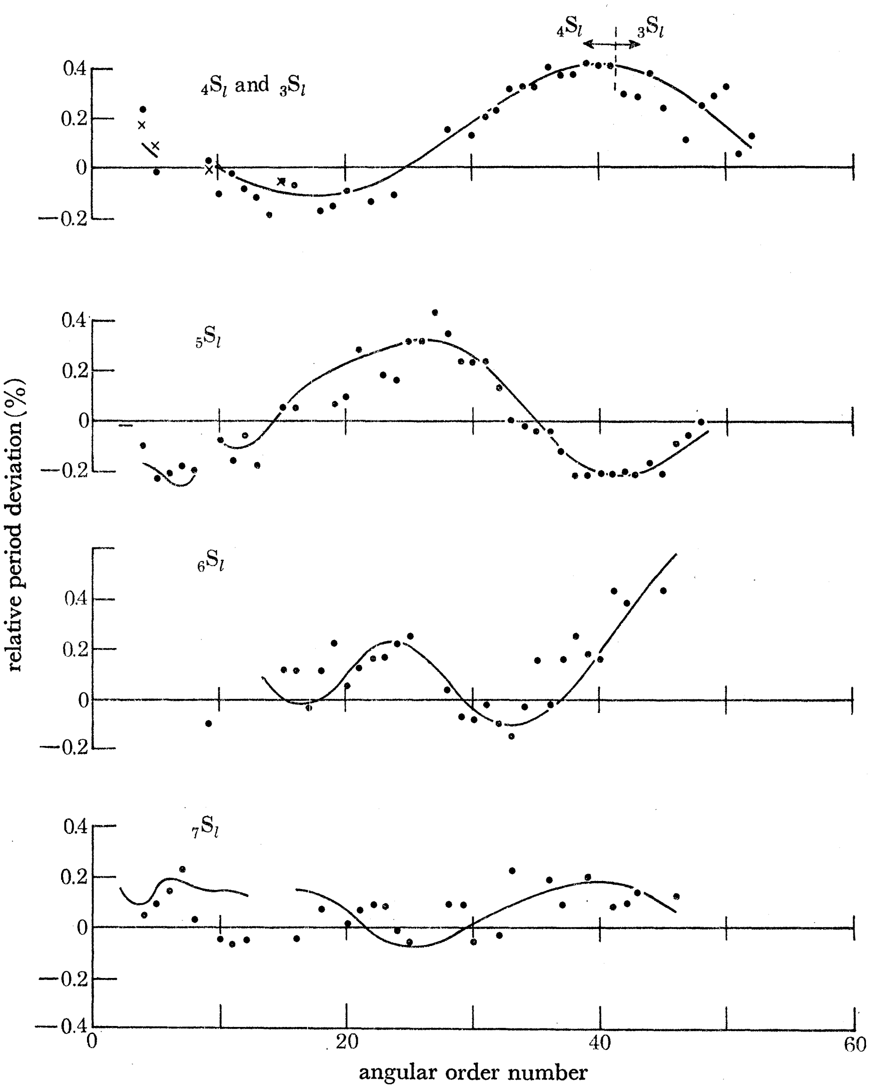

FIGURE 5. Relative deviations of the observed eigenperiods of the spheroidal overtones $_4S_l(_3S_l)$–$_7S_l$ from the periods computed for the model UTD124A′ are shown as dots. The solid line represents relative differences between theoretical eigenperiods for the models 508 and UTD124A′.

The same comparison is made in figure 5 for spheroidal overtones from the fourth (third) to seventh; ${}_4S_l$ enters the Stoneley branch for $l > 40$, and the properties of the mantle modes ${}_3S_l$ for $l > 40$ are continuous with those of ${}_4S_l$ for $l \leqslant 40$. The gaps in the solid lines correspond to those ranges of l, where ${}_nS_l$ are the inner core modes (Alaska II). For these modes (none of which has been observed) the differences between periods predicted by model 508 and UTD124A′ exceed the scale of the figure.

It is clear that model 508 satisfies the data much better than model UTD124A′ and it should represent a satisfactory model for retrieving the moment spectrum.

Our data derived from the spectra of the Colombian earthquake agree very closely, in nearly all cases, with those derived by Mendiguren (1973) for the same event. Some discrepancies may result from differences in selection of seismograms as well as digitization intervals. Perhaps differences in data processing techniques are more significant. Mendiguren performed summation in the epicentral coordinate system by rotating the observed spectra and he computed separate stacks for each component. We have computed a 'common' stack (2.2.14) in the standard coordinate system by rotating the theoretical spectra. This allows us to consider recordings from stations where only one horizontal component was available or of satisfactory quality.

Mendiguren performed stacking by using $\operatorname{sgn} a_{pj}$ rather than $\bar{a}_{pj}$ in (2.2.14). Also, if $|a_j|$ represents the average amplitude of the jth multiplet, he replaced $\bar{a}_{pj}$ by zero if $|\bar{a}_{pj}| < 0.5\,|a_j|$.

The principal reason why we were able to identify approximately twice as many modes as reported by Mendiguren is that he did not attempt to identify modes with radial order numbers greater than three for toroidal modes and greater than six for spheroidal modes. However, there are groups of modes, for example:

$$ {}_2T_l\,(43 \leqslant l \leqslant 58), \quad {}_3T_l\,(31 \leqslant l \leqslant 59), $$
$$ {}_4S_l\,(5 \leqslant l \leqslant 24), \quad {}_5S_l\,(4 \leqslant l \leqslant 23), $$

that were clearly identifiable in our stacks but were not reported by Mendiguren.

If the data of Mendiguren were included in figures 4 and 5 they would show smaller scatter for some ranges of l. It may be that the approach chosen by Mendiguren is preferable for well excited modes, while we seem to be more successful in recovering modes that were excited less strongly.

3.3. *The moment spectrum of two deep earthquakes*

The 165 spectra of the Colombian earthquake (table 1, §3.2) and the theoretical and computational methods of §§2.1–2.3 are used to retrieve the spectrum of the moment rate tensor. Model 508 (§3.2) was used to calculate the functions $A_k(\boldsymbol{r})$ and the eigenfrequencies ω_k.

Equations (2.3.19) and (2.3.11) represent a symmetric system of normal equations of order 6. Our stacking procedure and summation over multiplets is really a least-squares estimation procedure where the 'expected value' of $\boldsymbol{f}$ is (2.3.11). To the expected value, the solution (2.3.11), we can assign a variance in the usual way. In (2.3.16) let us write

$$ y_{pk} = \beta_k^{-1} I[U_{pk}(\omega)] = \boldsymbol{A}_{pk}\cdot\boldsymbol{f}g_k. \tag{1} $$

For (2.3.9) we have

$$ \boldsymbol{w}_k = \sum_p \boldsymbol{A}^T_{pk} g_k y_{pk}, \tag{2} $$

from which follows (2.3.10)

$$ \sum_{t=1}^{6} F_{st} f_t = h_s, \tag{3} $$

$$ \boldsymbol{h} = \sum_k \boldsymbol{w}_k. \tag{4} $$

If there are P seismic spectra and K multiplets and if $\boldsymbol{f}$, $\boldsymbol{h}$, $\boldsymbol{y}$ stand for either real or imaginary values then the unbiased estimate of the variance is

$$\sigma_t^2 = \frac{F_{tt}^{-1}}{PK-6}\left[\sum_{pk} y_{pk}^2 - \sum_s h_s f_s\right] \quad (t = 1, \ldots, 6) \tag{5}$$

(Kenney & Keeping 1951, ch. 10).

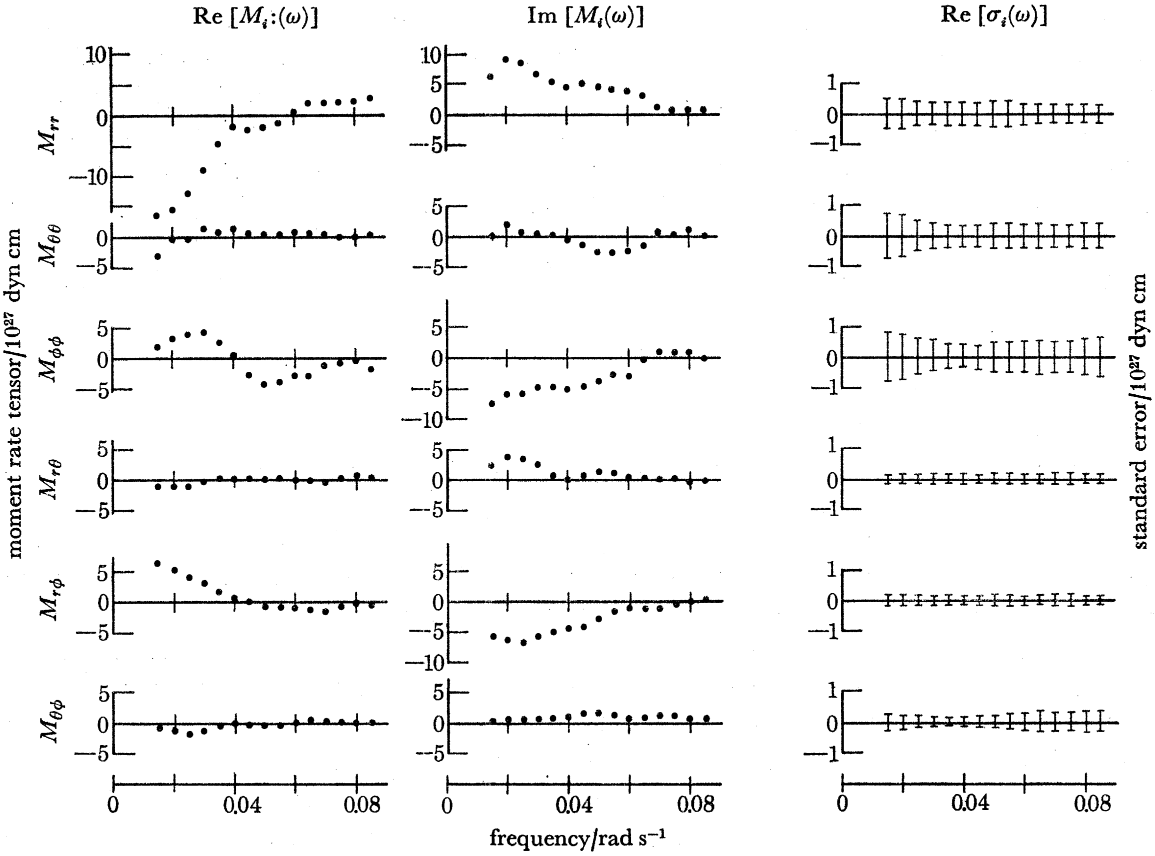

FIGURE 6. Spectrum of the moment rate tensor of the Colombian earthquake of 1970 July 31. Dots represent average values of the moment rate tensor determined for frequency intervals specified in the text. The error bars indicate estimates of standard errors of our solutions for the real component of the spectrum; the corresponding values for the imaginary component are approximately equal. Note that the error scale is expanded by a factor of five in comparison to that used in representing the spectra.

In figure 6 we present the spectra of the moment rate tensor of the Colombian earthquake. The frequency bands are of equal width, $0.005\,\mathrm{s}^{-1}$, and the centre frequencies are $0.005\mathrm{J}\,\mathrm{s}^{-1}$, $\mathrm{J} = 3(1)17$.

We used 1348 multiplets to retrieve the spectra in figure 6. The maximum angular order was $l = 30$ for ${}_0\mathrm{T}_l$ and $l = 40$ otherwise. That is, all horizontal wavelengths less than 1000 km were rejected.

There are two differences between figure 1 of Dziewonski & Gilbert (1974) and our figure 6. First, we have changed to the more prevalent convention in computing Fourier transforms. We use $\exp(-\mathrm{i}\omega t)$ as the time $\rightarrow$ frequency kernel. Second, in figure 6 we present the spectra without separating the moment rate tensor into its isotropic and deviatoric parts.

The scale for errors in figure 6 is expanded five times over that for the moment rate tensor itself. The real and imaginary parts appear to be approximately equally accurate.

If the moment tensor was a step function in time, the spectrum of the moment rate tensor would have a constant real part and a zero imaginary part. Figure 6 shows that not to be the case. The immediate conclusion is that stress release occurred over a finite period of time. This matter is discussed in §4.3.

The standard errors of the off-diagonal components of the tensor are approximately three times less than those of the diagonal elements. This suggests that, for the Colombian earthquake, the observed overall excitation pattern is roughly three times more sensitive to perturbations of the shear elements $M_{r\theta}$, $M_{r\phi}$ and $M_{\theta\phi}$ than the diagonal elements M_{rr}, $M_{\theta\theta}$ and $M_{\phi\phi}$. It is easy to see, therefore, why it might be possible to approximate the observed excitation with a tensor for which $T_R M = 0$. However, the isotropic part of the tensor is statistically significant. For a frequency of $0.015\,\mathrm{s}^{-1}$ (approximate period of 400 s) we find that $1/3\,\mathrm{Re}\,(f_1+f_2+f_3) = -6.0 \times 10^{27}$ dyn cm with a standard error of 6.9×10^{26} dyn cm, thus the inferred value of the isotropic part of the tensor is nearly nine times greater than the standard error. The probability that this would occur by chance alone is less than 10^{-17}.

The relative errors increase with frequency. This is, most likely, the result of increasing contamination of the integral $I[U_{pk}(\omega)]$ by the interference of other modes. Two factors are involved: (i) the number of possible modes per unit frequency interval is roughly proportional to frequency; (ii) the width of the integration interval is also proportional to frequency: $\mathrm{w} = N\omega_k/2Q_k$. The effect of the first factor is offset by the increase in frequency of the number of modes per fixed frequency interval (in (5) K is approximately proportional to J, the index of the frequency band being considered), but the net result is such that the relative errors can be expected to increase with frequency. This means that for a given set of observed spectra there will be an upper frequency limit beyond which the results lose their statistical significance. For the example shown in figure 6 this limit appears to correspond to a period of 80 seconds. It is possible to think of ways to circumvent this problem; for example by using in (2) only those modes that yield good 'stacks' for the moment tensor derived from the low frequency part of the spectra.

Figure 7 shows the results obtained from the analysis of 46 spectra of recordings of the Peru–Bolivia earthquake. The variations of the tensor spectrum are very similar in general character to those derived for the Colombian earthquake but the corresponding values are less by, roughly, a factor of three. The relative errors are larger, because we have fewer recordings with shorter digitization intervals.

An erroneous attenuation model and representing a finite dimensional source as a point in space must be considered the primary causes of possible systematic errors.

The estimates of Q_k are used to correct the observed spectra for phase distortions due to truncation (2.3.13) and to determine the integration interval (2.3.6). They are also used to evaluate the weighting factors.

For a given set of estimates of Q_k the left hand side in (3) is constant, except for the factor β_k. If the errors in the estimates of Q_k were to lead to systematic errors, the solutions of (3) should show statistically significant differences for different values of the parameter $N = \mathrm{w}/\alpha_k$, as the values h_s in (3) would change other than proportional to β_k. Thus, comparison of the results obtained by using different values of N may be used as a test for systematic bias due to an erroneous attenuation model. We have found that the results for $N = 2$ and $N = 4$ do not differ significantly from those for $N = 3$ that are shown in figures 6 and 7. Finally, we have increased the estimates of

Q_k for all the modes by 20 %; the resulting changes in the eigenvalues of the moment rate tensor were less than 5 % and the changes in their eigenvectors were even less significant.

The favourable outcome of the tests described above does not mean that a refinement of the attenuation model is not desirable. Better knowledge of the attenuation parameters, in addition to being of great interest from the standpoint of the physics of the Earth's interior, could result in a further reduction of errors in estimates of the source properties.

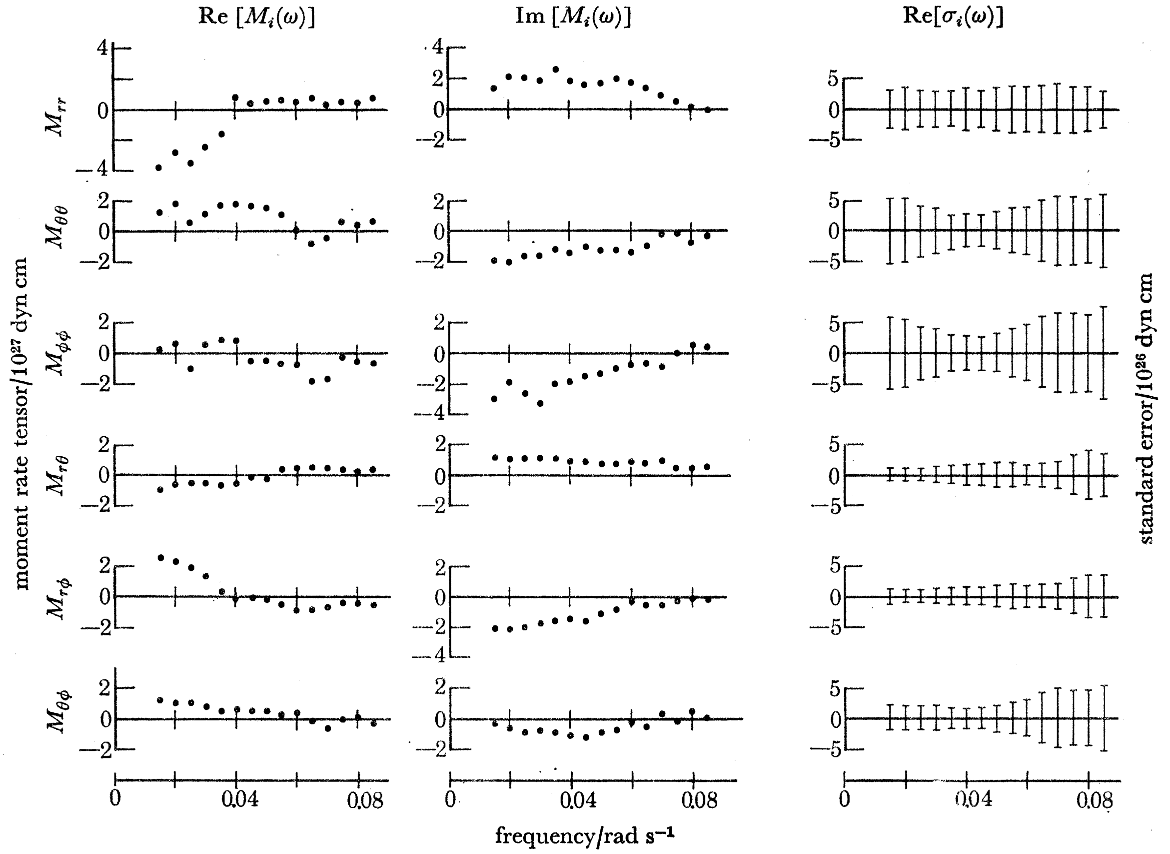

FIGURE 7. Spectrum of the moment rate tensor of the Peru–Bolivia border earthquake of 1963 August 15. For details see the caption to figure 6. The error scale is expanded by a factor of four.

The effect of finite dimensions of the source was tested by limiting the range of wavelengths of the modes used to evaluate expressions (2) and (2.3.10); that is, we have used only modes with an angular order number $l \leqslant l_{max}$. Computations were repeated for $l_{max} = 20$, 40 and 60 and the results obtained for the latter two were nearly identical, which means that solutions do not deteriorate within the considered range of wavelengths. Solutions for $l_{max} = 20$ had large errors at high frequencies, because only modes with very high phase velocities ($C_{ph} > 20\,km\,s^{-1}$ for periods less than 100 s) could be considered and these modes are not, in general, as strongly excited as those with phase velocities less than 10 km/s.

The test described above represents also a test for the effect of lateral heterogeneities, as the multiplet width can be expected to increase with increasing l (Luh 1974). The effect of lateral heterogeneities is, for a particular frequency range, the largest for the fundamental modes, because their energy is concentrated in the inhomogeneous upper mantle. Thus, in order to test further the effect of lateral heterogeneities we have obtained a solution based only on excitation of overtones ($n > 0$; $l \leqslant 40$). The results do not differ significantly from those shown in figures 6 and 7 but the errors are somewhat larger.

3.4. *Improved resolution of multiplets*

The 165 spectra of the Colombian earthquake (table 1, §3.1), the 46 spectra of the Peru–Bolivian earthquake (table 2, §3.1) and the source mechanisms shown in figures 6 and 7 have been used to apply the theoretical and computational methods of §§2.1 and 2.2. The spectra of the source mechanisms are represented as continuous functions of frequency *via* Fourier series. Those parameters that depend on Earth structure in §§2.1 and 2.2 have been computed for model 508 (Gilbert & Dziewonski (1973) and table 3).

There are two major points to be emphasized. Both are illustrated in figures 8 and 9. The first point is that the source mechanism derived by us in §3.2 for the Colombian earthquake gives better stripping results than the double-couple (3.2.1). The second point is that by combining data from different earthquakes we can improve the resolution of multiplets.

In the stripping process (2.2.7) adjacent multiplet stacks are recombined to enhance the multiplet being sought and to suppress the others. It is essential to have a good source mechanism not only to enhance one multiplet but also to suppress others, particularly those that are nearly coincident in frequency. For the multiplet ${}_2T_5$ in figure 8 stripping with the double-couple is a failure but stripping with the source mechanism in figure 6 is a success. Results for the well-resolved multiplet ${}_0S_{15}$ are also slightly improved. In general, figures 8 and 9 demonstrate that improvement is realized by using the better source mechanism in figure 6.

The results presented in the lower third of figures 8 and 9 were derived from the 211 spectra of the two earthquakes whose source mechanisms are shown in figures 6 and 7. We have already seen how a global network of seismographs can be used to resolve many normal mode multiplets. It is very suggestive, from the results presented in figures 8 and 9, that an array of sources could be used to improve the resolution of multiplets and to increase further the number of gross Earth data.

The final outcome of resolving multiplets is that we have obtained more than 1000 normal mode eigenfrequencies. More than 200 of inferior quality have been culled, leaving 812 eigenfrequencies. Typical results for ${}_nT_l$ ($n \leqslant 7$) are shown in figure 10. It is a relatively simple matter to select the centre frequency of a multiplet. It is more difficult to assign an error to the observation, especially for broad multiplets. Typical results for ${}_nS_l$ ($n \leqslant 30$) are shown in figures 11–13. Clearly, some of the multiplets are quite narrow (e.g. ${}_5S_6$, ${}_{13}S_2$) indicating little splitting, high Q or both.

In table 4 we present 812 normal mode eigenperiods whose multiplets have been resolved. We have tried to overcome the difficulty in assigning errors to the observations by using a few qualitative factors. From the discussion given in Alaska II (p. 433) we have chosen the minimum assigned error to be 0.05 %. To be assigned the minimum error a multiplet must have low noise, good symmetry or be very narrow. Poorly resolved multiplets, such as ${}_2S_l$, $l > 47$, were assigned the maximum error of 0.20 %. This *a priori* assignment of errors is subjective and open to criticism. The errors have the same order of magnitude as those in Alaska I and II and they appear to be reasonable, but a more realistic assignment can be made only after the data have been inverted to find improved models (§§4.1 and 4.2).

Although we continue to use the diagonal sum rule (Gilbert 1971*b*), in a statistical sense, to interpret the eigenperiods in table 4 as gross Earth data (degenerate multiplet periods) we

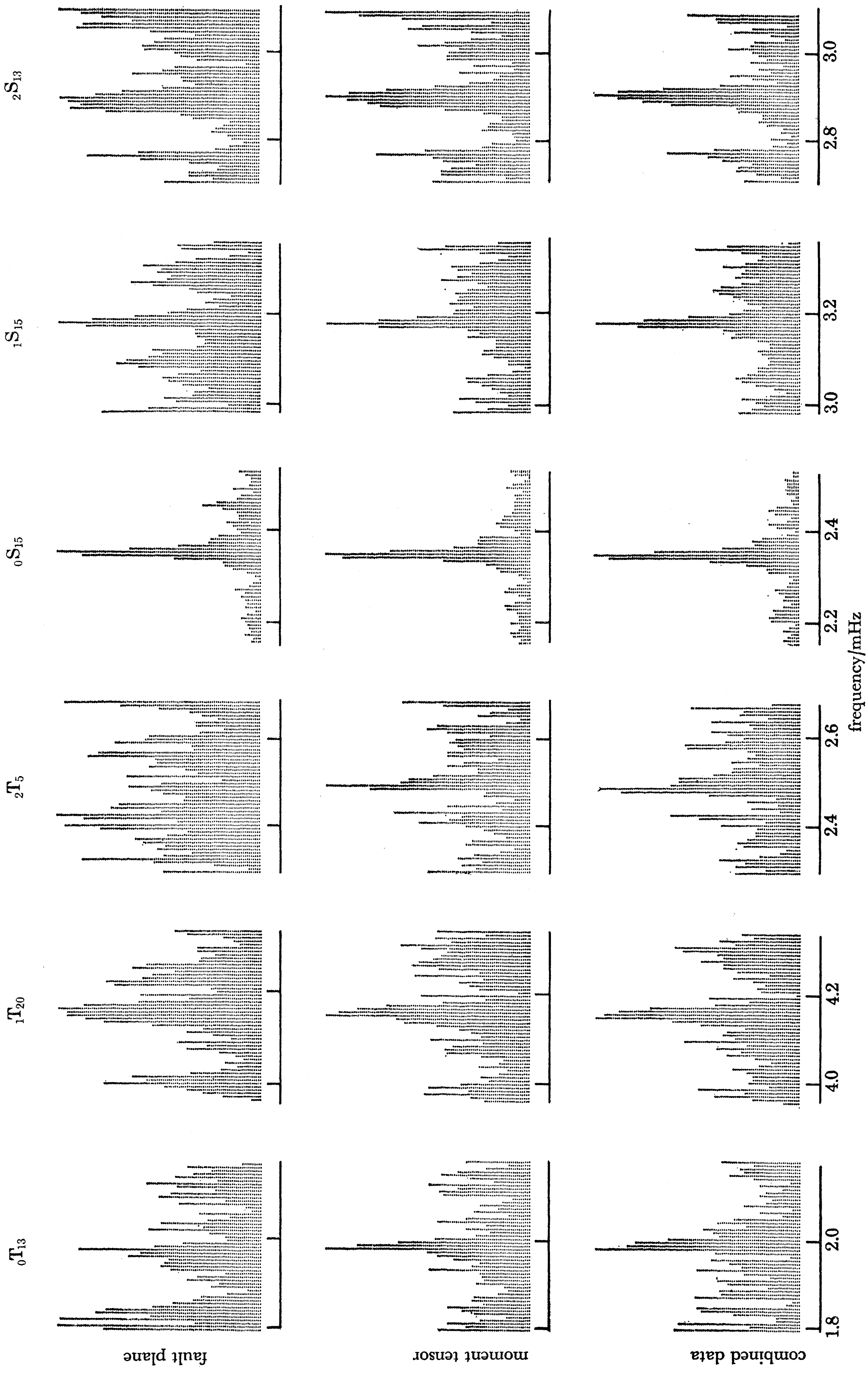

FIGURE 8. Comparison of the 'stripped stacks' obtained by using different source mechanisms and different sets of observed spectra; *top*, results obtained from processing 165 spectra of the Colombian earthquake by using the nodal plane solution of Mendiguren (1973); *middle*, results obtained from processing the same set of data with the interpolated spectrum of the moment rate tensor shown in figure 6; *bottom*, results obtained from the combined data set of 165 spectra of the Colombian earthquake and 46 spectra of the Peru–Bolivian earthquake and the interpolated spectra of the moment rate tensor shown in figures 6 and 7.

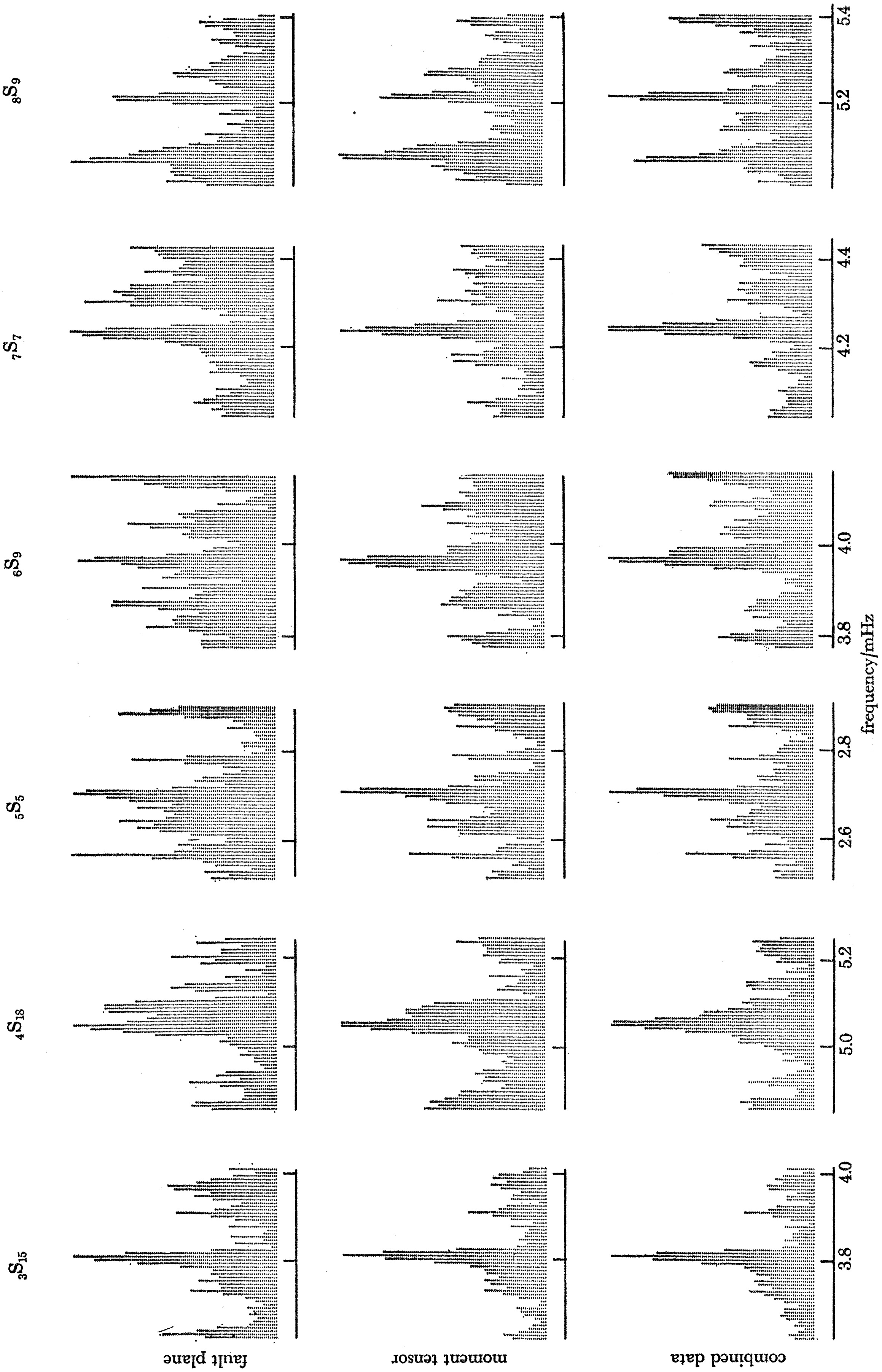

FIGURE 9. Results for higher spheroidal overtones described in the caption of figure 8 from the same procedure.

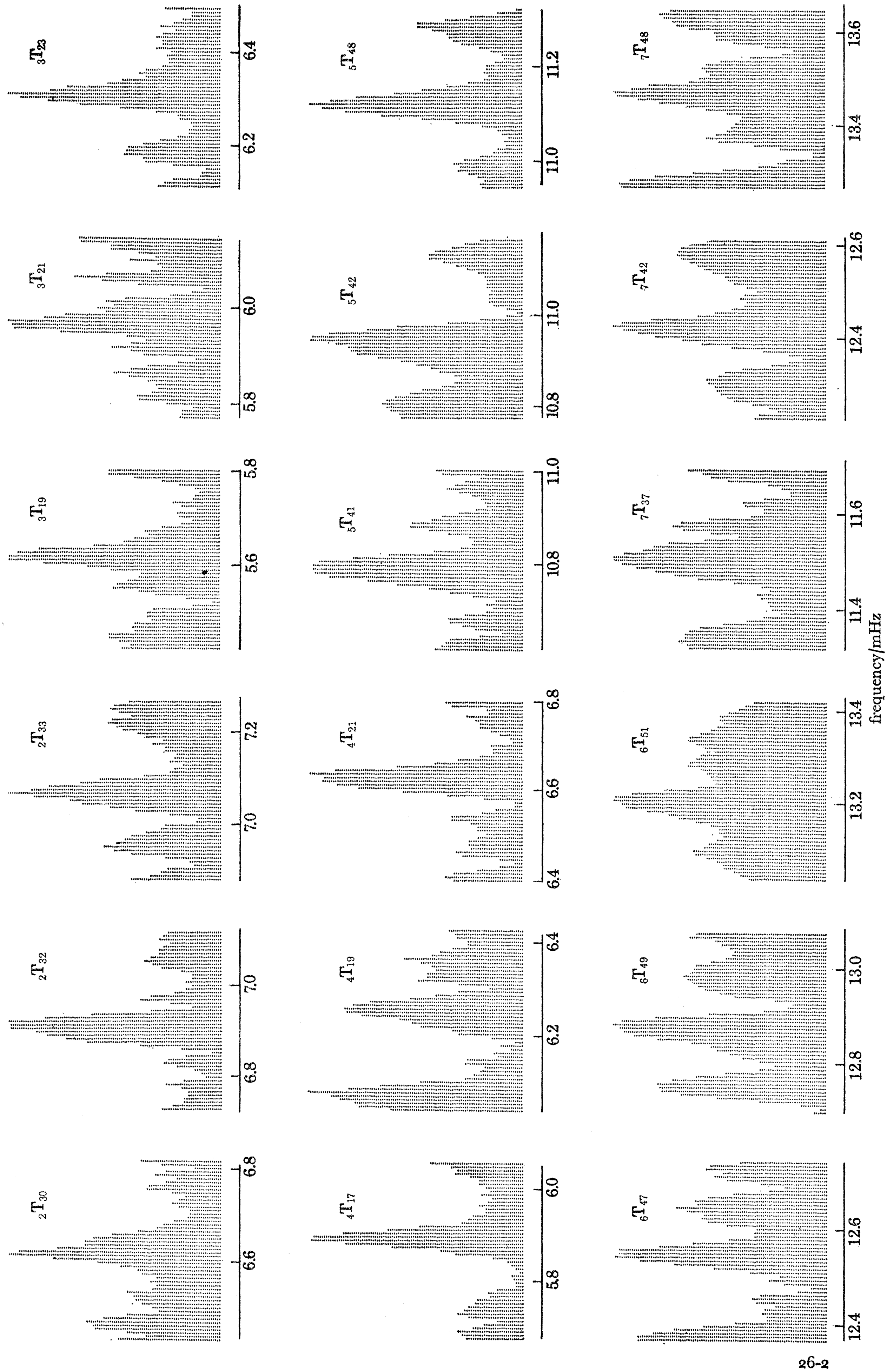

FIGURE 10. Examples of 'stacked' or 'stripped' spectra for toroidal overtones ($2 \leqslant n \leqslant 7$) obtained from processing 211 spectra of the combined dataset.

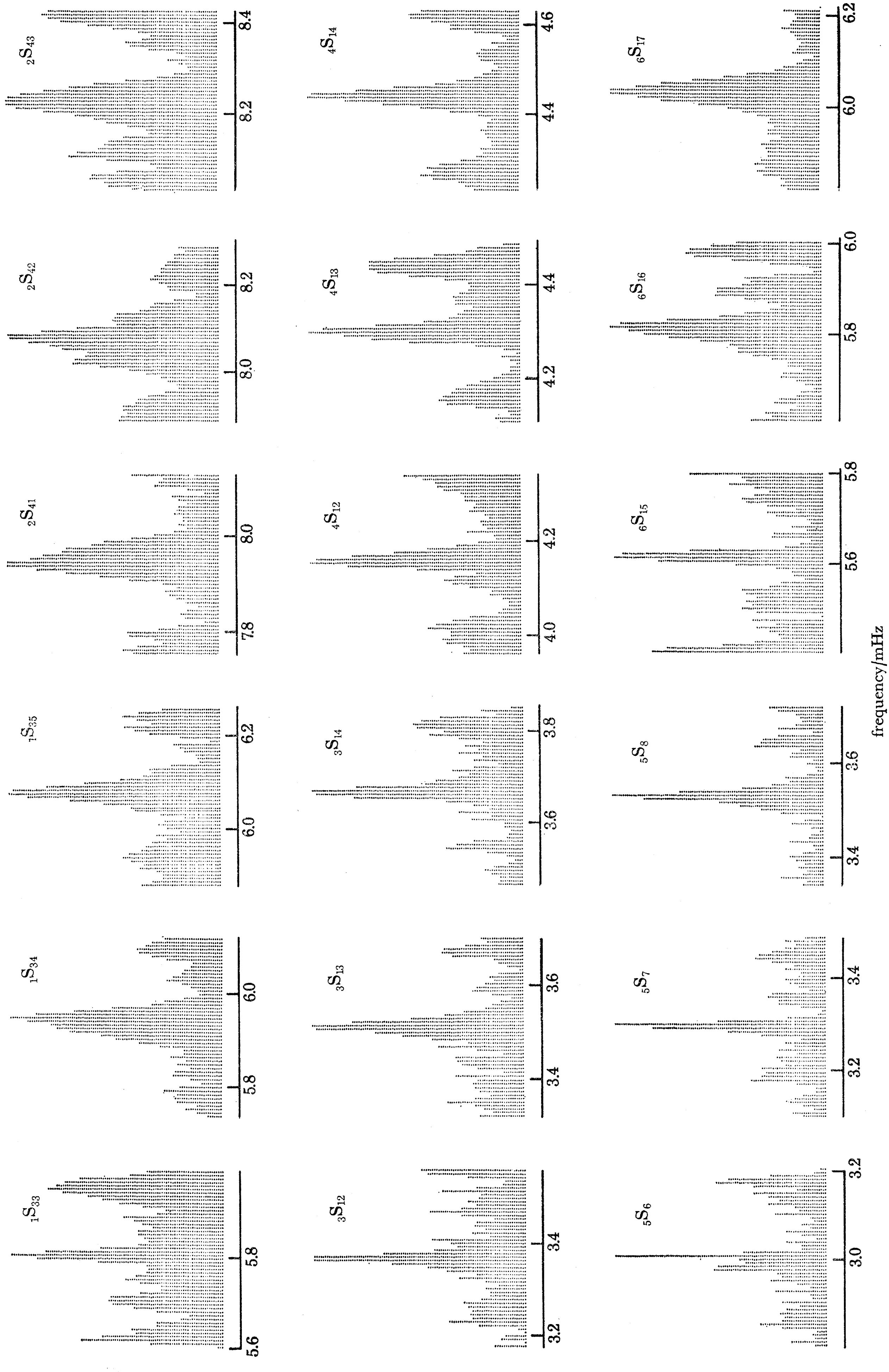

FIGURE 11. Examples of 'stacked' or 'stripped' spectra for spheroidal overtones ($1 \leqslant n \leqslant 6$).

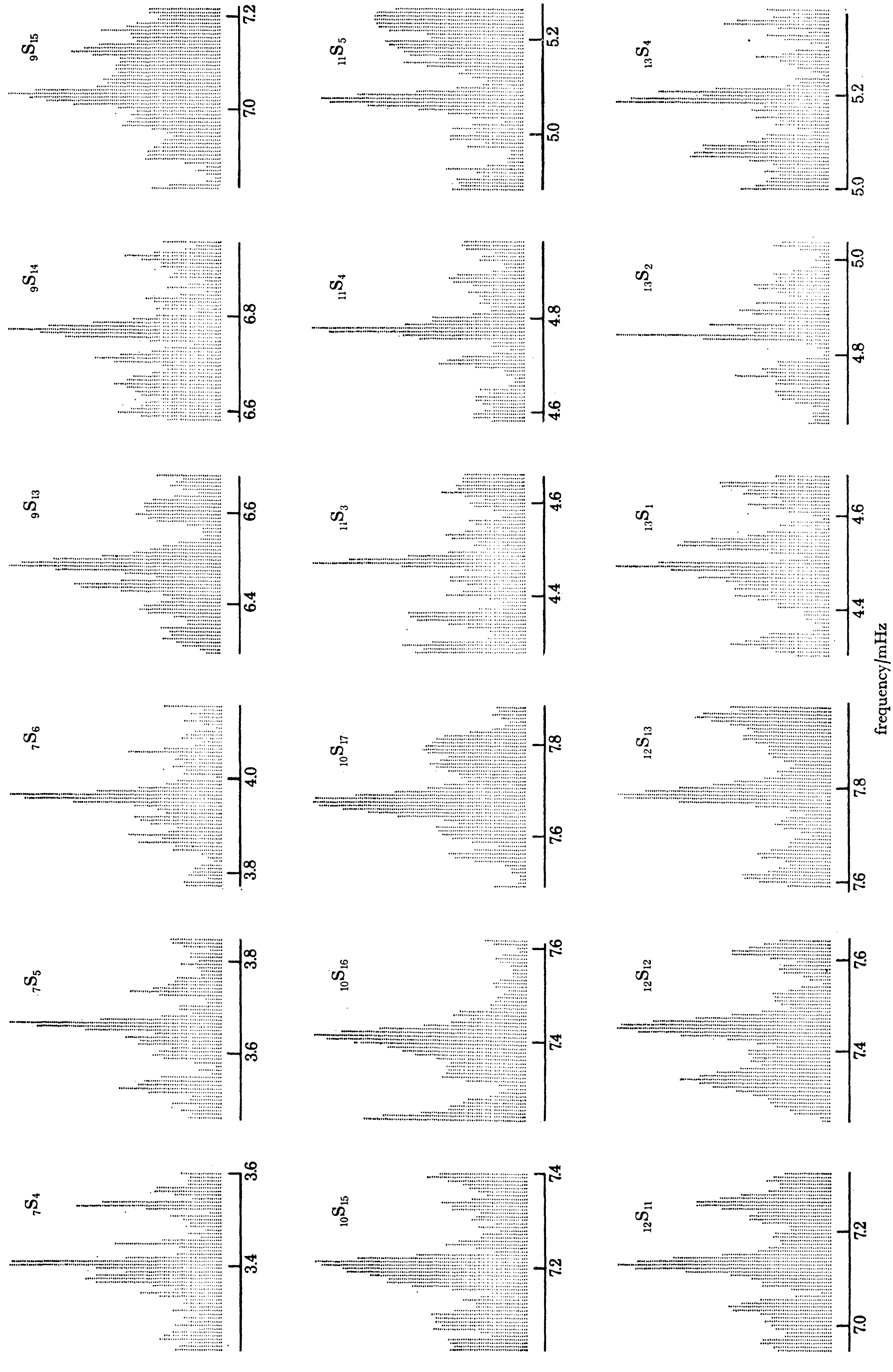

FIGURE 12. Examples of 'stacked' or 'stripped' spectra for spheroidal overtones ($7 \leqslant n \leqslant 13$).

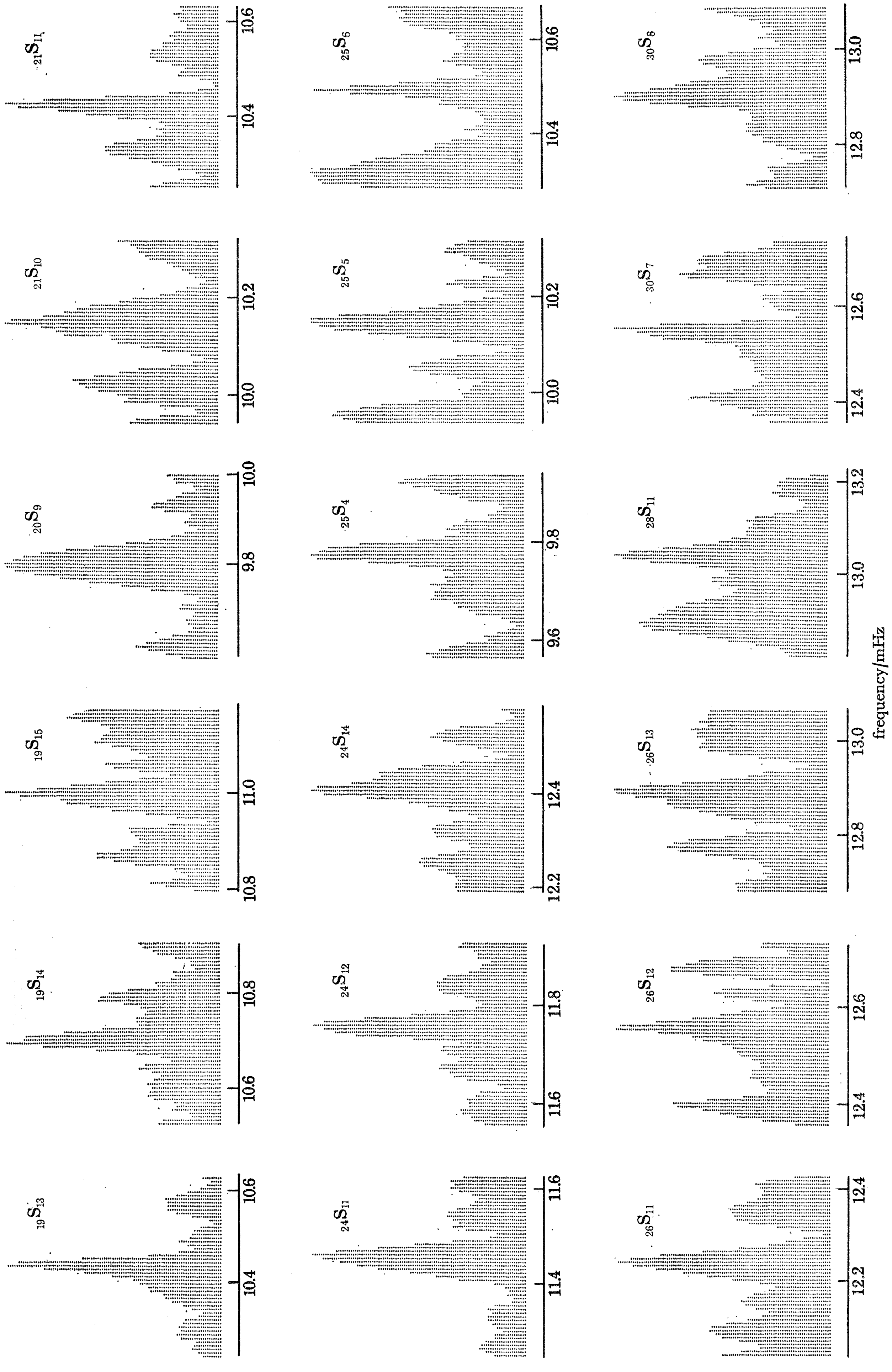

FIGURE 13. Examples of 'stacked' or 'stripped' spectra for spheroidal overtones ($19 \leqslant n \leqslant 30$).

TABLE 4. EIGENPERIODS AND RELATIVE ERRORS OF THE NORMAL MODES OBTAINED FROM PROCESSING THE COMBINED DATA SET OF 211 OBSERVED SPECTRA

mode	period (s)	error (%)	mode	period (s)	error (%)	mode	period (s)	error (%)
2 S 0	398.30	0.05	1 T 31	176.61	0.05	2 T 45	113.57	0.05
3 S 0	305.38	0.05	1 T 32	172.96	0.05	2 T 47	110.22	0.05
4 S 0	243.67	0.05	1 T 33	169.27	0.05	2 T 49	106.98	0.05
6 S 0	174.25	0.05	1 T 34	165.48	0.05	2 T 51	104.01	0.05
10 S 0	110.68	0.20	1 T 35	162.31	0.05	2 T 52	102.60	0.05
11 S 0	101.30	0.07	1 T 36	159.08	0.05	2 T 54	99.93	0.05
12 S 0	93.54	0.07	1 T 37	156.08	0.05	2 T 55	98.61	0.05
			1 T 38	153.11	0.05	2 T 56	97.40	0.05
0 T 12	539.19	0.10	1 T 39	150.28	0.05	2 T 58	95.08	0.05
0 T 13	506.18	0.10	1 T 40	147.58	0.05	2 T 61	91.85	0.05
0 T 14	478.03	0.10	1 T 41	144.99	0.05			
0 T 15	451.83	0.10	1 T 42	142.53	0.05	3 T 9	259.26	0.07
0 T 16	430.44	0.10	1 T 43	140.20	0.05	3 T 11	240.50	0.07
0 T 17	410.24	0.10	1 T 44	138.03	0.05	3 T 18	184.09	0.07
0 T 18	392.23	0.10	1 T 46	133.63	0.05	3 T 19	178.17	0.07
0 T 19	375.29	0.10	1 T 47	131.52	0.05	3 T 20	172.74	0.05
0 T 20	360.52	0.10	1 T 48	129.56	0.05	3 T 21	167.69	0.05
0 T 21	346.07	0.10	1 T 49	127.79	0.05	3 T 23	158.54	0.05
0 T 22	333.15	0.10	1 T 50	125.92	0.10	3 T 24	154.61	0.05
0 T 23	321.87	0.10	1 T 51	124.19	0.10	3 T 25	150.65	0.05
0 T 24	310.40	0.10	1 T 52	122.26	0.10	3 T 26	147.15	0.05
0 T 25	300.43	0.10	1 T 54	118.96	0.10	3 T 27	143.67	0.05
0 T 26	290.82	0.10	1 T 57	114.41	0.10	3 T 28	140.41	0.05
0 T 27	281.35	0.10	1 T 58	112.92	0.10	3 T 29	137.24	0.05
0 T 28	272.91	0.10	1 T 59	111.40	0.10	3 T 30	134.23	0.05
0 T 29	264.90	0.10	1 T 60	110.24	0.10	3 T 31	131.37	0.05
0 T 30	258.05	0.10	1 T 62	107.44	0.10	3 T 32	128.68	0.05
0 T 31	250.29	0.10	1 T 64	104.94	0.10	3 T 33	126.16	0.05
0 T 32	244.26	0.10	1 T 66	102.59	0.10	3 T 34	123.75	0.05
0 T 33	237.37	0.10				3 T 37	116.89	0.05
0 T 34	232.06	0.10	2 T 2	447.30	0.07	3 T 38	114.66	0.05
0 T 36	220.70	0.10	2 T 4	419.38	0.07	3 T 41	108.87	0.05
			2 T 5	401.82	0.07	3 T 42	107.04	0.05
1 T 6	519.74	0.10	2 T 17	219.95	0.05	3 T 46	100.56	0.05
1 T 7	475.39	0.07	2 T 18	211.90	0.05	3 T 47	99.08	0.05
1 T 8	438.86	0.07	2 T 19	204.63	0.05	3 T 51	93.67	0.07
1 T 9	407.73	0.07	2 T 21	191.91	0.05	3 T 53	91.15	0.07
1 T 11	359.14	0.05	2 T 22	186.19	0.05	3 T 54	89.90	0.07
1 T 12	339.54	0.05	2 T 25	170.90	0.05	3 T 56	87.67	0.07
1 T 13	322.12	0.05	2 T 26	166.50	0.05	3 T 57	86.41	0.07
1 T 14	307.02	0.05	2 T 27	162.34	0.05	3 T 58	85.33	0.07
1 T 15	293.33	0.05	2 T 28	158.43	0.05	3 T 59	84.35	0.07
1 T 16	280.59	0.05	2 T 29	154.70	0.05	3 T 61	82.44	0.07
1 T 17	269.68	0.05	2 T 31	147.71	0.05	3 T 62	81.44	0.07
1 T 18	258.97	0.05	2 T 32	144.59	0.05	3 T 65	78.69	0.07
1 T 19	249.61	0.05	2 T 33	141.54	0.05	3 T 68	76.19	0.07
1 T 20	240.82	0.05	2 T 34	138.62	0.05	3 T 69	75.42	0.07
1 T 22	225.24	0.05	2 T 35	135.73	0.05	3 T 72	73.16	0.07
1 T 23	218.25	0.05	2 T 36	133.14	0.05	3 T 73	72.36	0.07
1 T 24	211.87	0.05	2 T 37	130.51	0.05			
1 T 25	205.74	0.05	2 T 38	128.13	0.05	4 T 7	216.81	0.15
1 T 26	200.21	0.05	2 T 39	125.71	0.05	4 T 11	199.74	0.15
1 T 27	194.71	0.05	2 T 40	123.56	0.05	4 T 14	184.86	0.15
1 T 28	189.82	0.05	2 T 41	121.30	0.05	4 T 16	174.72	0.15
1 T 29	185.19	0.05	2 T 42	119.31	0.05	4 T 17	169.68	0.15
1 T 30	180.80	0.05	2 T 44	115.49	0.05	4 T 18	164.71	0.15

TABLE 4 (*cont.*)

mode	period s	error (%)
4 T 19	160.11	0.15
4 T 20	155.64	0.15
4 T 21	151.15	0.15
4 T 22	147.47	0.15
4 T 23	143.67	0.15
4 T 25	136.30	0.15
4 T 27	130.03	0.15
4 T 40	101.27	0.07
4 T 41	99.71	0.07
4 T 45	93.79	0.07
4 T 46	92.29	0.07
4 T 47	91.11	0.07
4 T 48	89.82	0.07
4 T 50	87.46	0.07
4 T 54	82.95	0.07
4 T 63	74.72	0.07
4 T 64	73.79	0.07
4 T 65	72.94	0.07
4 T 66	72.28	0.07
5 T 9	174.33	0.07
5 T 10	171.89	0.07
5 T 15	157.57	0.07
5 T 38	97.11	0.07
5 T 40	94.12	0.07
5 T 41	92.65	0.07
5 T 42	91.34	0.07
5 T 43	89.97	0.07
5 T 44	88.64	0.07
5 T 45	87.47	0.07
5 T 46	86.26	0.07
5 T 47	85.08	0.07
5 T 48	83.75	0.07
5 T 50	81.60	0.07
5 T 51	80.55	0.07
5 T 52	79.52	0.07
5 T 55	76.52	0.07
5 T 56	75.67	0.07
5 T 57	74.75	0.07
6 T 34	97.13	0.07
6 T 35	95.46	0.07
6 T 37	92.29	0.07
6 T 41	86.70	0.07
6 T 42	85.35	0.07
6 T 43	84.30	0.07
6 T 44	83.13	0.07
6 T 45	81.85	0.07
5 T 47	79.71	0.07
6 T 49	77.65	0.07
6 T 51	75.75	0.07
6 T 53	73.89	0.07
7 T 17	118.57	0.10
7 T 19	115.58	0.10
7 T 28	101.15	0.10

mode	period s	error (%)
7 T 29	99.53	0.10
7 T 30	97.93	0.10
7 T 34	91.46	0.10
7 T 38	85.45	0.10
7 T 40	82.84	0.10
7 T 42	80.51	0.10
7 T 45	77.23	0.10
7 T 46	76.18	0.10
7 T 48	74.28	0.10
7 T 49	73.36	0.10
0 S 11	536.98	0.05
0 S 12	502.33	0.05
0 S 13	473.17	0.05
0 S 14	448.13	0.05
0 S 15	426.07	0.05
0 S 16	406.70	0.05
0 S 17	389.27	0.05
0 S 18	373.84	0.05
0 S 19	360.23	0.05
0 S 20	347.69	0.05
0 S 21	335.98	0.05
0 S 22	325.22	0.05
0 S 23	315.26	0.05
0 S 24	306.21	0.05
0 S 25	297.72	0.05
0 S 26	289.61	0.05
0 S 27	282.23	0.05
0 S 28	275.20	0.05
0 S 29	268.45	0.05
0 S 30	262.14	0.05
0 S 31	256.07	0.05
0 S 32	250.34	0.05
0 S 33	244.95	0.05
0 S 34	239.64	0.05
0 S 35	234.62	0.05
0 S 36	229.86	0.05
0 S 37	225.18	0.05
0 S 38	220.75	0.05
0 S 39	216.47	0.05
0 S 40	212.41	0.05
0 S 41	208.39	0.05
0 S 42	204.57	0.05
0 S 43	200.92	0.05
0 S 44	197.39	0.05
0 S 45	193.94	0.05
0 S 46	190.57	0.05
0 S 47	187.38	0.05
0 S 48	184.18	0.05
0 S 49	181.19	0.05
0 S 50	178.31	0.05
0 S 51	175.41	0.05
0 S 52	172.56	0.05
0 S 53	170.07	0.07
0 S 54	167.60	0.07
0 S 55	165.02	0.07
0 S 56	162.41	0.07

mode	period s	error (%)
0 S 57	160.24	0.07
0 S 58	157.69	0.07
0 S 59	155.58	0.07
0 S 60	153.39	0.07
0 S 61	151.19	0.07
0 S 62	149.21	0.07
0 S 63	147.12	0.07
0 S 64	144.96	0.07
0 S 65	142.99	0.07
0 S 66	141.22	0.07
1 S 8	556.03	0.07
1 S 16	299.50	0.07
1 S 17	286.22	0.07
1 S 19	263.63	0.07
1 S 20	253.97	0.07
1 S 21	244.93	0.07
1 S 22	236.21	0.07
1 S 23	228.42	0.07
1 S 24	220.99	0.07
1 S 25	214.44	0.07
1 S 26	207.71	0.07
1 S 27	201.70	0.07
1 S 28	196.31	0.07
1 S 29	190.77	0.07
1 S 30	185.94	0.07
1 S 32	176.71	0.10
1 S 33	172.34	0.10
1 S 34	168.30	0.10
1 S 35	164.60	0.10
1 S 36	161.43	0.10
1 S 37	157.67	0.10
1 S 38	154.69	0.07
1 S 39	151.64	0.07
1 S 40	148.61	0.07
1 S 41	145.71	0.07
1 S 42	143.17	0.07
1 S 43	140.61	0.07
1 S 44	138.25	0.07
1 S 47	131.50	0.10
1 S 48	129.18	0.10
1 S 49	127.14	0.10
1 S 50	125.30	0.10
1 S 52	121.68	0.10
1 S 53	119.86	0.10
1 S 54	118.50	0.10
1 S 55	116.81	0.10
1 S 56	115.32	0.10
1 S 58	112.25	0.10
1 S 59	110.91	0.10
1 S 61	108.06	0.10
1 S 63	105.69	0.10
1 S 64	104.41	0.10
1 S 68	99.71	0.10
1 S 75	92.48	0.10
2 S 7	535.70	0.10

TABLE 4 (*cont.*)

mode	period s	error (%)
2 S 8	488.51	0.10
2 S 9	447.71	0.10
2 S 10	415.23	0.10
2 S 11	387.92	0.10
2 S 12	364.52	0.10
2 S 13	344.72	0.07
2 S 14	326.59	0.07
2 S 26	179.24	0.05
2 S 27	174.03	0.05
2 S 28	169.33	0.05
2 S 29	164.87	0.05
2 S 30	160.51	0.05
2 S 31	156.55	0.05
2 S 33	149.32	0.05
2 S 34	145.95	0.05
2 S 35	142.64	0.05
2 S 36	139.66	0.05
2 S 37	136.68	0.05
2 S 38	133.90	0.05
2 S 39	131.08	0.05
2 S 40	128.61	0.05
2 S 42	123.84	0.05
2 S 43	121.65	0.05
2 S 44	119.49	0.05
2 S 45	117.34	0.05
2 S 46	115.33	0.05
2 S 48	111.87	0.20
2 S 49	110.07	0.20
2 S 50	108.37	0.20
2 S 51	106.71	0.20
2 S 57	98.04	0.20
2 S 58	96.61	0.20
2 S 59	95.29	0.20
2 S 60	94.14	0.20
2 S 62	91.76	0.20
2 S 63	90.59	0.20
2 S 64	89.66	0.20
2 S 65	88.65	0.20
2 S 66	87.66	0.22
2 S 67	86.51	0.20
2 S 71	82.97	0.20
2 S 72	82.02	0.20
2 S 74	80.53	0.20
2 S 76	78.89	0.20
3 S 6	392.36	0.06
3 S 7	371.79	0.06
3 S 8	354.34	0.06
3 S 9	338.90	0.06
3 S 10	323.86	0.06
3 S 11	310.27	0.06
3 S 12	297.41	0.06
3 S 13	285.08	0.06
3 S 14	273.30	0.06
3 S 15	262.44	0.06
3 S 16	252.40	0.06
3 S 17	242.62	0.06
3 S 18	233.21	0.06
3 S 19	225.07	0.06
3 S 20	217.04	0.06
3 S 21	209.72	0.06
3 S 22	202.77	0.06
3 S 23	196.28	0.06
3 S 24	190.06	0.06
3 S 25	184.32	0.06
3 S 41	113.31	0.06
3 S 42	111.36	0.06
3 S 43	109.38	0.06
3 S 44	107.75	0.06
3 S 45	106.02	0.06
3 S 47	102.44	0.06
3 S 48	101.00	0.06
3 S 50	97.97	0.06
3 S 51	96.41	0.06
3 S 53	93.73	0.06
3 S 54	92.39	0.06
3 S 57	88.72	0.10
3 S 63	82.38	0.10
3 S 67	78.76	0.10
3 S 70	76.11	0.10
3 S 73	73.78	0.10
3 S 75	72.12	0.10
4 S 4	439.35	0.10
4 S 5	414.62	0.05
4 S 9	269.59	0.05
4 S 10	258.64	0.05
4 S 11	249.38	0.05
4 S 12	240.78	0.05
4 S 13	232.75	0.05
4 S 14	225.08	0.05
4 S 15	218.20	0.05
4 S 16	211.24	0.05
4 S 17	204.66	0.05
4 S 18	198.16	0.05
4 S 19	191.96	0.05
4 S 20	186.33	0.05
4 S 24	165.68	0.05
4 S 30	141.97	0.05
4 S 31	138.72	0.05
4 S 32	135.65	0.05
4 S 33	132.70	0.05
4 S 34	129.81	0.05
4 S 35	127.12	0.05
4 S 36	124.66	0.05
4 S 37	122.19	0.05
4 S 38	119.89	0.05
4 S 39	117.68	0.05
4 S 40	115.41	0.05
4 S 62	77.77	0.10
4 S 63	76.65	0.10
5 S 3	461.80	0.10
5 S 4	420.36	0.05
5 S 5	370.10	0.05
5 S 6	331.83	0.05
5 S 7	303.56	0.05
5 S 8	283.20	0.05
5 S 10	237.81	0.05
5 S 11	224.49	0.05
5 S 12	213.02	0.05
5 S 13	203.10	0.05
5 S 15	187.51	0.05
5 S 16	181.74	0.05
5 S 19	166.78	0.05
5 S 20	162.45	0.05
5 S 21	158.47	0.05
5 S 23	150.57	0.05
5 S 24	146.92	0.05
5 S 25	143.60	0.05
5 S 26	140.23	0.05
5 S 28	134.09	0.05
5 S 29	131.17	0.05
5 S 30	128.51	0.05
5 S 31	125.92	0.05
5 S 32	123.38	0.05
5 S 33	121.02	0.05
5 S 34	118.74	0.05
5 S 35	116.66	0.05
5 S 36	114.60	0.05
5 S 37	112.57	0.05
5 S 38	110.56	0.05
5 S 39	108.65	0.05
5 S 40	106.83	0.05
5 S 41	105.07	0.05
5 S 42	103.37	0.05
5 S 43	101.67	0.05
5 S 44	100.10	0.05
5 S 45	98.45	0.05
5 S 46	96.98	0.05
5 S 47	95.51	0.05
5 S 51	89.91	0.05
6 S 9	252.63	0.07
6 S 15	178.76	0.07
6 S 16	172.01	0.07
6 S 17	166.02	0.07
6 S 18	160.39	0.07
6 S 19	155.23	0.07
6 S 20	150.17	0.05
6 S 21	145.73	0.05
6 S 22	141.82	0.05
6 S 23	138.13	0.05
6 S 24	134.85	0.05
6 S 25	131.82	0.05
6 S 26	128.85	0.05
6 S 27	125.98	0.05
6 S 28	123.48	0.05
6 S 29	120.97	0.05
6 S 30	118.75	0.07
6 S 31	116.40	0.07

TABLE 4 (*cont.*)

mode	period s	error (%)
6 S 32	114.10	0.07
6 S 33	112.06	0.07
6 S 34	109.90	0.07
6 S 35	107.96	0.07
6 S 36	106.06	0.07
6 S 37	104.18	0.07
6 S 38	102.38	0.07
6 S 39	100.68	0.07
6 S 40	98.97	0.07
6 S 41	97.47	0.07
6 S 42	95.80	0.07
6 S 43	94.32	0.07
6 S 47	89.02	0.07
6 S 48	87.62	0.07
6 S 49	86.41	0.07
6 S 51	84.07	0.07
6 S 52	82.99	0.07
6 S 53	81.93	0.07
6 S 54	81.05	0.07
6 S 55	79.95	0.07
6 S 56	78.92	0.07
6 S 57	77.97	0.07
6 S 58	77.11	0.07
6 S 59	76.20	0.07
6 S 60	75.33	0.07
6 S 61	74.46	0.07
7 S 4	293.37	0.10
7 S 5	273.27	0.10
7 S 6	252.71	0.10
7 S 7	236.12	0.10
7 S 8	224.36	0.10
7 S 9	216.62	0.10
7 S 10	209.42	0.10
7 S 11	203.09	0.10
7 S 12	197.12	0.10
7 S 16	154.52	0.07
7 S 18	147.82	0.07
7 S 20	141.23	0.07
7 S 21	138.06	0.07
7 S 22	134.81	0.07
7 S 23	131.81	0.07
7 S 24	128.57	0.07
7 S 25	125.48	0.07
7 S 27	119.96	0.07
7 S 28	117.21	0.07
7 S 29	114.65	0.07
7 S 30	112.16	0.07
7 S 33	105.75	0.07
7 S 35	101.74	0.07
7 S 36	99.98	0.07
7 S 37	98.19	0.07
7 S 38	96.51	0.07
7 S 39	94.89	0.07
7 S 41	91.72	0.07
7 S 42	90.30	0.07
7 S 43	88.99	0.07

mode	period s	error (%)
7 S 45	86.37	0.07
7 S 46	85.13	0.07
7 S 47	84.09	0.07
7 S 48	82.76	0.07
7 S 50	80.42	0.07
7 S 52	78.34	0.07
7 S 55	75.53	0.07
7 S 56	74.59	0.07
7 S 57	73.68	0.07
8 S 1	348.12	0.07
8 S 6	225.12	0.07
8 S 9	191.89	0.07
8 S 15	158.50	0.07
8 S 23	120.87	0.07
8 S 24	118.67	0.07
8 S 29	108.08	0.07
8 S 30	106.04	0.07
8 S 32	102.20	0.07
8 S 38	91.81	0.07
8 S 41	87.28	0.07
8 S 46	80.79	0.07
8 S 47	79.78	0.07
8 S 48	78.57	0.07
8 S 51	75.51	0.07
8 S 52	74.60	0.07
9 S 2	310.04	0.07
9 S 3	281.42	0.07
9 S 4	258.10	0.07
9 S 6	216.26	0.07
9 S 7	205.01	0.07
9 S 8	194.22	0.07
9 S 10	178.72	0.07
9 S 11	170.05	0.07
9 S 12	161.63	0.07
9 S 13	154.30	0.07
9 S 14	147.95	0.07
9 S 15	142.19	0.07
9 S 16	137.91	0.07
9 S 18	132.47	0.07
9 S 19	129.87	0.07
9 S 23	110.56	0.07
9 S 29	100.32	0.07
9 S 35	91.16	0.07
9 S 37	88.49	0.07
9 S 38	87.07	0.07
10 S 13	145.46	0.07
10 S 14	142.06	0.05
10 S 15	138.77	0.05
10 S 16	135.01	0.10
10 S 17	130.40	0.10
10 S 18	126.12	0.10
10 S 19	121.95	0.05
10 S 20	118.35	0.05

mode	period s	error (%)
10 S 21	115.20	0.05
10 S 25	101.73	0.07
10 S 26	99.63	0.07
10 S 28	95.58	0.07
10 S 29	93.90	0.07
10 S 31	91.14	0.07
10 S 32	89.78	0.07
10 S 34	87.21	0.07
10 S 36	84.86	0.07
10 S 37	83.58	0.07
10 S 41	79.18	0.07
10 S 42	78.04	0.07
10 S 44	76.05	0.07
11 S 1	271.36	0.07
11 S 3	224.01	0.07
11 S 4	209.45	0.07
11 S 5	197.19	0.07
11 S 6	186.73	0.10
11 S 7	179.70	0.10
11 S 8	163.26	0.10
11 S 9	155.56	0.07
11 S 13	134.99	0.07
11 S 15	126.44	0.07
11 S 16	123.22	0.07
11 S 17	120.89	0.07
11 S 21	112.16	0.07
11 S 22	109.66	0.07
11 S 23	107.15	0.07
11 S 24	104.43	0.07
11 S 31	87.29	0.07
11 S 32	85.78	0.07
11 S 33	84.11	0.07
11 S 34	82.87	0.07
11 S 35	81.45	0.07
11 S 37	79.15	0.07
11 S 39	77.24	0.07
11 S 40	76.21	0.07
11 S 41	75.21	0.07
11 S 43	73.39	0.07
11 S 44	72.53	0.07
11 S 46	70.68	0.07
11 S 47	69.99	0.07
12 S 7	170.65	0.05
12 S 10	145.67	0.05
12 S 11	140.33	0.05
12 S 12	134.25	0.05
12 S 13	128.70	0.05
12 S 14	123.50	0.05
12 S 16	115.07	0.07
12 S 17	111.79	0.07
12 S 18	109.39	0.07
12 S 22	102.08	0.07
12 S 23	100.48	0.07
12 S 26	95.80	0.07
12 S 33	81.43	0.07

TABLE 4 (*cont.*)

mode	period s	error (%)
13 S 1	222.69	0.07
13 S 2	206.78	0.07
13 S 3	192.92	0.07
13 S 5	170.74	0.10
13 S 8	152.39	0.10
13 S 12	125.76	0.10
13 S 13	123.21	0.10
13 S 14	120.96	0.10
13 S 17	110.11	0.10
13 S 18	106.77	0.10
13 S 19	103.36	0.10
13 S 21	97.65	0.10
13 S 22	95.32	0.10
13 S 23	93.62	0.10
13 S 25	90.52	0.10
13 S 26	89.31	0.10
13 S 27	88.02	0.10
13 S 29	85.94	0.10
13 S 37	73.52	0.10
13 S 38	72.74	0.10
14 S 4	180.81	0.10
14 S 8	142.13	0.10
14 S 9	136.22	0.10
14 S 10	131.27	0.10
14 S 17	104.97	0.07
14 S 19	99.97	0.07
14 S 23	91.18	0.07
14 S 25	87.15	0.07
14 S 28	82.07	0.07
14 S 31	78.89	0.07
15 S 11	122.85	0.07
15 S 12	118.60	0.07
15 S 14	107.15	0.07
15 S 15	103.97	0.07
15 S 16	100.57	0.07
15 S 18	96.03	0.07
15 S 20	92.69	0.07
15 S 21	91.13	0.07
15 S 24	85.73	0.07
15 S 28	80.39	0.07
15 S 30	77.63	0.07
15 S 31	76.21	0.07
15 S 32	74.83	0.07
16 S 2	175.20	0.10
16 S 5	146.60	0.07
16 S 7	133.90	0.07
16 S 9	123.05	0.07
16 S 10	118.53	0.07
16 S 18	94.00	0.07
16 S 19	91.18	0.07
16 S 20	88.61	0.07
16 S 25	80.23	0.07
16 S 26	78.81	0.07
16 S 31	73.61	0.07
16 S 33	71.86	0.07
17 S 12	109.11	0.07
17 S 13	105.93	0.07
17 S 14	102.96	0.07
17 S 15	100.48	0.07
17 S 18	88.85	0.07
17 S 22	83.54	0.07
17 S 23	81.61	0.07
17 S 24	79.76	0.07
17 S 26	76.47	0.07
17 S 27	75.01	0.07
17 S 28	73.56	0.07
17 S 29	72.26	0.07
17 S 30	71.11	0.07
17 S 31	69.98	0.07
18 S 15	95.68	0.07
18 S 16	93.28	0.07
18 S 17	90.84	0.07
18 S 25	76.19	0.07
18 S 27	73.62	0.07
18 S 28	72.37	0.07
19 S 9	110.78	0.12
19 S 10	106.84	0.07
19 S 11	103.63	0.07
19 S 13	95.86	0.07
19 S 14	93.36	0.07
19 S 15	90.91	0.07
19 S 22	75.93	0.07
20 S 9	102.09	0.05
20 S 11	99.66	0.05
20 S 12	98.18	0.05
20 S 14	90.38	0.05
20 S 15	89.12	0.05
20 S 16	87.39	0.07
20 S 17	85.30	0.07
20 S 18	83.16	0.07
20 S 19	81.12	0.07
20 S 20	79.46	0.07
20 S 22	75.24	0.07
20 S 25	70.75	0.07
21 S 7	108.94	0.05
21 S 8	105.40	0.10
21 S 10	98.70	0.05
21 S 11	95.84	0.05
21 S 12	93.32	0.05
22 S 1	127.88	0.07
22 S 12	89.88	0.07
22 S 13	88.23	0.07
22 S 14	86.08	0.07
22 S 15	83.98	0.07
22 S 17	78.92	0.07
22 S 19	75.35	0.07
22 S 23	70.88	0.07
23 S 4	111.80	0.07
23 S 5	107.47	0.07
23 S 7	100.14	0.07
23 S 8	97.06	0.07
23 S 9	94.16	0.07
23 S 10	92.14	0.07
23 S 13	83.03	0.07
23 S 22	69.59	0.07
24 S 10	89.52	0.10
24 S 11	87.33	0.10
24 S 12	85.06	0.10
24 S 14	80.65	0.10
24 S 15	78.63	0.10
24 S 16	76.71	0.10
24 S 17	75.20	0.10
24 S 18	74.26	0.10
24 S 20	70.05	0.10
25 S 1	115.46	0.07
25 S 2	110.90	0.07
25 S 5	98.65	0.10
25 S 6	95.32	0.10
25 S 10	84.78	0.10
25 S 18	72.99	0.10
26 S 1	105.40	0.07
26 S 8	89.19	0.07
26 S 9	86.82	0.07
26 S 11	81.77	0.07
26 S 12	79.66	0.07
26 S 13	77.58	0.07
27 S 2	101.44	0.07
27 S 4	94.37	0.07
27 S 14	75.18	0.15
27 S 15	73.43	0.15
27 S 16	71.60	0.15
28 S 5	91.39	0.07
28 S 6	88.61	0.07
28 S 10	78.59	0.07
28 S 11	76.75	0.07
28 S 13	72.77	0.07
29 S 1	97.04	0.10
30 S 3	90.61	0.07
30 S 7	79.69	0.07
30 S 8	77.52	0.07
30 S 10	73.78	0.07
32 S 1	90.03	0.07
33 S 6	77.00	0.10
34 S 1	83.83	0.10

must still realize that we do not have a proper ensemble of sources and receivers. However, comparing eigenperiods common to table 4 and Alaska I and II we find that the differences are generally less than 0.1 %, except for ${}_0T_l$ where they average 0.3 %. Thus, it appears that our subjective *a priori* assignment of errors is realistic and that the data in table 4 can be regarded as gross Earth data.

4. Solutions of two geophysical inverse problems

We have a wealth of new gross Earth data with which we anticipate that more can be learned about the mechanical structure of the interior of the Earth. We use a set of 1463 data, of which 1066 are distinct, to derive models 1066A and 1066B in §4.1.

Although an analysis of the resolving power of the dataset is postponed to a later date, numerous traditional arguments are presented about the credibility of the two models. They are nearly identical in the fluid outer core and in the lower mantle below a depth of 950 km. There are only minor differences in the inner core, but there are (probably unresolvable) major differences in the upper mantle. These latter arise from the fact that model 1066A has a smooth, continuous upper mantle while model 1066B has a discontinuous one. The two models are equally good fits to the data and both show the need for baseline corrections to the travel times.

After tabulating a standard set of 1064 gross Earth data (eigenperiods) in §4.2 we discuss the temporal behaviour of the moment tensor in §4.3. For each of the two events studied in this report, there is a significant isotropic (compressive) component. It appears to be precursive by over 80 s. Both source mechanisms support an interpretation made by Isacks, Oliver & Sykes (1968) about focal mechanisms of deep earthquakes, and that interpretation is extended *intra* event.

4.1. *Properties of Earth models 1066A and 1066B*

In addition to the mass and moment of inertia (Jeffreys 1970) we have a very large number of observed eigenperiods.

Derr (1969) compiled a list of eigenperiods observed through 1968. We have chosen his values for ${}_0S_2$ and ${}_0S_3$. His other ${}_0S_l$ values have been averaged into table 2 (all data) of Alaska I.

Brune & Gilbert (1974) have presented 154 (actually 153) ${}_nT_l$ overtones derived from the phase spectra of SH pulses. The compatibility of their data for $n \geqslant 6$ with the data of Alaska I and II (Gilbert, Dziewonski & Brune 1973) has lent credibility to their unreported observations of $n = 4$ and 5 which we now have (J. N. Brune & F. Gilbert, personal communication). By combining redundant observations we have 159 ${}_nT_l$ data ($4 \leqslant n \leqslant 18$) from these authors.

Mendiguren (1973) has presented 240 eigenperiods from his study of the Colombian (1970 July 31) earthquake.

From Alaska I and II we have 248 modal data (${}_0S_3$ has been rejected) and in this report we have 812 modal data (table 4).

Neglecting travel times for the present we have 1463 gross Earth data (g.e.d.) of which 1066 are distinct. The minimum error assigned to a g.e.d. is 0.05 %. Many of the data are common to two or more of the studies listed previously but we have chosen not to select *a priori* a 'best value' or to average redundant observations. Instead, in solving the inverse problem, we have winnowed the dataset (Gilbert 1971 *c*).

Using the 'Dirichlet' criterion (Backus & Gilbert 1968; Sabatier 1974, pp. 50–58) and rejecting a datum with a relative variance greater than unity, we find that there are 222 significant

TABLE 5. PARAMETERS OF MODEL 1066A

level	radius km	depth km	ρ g cm^{-3}	V_p km s^{-1}	V_s km s^{-1}	ϕ km^2 s^{-2}	κ kbar	μ kbar	λ kbar	σ	pressure kbar	g cm s^{-2}
1	0.0	6371.0	13.421	11.338	3.630	110.99	14896	1768	13717	0.4429	3690.6	0.0
2	38.4	6332.6	13.418	11.337	3.630	110.97	14889	1767	13711	0.4429	3689.5	14.4
3	76.8	6294.2	13.411	11.335	3.629	110.91	14874	1766	13696	0.4429	3687.6	28.8
4	115.2	6255.8	13.406	11.330	3.629	110.81	14855	1765	13678	0.4429	3685.0	43.2
5	153.6	6217.4	13.399	11.324	3.628	110.67	14829	1763	13653	0.4428	3681.7	57.5
6	192.0	6179.0	13.393	11.315	3.627	110.50	14798	1761	13624	0.4428	3677.6	71.9
7	230.4	6140.6	13.385	11.306	3.626	110.29	14761	1759	13588	0.4427	3672.8	86.2
8	268.8	6102.2	13.377	11.294	3.624	110.04	14719	1757	13547	0.4426	3667.3	100.6
9	307.2	6063.8	13.368	11.281	3.623	109.76	14672	1754	13502	0.4425	3661.0	114.9
10	345.6	6025.4	13.357	11.267	3.621	109.46	14620	1751	13452	0.4424	3654.0	129.2
11	384.0	5987.0	13.345	11.251	3.619	109.13	14563	1747	13398	0.4423	3646.3	143.5
12	422.4	5948.6	13.331	11.235	3.616	108.79	14502	1743	13340	0.4422	3637.9	157.7
13	460.8	5910.2	13.316	11.218	3.614	108.43	14439	1738	13280	0.4421	3628.7	171.9
14	499.2	5871.8	13.300	11.201	3.611	108.08	14374	1734	13218	0.4420	3618.9	186.1
15	537.6	5833.4	13.284	11.184	3.608	107.73	14310	1728	13158	0.4420	3608.3	200.3
16	576.0	5795.0	13.267	11.167	3.604	107.39	14247	1723	13098	0.4419	3597.0	214.4
17	614.4	5756.6	13.251	11.151	3.600	107.06	14186	1717	13041	0.4418	3585.1	228.5
18	652.9	5718.1	13.235	11.135	3.596	106.74	14128	1711	12987	0.4418	3572.4	242.6
19	691.3	5679.7	13.220	11.120	3.592	106.45	14072	1705	12935	0.4418	3559.0	256.6
20	729.7	5641.3	13.205	11.106	3.588	106.18	14020	1699	12887	0.4418	3544.9	270.7
21	768.1	5602.9	13.190	11.092	3.583	105.93	13971	1693	12842	0.4418	3530.2	284.7
22	806.5	5564.5	13.175	11.080	3.578	105.69	13925	1686	12801	0.4418	3514.7	298.6
23	844.9	5526.1	13.160	11.068	3.572	105.48	13881	1679	12761	0.4419	3498.6	312.6
24	883.3	5487.7	13.145	11.056	3.567	105.28	13839	1672	12724	0.4419	3481.7	326.5
25	921.7	5449.3	13.131	11.045	3.561	105.09	13799	1665	12689	0.4420	3464.2	340.4
26	960.1	5410.9	13.116	11.035	3.555	104.92	13761	1657	12656	0.4421	3446.0	354.3
27	998.5	5372.5	13.102	11.025	3.549	104.75	13724	1650	12624	0.4422	3427.2	368.2
28	1036.9	5334.1	13.088	11.015	3.543	104.59	13689	1642	12594	0.4423	3407.6	382.0
29	1075.3	5295.7	13.074	11.005	3.536	104.44	13653	1635	12563	0.4424	3387.4	395.8
30	1113.7	5257.3	13.060	10.995	3.530	104.28	13618	1627	12533	0.4425	3366.6	409.6
31	1152.1	5218.9	13.045	10.986	3.524	104.13	13583	1619	12503	0.4427	3345.0	423.4
32	1190.5	5180.5	13.031	10.976	3.517	103.97	13548	1612	12473	0.4428	3322.8	437.2
33	1229.5	5141.5	13.021	10.969	3.512	103.87	13525	1605	12455	0.4429	3300.7	451.1
34	1229.5	5141.5	12.153	10.414	0.000	108.45	13180	0	13180	0.5000	3300.7	451.1
35	1299.4	5071.6	12.110	10.352	0.000	107.16	12976	0	12976	0.5000	3260.0	471.2
36	1369.8	5001.2	12.068	10.292	0.000	105.93	12783	0	12783	0.5000	3217.4	491.8
37	1440.3	4930.7	12.026	10.235	0.000	104.76	12597	0	12597	0.5000	3173.1	512.5
38	1510.7	4860.3	11.985	10.181	0.000	103.65	12421	0	12421	0.5000	3127.3	533.5
39	1581.2	4789.8	11.944	10.130	0.000	102.61	12255	0	12255	0.5000	3079.8	554.6
40	1651.7	4719.3	11.904	10.079	0.000	101.58	12091	0	12091	0.5000	3030.7	575.7
41	1722.1	4648.9	11.863	10.028	0.000	100.57	11930	0	11930	0.5000	2980.0	596.9
42	1792.6	4578.4	11.818	9.979	0.000	99.58	11768	0	11768	0.5000	2927.8	618.1
43	1863.0	4508.0	11.769	9.931	0.000	98.62	11606	0	11606	0.5000	2874.0	639.3
44	1933.5	4437.5	11.716	9.884	0.000	97.68	11444	0	11444	0.5000	2818.8	660.4
45	2003.9	4367.1	11.660	9.835	0.000	96.73	11279	0	11279	0.5000	2762.1	681.4
46	2074.4	4296.6	11.602	9.782	0.000	95.70	11102	0	11102	0.5000	2704.0	702.3
47	2144.9	4226.1	11.541	9.721	0.000	94.50	10905	0	10905	0.5000	2644.5	723.0
48	2215.3	4155.7	11.475	9.652	0.000	93.16	10690	0	10690	0.5000	2583.8	743.6
49	2285.8	4085.2	11.406	9.581	0.000	91.79	10468	0	10468	0.5000	2521.8	763.9
50	2356.2	4014.8	11.335	9.512	0.000	90.47	10254	0	10254	0.5000	2458.5	784.1
51	2426.7	3944.3	11.265	9.446	0.000	89.24	10052	0	10052	0.5000	2394.2	804.0
52	2497.2	3873.8	11.192	9.383	0.000	88.04	9853	0	9853	0.5000	2328.7	823.8
53	2567.6	3803.4	11.116	9.317	0.000	86.80	9648	0	9648	0.5000	2262.1	843.2
54	2638.1	3732.9	11.033	9.244	0.000	85.46	9428	0	9428	0.5000	2194.6	862.5
55	2708.5	3662.5	10.946	9.166	0.000	84.01	9195	0	9195	0.5000	2126.2	881.4
56	2779.0	3592.0	10.858	9.083	0.000	82.51	8958	0	8958	0.5000	2056.9	900.0
57	2849.5	3521.5	10.772	8.999	0.000	80.98	8722	0	8722	0.5000	1986.8	918.4

TABLE 5 (*cont.*)

level	radius km	depth km	ρ g cm^{-3}	V_p km s^{-1}	V_s km s^{-1}	ϕ km^2 s^{-2}	κ kbar	μ kbar	λ kbar	σ	pressure kbar	g cm s^{-2}
58	2919.9	3451.1	10.687	8.912	0.000	79.42	8487	0	8487	0.5000	1915.9	936.4
59	2990.4	3380.6	10.603	8.820	0.000	77.79	8248	0	8248	0.5000	1844.2	954.2
60	3060.8	3310.2	10.516	8.722	0.000	76.08	8000	0	8000	0.5000	1771.9	971.7
61	3131.3	3239.7	10.427	8.617	0.000	74.25	7742	0	7742	0.5000	1699.0	989.0
62	3201.8	3169.2	10.333	8.503	0.000	72.30	7471	0	7471	0.5000	1625.5	1005.9
63	3272.2	3098.8	10.235	8.318	0.000	70.24	7188	0	7188	0.5000	1551.5	1022.5
64	3342.7	3028.3	10.134	8.256	0.000	68.15	6906	0	6906	0.5000	1477.2	1038.7
65	3413.1	2957.9	10.028	8.132	0.000	66.13	6631	0	6631	0.5000	1402.6	1054.6
66	3484.3	2886.7	9.914	8.011	0.000	64.18	6362	0	6362	0.5000	1343.8	1070.2
67	3484.3	2886.7	5.528	13.717	7.250	118.08	6527	2905	4590	0.3062	1343.8	1070.2
68	3518.2	2852.8	5.518	13.713	7.238	118.21	6522	2890	4595	0.3069	1323.9	1065.2
69	3552.9	2818.1	5.506	13.709	7.224	118.35	6516	2873	4600	0.3078	1303.7	1060.4
70	3587.5	2783.5	5.495	13.681	7.210	117.85	6475	2856	4571	0.3077	1283.7	1055.8
71	3622.1	2748.9	5.483	13.652	7.196	117.32	6432	2839	4539	0.3076	1263.8	1051.5
72	3656.7	2714.3	5.471	13.625	7.183	116.85	6393	2823	4511	0.3075	1244.0	1047.4
73	3691.4	2679.6	5.460	13.592	7.170	116.19	6343	2806	4472	0.3072	1224.3	1043.6
74	3726.0	2645.0	5.447	13.556	7.157	115.48	6290	2790	4430	0.3068	1204.8	1040.0
75	3760.6	2610.4	5.434	13.517	7.144	114.64	6229	2773	4380	0.3062	1185.3	1036.5
76	3795.3	2575.7	5.421	13.473	7.132	113.69	6162	2757	4324	0.3053	1166.0	1033.3
77	3829.9	2541.1	5.406	13.425	7.120	112.64	6089	2740	4262	0.3043	1146.7	1030.3
78	3864.5	2506.5	5.391	13.374	7.107	111.52	6011	2723	4195	0.3032	1127.6	1027.4
79	3899.2	2471.8	5.374	13.322	7.095	110.34	5930	2705	4126	0.3020	1108.6	1024.8
80	3933.8	2437.2	5.357	13.268	7.083	109.14	5846	2687	4054	0.3007	1089.7	1022.2
81	3968.4	2402.6	5.338	13.214	7.071	107.95	5762	2669	3982	0.2994	1070.9	1019.9
82	4003.1	2367.9	5.318	13.162	7.059	106.79	5679	2650	3912	0.2981	1052.2	1017.6
83	4037.7	2333.3	5.298	13.111	7.047	105.69	5599	2630	3845	0.2969	1033.6	1015.5
84	4072.3	2298.7	5.277	13.063	7.035	104.66	5522	2611	3781	0.2958	1015.2	1013.5
85	4107.0	2264.0	5.255	13.017	7.022	103.71	5449	2591	3721	0.2948	996.8	1011.7
86	4141.6	2229.4	5.233	12.975	7.009	102.84	5382	2570	3668	0.2940	978.6	1009.9
87	4176.2	2194.8	5.212	12.935	6.995	102.07	5319	2549	3619	0.2934	960.4	1008.3
88	4210.8	2160.2	5.190	12.898	6.980	101.38	5261	2528	3575	0.2929	942.4	1006.7
89	4245.5	2125.5	5.169	12.864	6.965	100.79	5209	2507	3537	0.2926	924.4	1005.3
90	4280.1	2090.9	5.147	12.832	6.949	100.27	5161	2485	3504	0.2925	906.6	1003.9
91	4314.7	2056.3	5.127	12.802	6.933	99.81	5116	2464	3473	0.2925	888.8	1002.7
92	4349.4	2021.6	5.106	12.774	6.916	99.39	5074	2442	3446	0.2926	871.2	1001.5
93	4384.0	1987.0	5.086	12.746	6.899	99.00	5035	2420	3421	0.2928	853.6	1000.4
94	4418.6	1952.4	5.066	12.719	6.882	98.61	4995	2399	3395	0.2930	836.1	999.4
95	4453.3	1917.7	5.046	12.690	6.865	98.20	4955	2378	3369	0.2931	818.7	998.5
96	4487.9	1883.1	5.027	12.661	6.849	97.76	4913	2358	3341	0.2931	801.3	997.6
97	4522.5	1848.5	5.008	12.630	6.833	97.26	4870	2338	3311	0.2931	784.1	996.9
98	4557.2	1813.8	4.988	12.598	6.818	96.72	4824	2318	3278	0.2929	766.9	996.2
99	4591.8	1779.2	4.969	12.564	6.804	96.13	4776	2299	3243	0.2926	749.8	995.6
100	4626.4	1744.6	4.949	12.528	6.789	95.48	4725	2281	3204	0.2921	732.8	995.0
101	4661.1	1709.9	4.930	12.489	6.774	94.79	4673	2262	3165	0.2916	715.9	994.5
102	4695.7	1675.3	4.911	12.448	6.759	94.05	4618	2243	3122	0.2910	699.0	994.1
103	4730.3	1640.7	4.892	12.405	6.743	93.27	4562	2224	3079	0.2903	682.2	993.7
104	4764.9	1606.1	4.874	12.359	6.725	92.44	4505	2204	3035	0.2897	665.5	993.4
105	4799.6	1571.4	4.857	12.310	6.707	91.56	4447	2184	2991	0.2890	648.8	993.1
106	4834.2	1536.8	4.841	12.260	6.688	90.66	4388	2165	2944	0.2881	632.2	992.9
107	4868.8	1502.2	5.825	12.207	6.668	89.73	4329	2145	2899	0.2874	615.6	992.7
108	4903.5	1467.5	4.811	12.154	6.648	88.78	4270	2126	2852	0.2865	599.1	992.7
109	4938.1	1432.9	4.797	12.100	6.629	87.82	4212	2107	2807	0.2856	582.6	992.6
110	4972.7	1398.3	4.783	12.046	6.610	86.85	4154	2089	2761	0.2846	566.2	992.7
111	5007.4	1363.6	4.770	11.992	6.591	85.89	4096	2072	2714	0.2835	549.8	992.7
112	5042.0	1329.0	4.756	11.937	6.573	84.89	4037	2054	2667	0.2825	533.5	992.9
113	5076.6	1294.4	4.741	11.880	6.555	83.86	3975	2036	2617	0.2812	517.2	993.1
114	5111.3	1259.7	4.724	11.820	6.535	82.77	3909	2017	2564	0.2799	501.0	993.3

TABLE 5 (*cont.*)

level	radius km	depth km	ρ g cm^{-3}	V_p km s^{-1}	V_s km s^{-1}	ϕ km^2 s^{-2}	κ kbar	μ kbar	λ kbar	σ	pressure kbar	g cm s^{-2}
115	5145.9	1225.1	4.705	11.755	6.513	81.63	3840	1996	2509	0.2785	484.9	993.6
116	5180.5	1190.5	4.683	11.684	6.488	80.40	3765	1971	2451	0.2771	468.8	993.9
117	5215.2	1155.8	4.660	11.608	6.459	79.11	3686	1944	2390	0.2757	452.8	994.2
118	5249.8	1121.2	4.635	11.531	6.429	77.86	3608	1915	2331	0.2745	436.9	994.5
119	5284.4	1086.6	4.610	11.458	6.398	76.71	3536	1886	2278	0.2735	421.0	994.8
120	5319.1	1051.9	4.587	11.393	6.368	75.74	3473	1860	2233	0.2728	405.2	995.2
121	5353.7	1017.3	4.567	11.342	6.343	74.99	3424	1837	2199	0.2724	389.5	995.6
122	5388.3	982.7	4.552	11.309	6.324	74.57	3394	1820	2180	0.2725	373.8	996.0
123	5422.9	948.1	4.542	11.294	6.311	74.44	3381	1809	2175	0.2730	358.2	996.4
124	5457.6	913.4	4.537	11.291	6.304	74.51	3380	1802	2178	0.2736	342.5	996.9
125	5492.2	878.8	4.537	11.305	6.305	74.79	3393	1803	2191	0.2743	326.8	997.4
126	5526.8	844.2	4.535	11.312	6.302	75.01	3401	1801	2200	0.2749	311.2	998.1
127	5561.5	809.5	4.511	11.264	6.264	74.56	3363	1770	2183	0.2761	295.7	998.7
128	5596.1	774.9	4.468	11.163	6.195	73.46	3281	1714	2138	0.2775	280.3	999.3
129	5630.7	740.3	4.403	11.006	6.091	71.67	3155	1633	2066	0.2793	265.2	999.9
130	5665.4	705.6	4.319	10.796	5.955	69.26	2991	1531	1970	0.2813	250.4	1000.3
131	5700.0	671.0	4.208	10.514	5.776	66.08	2780	1403	1844	0.2840	235.8	1000.5
132	5700.0	671.0	4.208	10.514	5.776	66.08	2780	1403	1844	0.2840	235.8	1000.5
133	5731.2	639.7	4.106	10.251	5.608	63.15	2592	1291	1731	0.2864	223.1	1000.4
134	5762.5	608.5	4.025	10.040	5.475	60.84	2448	1206	1644	0.2884	210.7	1000.2
135	5793.8	577.2	3.961	9.865	5.365	58.93	2334	1140	1574	0.2900	198.4	999.8
136	5825.0	546.0	3.903	9.709	5.266	57.27	2235	1082	1513	0.2915	186.3	999.4
137	5856.2	514.7	3.850	9.568	5.176	55.82	2149	1031	1461	0.2931	174.3	998.8
138	5887.5	483.5	3.805	9.451	5.100	54.65	2079	989	1419	0.2946	162.5	998.2
139	5918.8	452.3	3.764	9.351	5.032	53.68	2020	953	1384	0.2961	150.9	997.6
140	5950.0	421.0	3.712	9.228	4.949	52.51	1949	909	1343	0.2982	139.3	996.9
141	5950.0	421.0	3.712	9.228	4.949	52.51	1949	909	1343	0.2982	139.3	996.9
142	5975.6	395.4	3.657	9.109	4.867	51.39	1879	866	1301	0.3002	130.1	996.2
143	6001.3	369.8	3.600	8.982	4.781	50.21	1807	822	1259	0.3025	120.9	995.5
144	6026.9	344.1	3.551	8.859	4.699	49.04	1741	784	1218	0.3042	111.9	994.7
145	6052.5	318.5	3.509	8.739	4.621	47.89	1680	749	1180	0.3059	103.1	993.8
146	6078.1	292.9	3.473	8.619	4.548	46.71	1622	718	1143	0.3071	94.3	992.9
147	6103.8	267.2	3.443	8.502	4.488	45.42	1563	693	1101	0.3069	85.5	992.0
148	6129.4	241.6	3.419	8.387	4.442	44.03	1505	674	1055	0.3051	76.9	991.1
149	6155.0	216.0	3.402	8.274	4.408	42.54	1447	661	1006	0.3017	68.3	990.1
150	6180.6	190.4	3.393	8.158	4.387	40.90	1387	653	951	0.2964	59.7	989.2
151	6206.3	164.7	3.387	8.054	4.379	39.29	1330	649	897	0.2901	51.1	988.3
152	6231.9	139.1	3.379	7.965	4.390	37.74	1275	651	841	0.2818	42.6	987.4
153	6257.5	113.5	3.372	7.873	4.433	35.79	1206	662	764	0.2679	34.1	986.6
154	6283.1	87.9	3.365	7.797	4.483	34.00	1144	676	693	0.2531	25.6	985.7
155	6308.8	62.2	3.358	7.739	4.539	32.42	1088	691	627	0.2379	17.1	984.9
156	6334.4	36.6	3.351	7.713	4.604	31.23	1046	710	572	0.2231	8.7	984.2
157	6360.0	11.0	3.343	7.705	4.649	30.55	1021	722	539	0.2137	1.7	983.4
158	6360.0	11.0	2.183	4.702	2.581	13.23	288	145	191	0.2842	1.7	983.4
159	6365.5	5.5	2.183	4.700	2.581	13.21	288	145	191	0.2842	0.5	982.7
160	6371.0	0.0	2.183	4.698	2.582	13.18	287	145	190	0.2836	0.0	982.0

Earth data (s.e.d.), while the 'smoothness' criterion (Gilbert, Dziewonski & Brune 1973) yields 57 s.e.d. In this report we use the smoothness criterion to obtain improved Earth models.

Two inversions have been performed with the set of 1463 g.e.d. The two initial models are model 508 (table 3) and model B1 (Jordan & Anderson 1974). They are shown in figure 14. The two final models are model 1066A derived from model 508, and model 1066B, derived from model B1. They are shown in figure 15. The parameters of model 1066A are given in table 5 and those of model 1066B in table 6.

In deriving model 1066A two calculations were made. In the first the smoothness criterion was applied throughout the mantle; discontinuities were not permitted to develop. In the second, discontinuities were permitted to develop at depths of 421 and 671 km. Discontinuities did develop but were less than 0.08 % in magnitude. Consequently the first calculation was chosen to yield model 1066 A.

Since model B1 has discontinuities in the upper mantle its perturbation was permitted to develop discontinuities.

The differences between the two initial models in figure 14 are not great. Both were derived to fit a large number of g.e.d. including, in the case of model B 1, differential travel times. The differences between the two final models are remarkably small. From the boundary of the inner

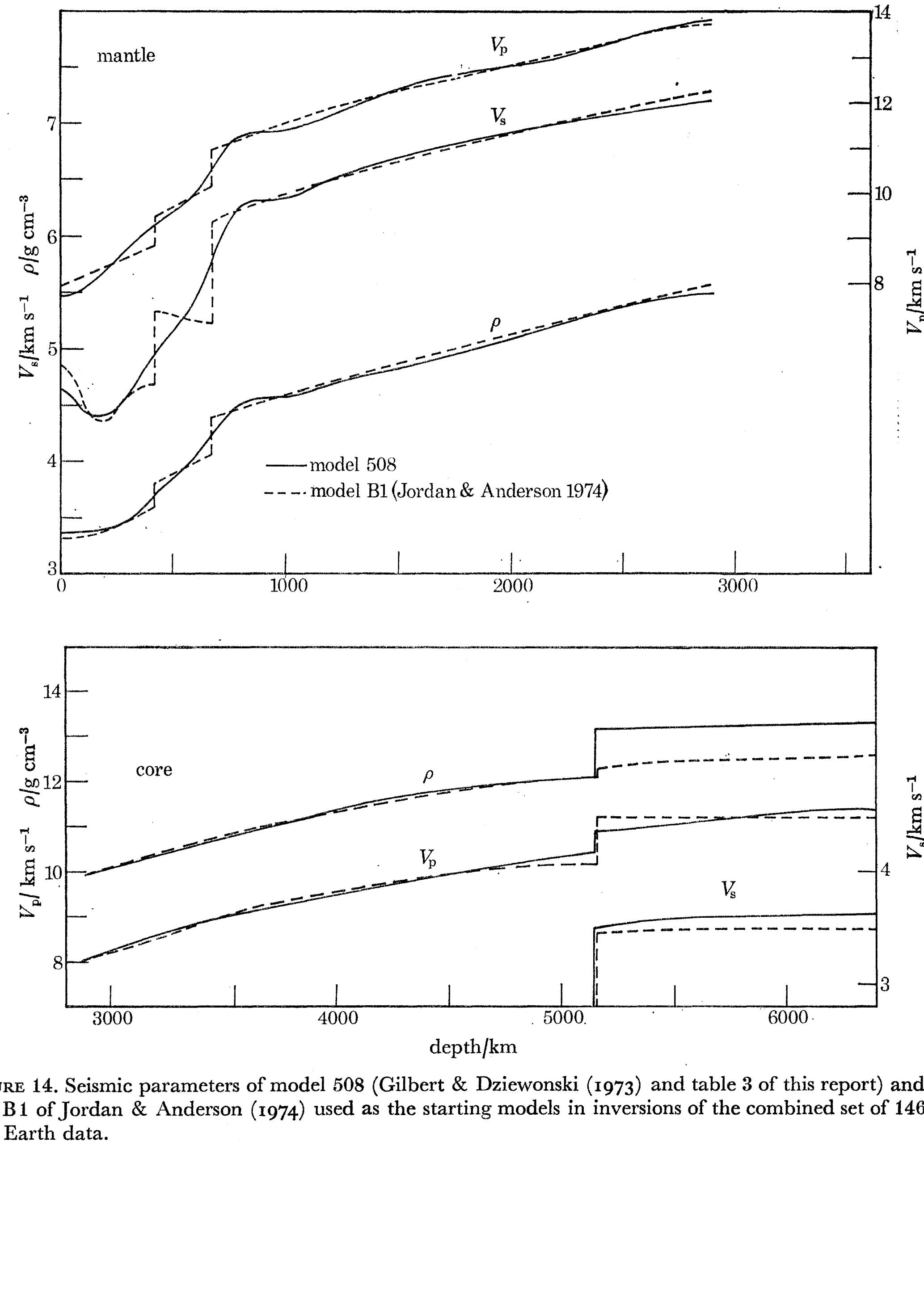

FIGURE 14. Seismic parameters of model 508 (Gilbert & Dziewonski (1973) and table 3 of this report) and model B1 of Jordan & Anderson (1974) used as the starting models in inversions of the combined set of 1463 gross Earth data.

core to a depth of about 950 km, models 1066 A and 1066 B are virtually identical. In the inner core the differences are relatively minor, especially for V_p. Only in the upper mantle are there major differences and these are related to the smoothness of model 1066 A and the discontinuities of model 1066 B. An averaging length of, say, 200 km appears to be sufficient to eliminate the major differences.

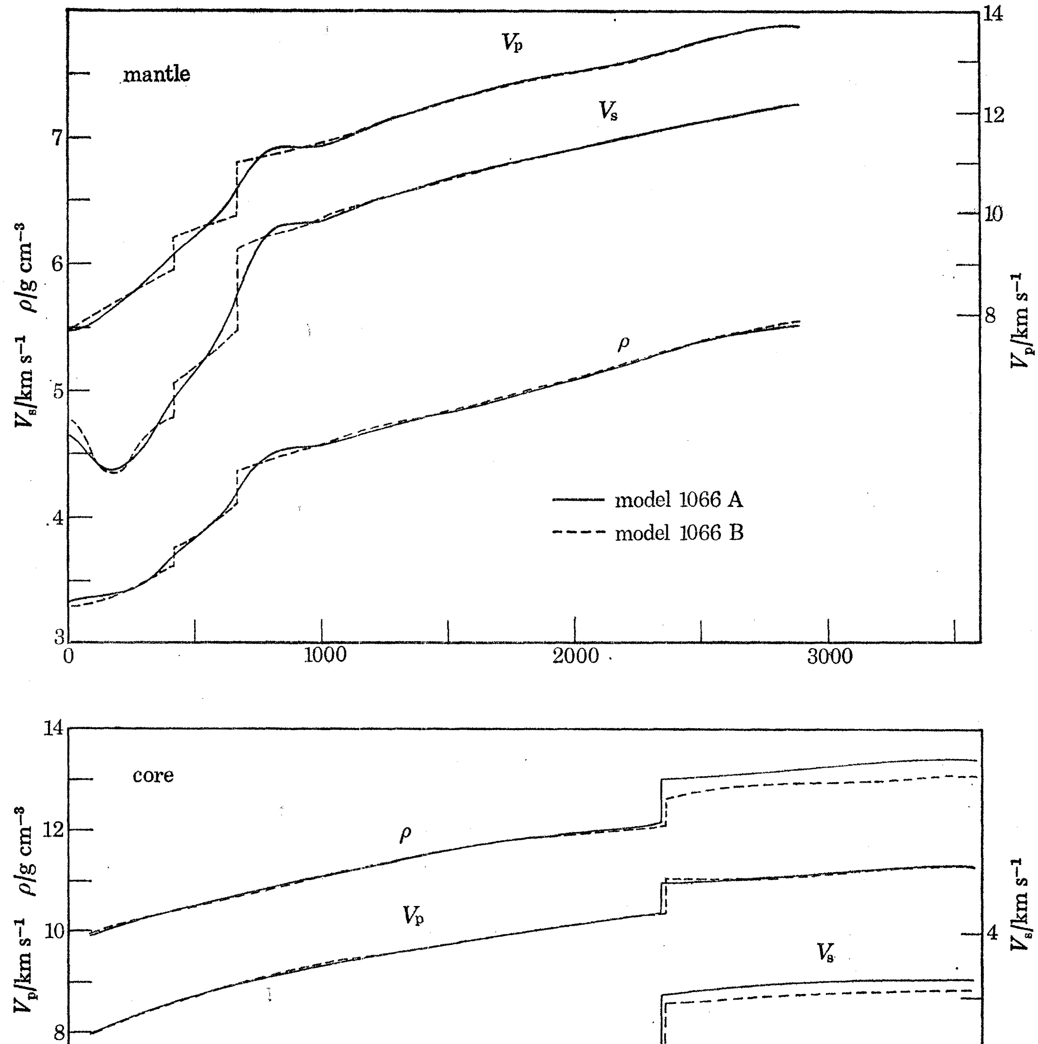

Figure 15. The Earth models obtained as a result of inverting 1463 gross Earth data, of which 1066 are distinct. model 1066 A was derived from model 508 and model 1066 B was derived from model B1.

Some idea of the extent to which the modal data sample different regions of the Earth can be gained from the (ω, l) diagram of observed eigenperiods. In figure 16 we present the (ω, l) diagram for ${}_nT_l$ modes and in figure 17 for ${}_nS_l$ modes ($\omega \leqslant 0.09\,\mathrm{s}^{-1}$, $l \leqslant 80$). Low phase velocities are not well represented; consequently the upper mantle is not well constrained. This is clear from figure 15. Phase velocities greater than, say $7\,\mathrm{km\,s^{-1}}$ are well represented in figure 17 including values that correspond to rays that turn in the inner core. In figure 16 there is a nearly

Table 6. Parameters of model 1066B

level	radius km	depth km	ρ g cm^{-3}	V_p km s^{-1}	V_s km s^{-1}	ϕ km^2 s^{-2}	κ kbar	μ kbar	λ kbar	σ	pressure kbar	g cm s^{-2}
1	0.0	6371.0	13.077	11.281	3.550	110.45	14444	1648	13345	0.4450	3660.4	0.0
2	38.0	6333.0	13.074	11.280	3.550	110.45	14440	1647	13342	0.4451	3659.4	13.9
3	75.9	6295.1	13.069	11.279	3.550	110.42	14430	1646	13332	0.4451	3657.6	27.7
4	113.9	6257.1	13.064	11.277	3.549	110.37	14418	1645	13321	0.4450	3655.2	41.6
5	151.9	6219.1	13.060	11.273	3.548	110.30	14404	1643	13308	0.4451	3652.1	55.4
6	189.8	6181.2	13.053	11.269	3.546	110.22	14386	1641	13292	0.4451	3648.4	69.3
7	227.8	6143.2	13.040	11.263	3.545	110.11	14358	1638	13266	0.4450	3643.9	83.1
8	265.8	6105.2	13.024	11.257	3.543	109.99	14325	1634	13235	0.4451	3638.8	96.9
9	303.7	6067.3	13.010	11.250	3.540	109.85	14291	1630	13204	0.4451	3633.0	110.6
10	341.7	6029.3	13.001	11.242	3.538	109.69	14260	1627	13175	0.4450	3626.5	124.4
11	379.7	5991.3	12.994	11.233	3.535	109.52	14230	1623	13148	0.4451	3619.4	138.1
12	417.7	5953.3	12.987	11.224	3.532	109.33	14198	1620	13118	0.4450	3611.5	151.8
13	455.6	5915.4	12.977	11.213	3.529	109.14	14163	1616	13085	0.4450	3603.0	165.6
14	493.6	5877.4	12.969	11.203	3.526	108.93	14126	1612	13051	0.4450	3593.9	179.3
15	531.6	5839.4	12.963	11.191	3.523	108.70	14090	1609	13017	0.4450	3584.0	192.9
16	569.5	5801.5	12.958	11.180	3.520	108.47	14055	1605	12985	0.4450	3573.5	206.6
17	607.5	5763.5	12.951	11.169	3.516	108.26	14021	1601	12953	0.4450	3562.4	220.3
18	645.5	5725.5	12.942	11.158	3.510	108.07	13986	1594	12923	0.4451	3550.6	234.0
19	683.4	5687.6	12.931	11.146	3.503	107.88	13949	1586	12891	0.4452	3538.1	247.6
20	721.4	5649.6	12.923	11.132	3.496	107.63	13908	1579	12855	0.4453	3524.9	261.3
21	759.4	5611.6	12.917	11.117	3.489	107.35	13856	1572	12817	0.4454	3511.1	274.9
22	797.3	5573.7	12.911	11.102	3.484	107.07	13823	1567	12778	0.4454	3496.6	288.5
23	835.3	5535.7	12.902	11.091	3.482	106.84	13784	1564	12741	0.4453	3481.5	302.1
24	873.3	5497.7	12.891	11.081	3.481	106.64	13747	1561	12706	0.4453	3465.7	315.7
25	911.2	5459.8	12.878	11.072	3.478	106.45	13709	1558	12670	0.4452	3449.3	329.2
26	949.2	5421.8	12.863	11.062	3.474	106.27	13669	1552	12634	0.4453	3432.3	342.8
27	987.2	5383.8	12.843	11.053	3.468	106.15	13632	1544	12602	0.4454	3414.6	356.3
28	1025.2	5345.8	12.817	11.050	3.461	106.13	13602	1535	12578	0.4456	3396.3	369.7
29	1063.1	5307.9	12.784	11.051	3.456	106.19	13575	1526	12557	0.4458	3377.4	383.1
30	1101.1	5269.9	12.747	11.051	3.452	106.24	13543	1518	12531	0.4460	3357.9	396.3
31	1139.1	5231.9	12.708	11.049	3.449	106.22	13499	1511	12491	0.4460	3337.9	409.5
32	1177.0	5194.0	12.666	11.045	3.447	106.14	13443	1505	12439	0.4460	3317.3	422.6
33	1216.8	5154.2	12.620	11.038	3.447	106.00	13377	1499	12377	0.4460	3295.9	436.2
34	1216.8	5154.2	12.057	10.366	0.000	107.45	12954	0	12954	0.5000	3295.9	436.2
35	1285.9	5085.1	12.029	10.335	0.000	106.81	12848	0	12848	0.5000	3257.0	456.7
36	1356.9	5014.1	12.000	10.297	0.000	106.03	12723	0	12723	0.5000	3215.5	477.9
37	1427.8	4943.2	11.968	10.255	0.000	105.16	12585	0	12585	0.5000	3172.3	499.4
38	1498.7	4872.2	11.932	10.211	0.000	104.27	12441	0	12441	0.5000	3127.3	521.0
39	1569.7	4801.3	11.894	10.169	0.000	103.40	12298	0	12298	0.5000	3080.7	542.6
40	1640.6	4730.4	11.859	10.120	0.000	102.41	12144	0	12144	0.5000	3032.4	564.3
41	1711.6	4659.4	11.827	10.062	0.000	101.24	11974	0	11974	0.5000	2982.4	586.1
42	1782.5	4588.5	11.791	10.002	0.000	100.03	11794	0	11794	0.5000	2930.7	607.8
43	1853.4	4517.6	11.749	9.945	0.000	98.90	11620	0	11620	0.5000	2877.4	629.5
44	1924.4	4446.6	11.703	9.892	0.000	97.86	11452	0	11452	0.5000	2822.6	651.1
45	1995.3	4375.7	11.654	9.839	0.000	96.80	11281	0	11281	0.5000	2766.2	672.7
46	2066.2	4304.8	11.601	9.778	0.000	95.61	11091	0	11091	0.5000	2708.4	694.0
47	2137.2	4233.8	11.537	9.715	0.000	94.38	10888	0	10888	0.5000	2649.2	715.3
48	2208.1	4162.9	11.466	9.652	0.000	93.17	10682	0	10682	0.5000	2588.7	736.3
49	2279.1	4091.9	11.398	9.589	0.000	91.96	10481	0	10481	0.5000	2526.8	757.0
50	2350.0	4021.0	11.323	9.535	0.000	90.92	10295	0	10295	0.5000	2463.8	777.5
51	2420.9	3950.1	11.244	9.482	0.000	89.90	10108	0	10108	0.5000	2399.6	797.8
52	2491.9	3879.1	11.166	9.417	0.000	88.67	9901	0	9901	0.5000	2334.3	817.7
53	2562.8	3808.2	11.085	9.342	0.000	87.27	9674	0	9674	0.5000	2267.9	837.4
54	2633.7	3737.2	11.001	9.268	0.000	85.90	9450	0	9450	0.5000	2200.6	856.8
55	2704.7	3666.3	10.917	9.196	0.000	84.57	9232	0	9232	0.5000	2132.3	875.9
56	2775.6	3595.4	10.833	9.116	0.000	83.10	9002	0	9002	0.5000	2063.0	894.8
57	2846.6	3524.4	10.759	9.029	0.000	81.53	8771	0	8771	0.5000	1992.9	913.3

TABLE 6 (*cont.*)

level	radius km	depth km	ρ g cm^{-3}	V_p km s^{-1}	V_s km s^{-1}	ϕ km^2 s^{-2}	κ kbar	μ kbar	λ kbar	σ	pressure kbar	g cm s^{-2}
58	2917.5	3453.5	10.686	8.933	0.000	79.80	8527	0	8527	0.5000	1921.8	931.7
59	2988.4	3382.6	10.607	8.827	0.000	77.92	8264	0	8264	0.5000	1849.9	949.8
60	3059.4	3311.6	10.532	8.725	0.000	76.13	8017	0	8017	0.5000	1777.3	967.6
61	3130.3	3240.7	10.452	8.613	0.000	74.19	7754	0	7754	0.5000	1703.9	985.2
62	3201.3	3169.8	10.365	8.489	0.000	72.06	7468	0	7468	0.5000	1629.9	1002.6
63	3272.2	3098.8	10.280	8.368	0.000	70.02	7197	0	7197	0.5000	1555.2	1019.6
64	3343.1	3027.9	10.189	8.243	0.000	67.95	6924	0	6924	0.5000	1480.1	1036.4
65	3414.1	2956.9	10.088	8.110	0.000	65.77	6634	0	6634	0.5000	1404.6	1052.8
66	3485.5	2885.5	9.977	7.967	0.000	63.48	6333	0	6333	0.5000	1345.2	1069.0
67	3485.5	2885.5	5.563	13.670	7.242	116.93	6504	2917	4559	0.3049	1345.2	1069.0
68	3519.6	2851.4	5.542	13.670	7.243	116.92	6479	2907	4541	0.3048	1325.2	1064.1
69	3554.2	2816.8	5.530	13.663	7.235	116.87	6463	2895	4533	0.3051	1305.0	1059.3
70	3588.8	2782.2	5.517	13.653	7.220	116.91	6450	2875	4533	0.3060	1284.9	1054.9
71	3623.4	2747.6	5.503	13.639	7.203	116.84	6429	2854	4526	0.3066	1265.0	1050.7
72	3658.0	2713.0	5.488	13.616	7.190	116.47	6392	2837	4500	0.3067	1245.2	1046.7
73	3692.7	2678.3	5.474	13.586	7.180	115.85	6341	2821	4460	0.3063	1225.5	1042.9
74	3727.3	2643.7	5.459	13.551	7.168	115.11	6284	2805	4414	0.3057	1205.9	1039.3
75	3761.9	2609.1	5.444	13.511	7.157	114.27	6220	2788	4361	0.3050	1186.4	1036.0
76	3796.5	2574.5	5.428	13.468	7.146	113.30	6149	2771	4301	0.3041	1167.1	1032.8
77	3831.1	2539.9	5.411	13.422	7.135	112.27	6075	2754	4239	0.3031	1147.9	1029.8
78	3865.7	2505.3	5.394	13.375	7.121	111.27	6002	2735	4178	0.3022	1128.7	1027.0
79	3900.3	2470.7	5.376	13.327	7.104	110.32	5930	2713	4121	0.3015	1109.7	1024.3
80	3934.9	2436.1	5.358	13.279	7.089	109.32	5857	2692	4062	0.3007	1090.8	1021.8
81	3969.5	2401.5	5.339	13.230	7.077	108.25	5780	2674	3997	0.2996	1072.1	1019.4
82	4004.1	2366.9	5.321	13.182	7.067	107.19	5702	2656	3931	0.2984	1053.4	1017.2
83	4038.7	2332.3	5.301	13.136	7.056	106.17	5628	2639	3868	0.2972	1034.8	1015.1
84	4073.4	2297.6	5.282	13.088	7.042	105.18	5555	2618	3809	0.2963	1016.3	1013.2
85	4108.0	2263.0	5.261	13.038	7.024	104.20	5481	2595	3751	0.2955	998.0	1011.3
86	4142.6	2228.4	5.241	12.990	7.006	103.30	5413	2572	3698	0.2949	979.7	1009.6
87	4177.2	2193.8	5.224	12.951	6.991	102.56	5358	2553	3656	0.2944	961.5	1008.0
88	4211.8	2159.2	5.209	12.918	6.977	101.96	5310	2535	3620	0.2941	943.4	1006.5
89	4246.4	2124.6	5.191	12.884	6.961	101.39	5262	2514	3586	0.2939	925.4	1005.1
90	4281.0	2090.0	5.169	12.848	6.941	100.83	5212	2490	3552	0.2939	907.5	1003.9
91	4315.6	2055.4	5.148	12.814	6.921	100.33	5164	2465	3520	0.2941	889.7	1002.7
92	4350.2	2020.8	5.127	12.782	6.902	99.86	5119	2442	3491	0.2942	872.0	1001.6
93	4384.8	1986.2	5.105	12.751	6.886	99.36	5072	2420	3458	0.2941	854.3	1000.5
94	4419.4	1951.6	5.083	12.720	6.874	98.81	5022	2401	3421	0.2938	836.8	999.6
95	4454.1	1916.9	5.063	12.689	6.861	98.25	4974	2383	3385	0.2934	819.3	998.7
96	4488.7	1882.3	5.046	12.658	6.846	97.73	4931	2364	3355	0.2933	801.9	997.9
97	4523.3	1847.7	5.029	12.625	6.829	97.21	4888	2345	3324	0.2932	784.6	997.2
98	4557.9	1813.1	5.008	12.591	6.812	96.66	4841	2324	3291	0.2931	767.4	996.6
99	4592.5	1778.5	4.985	12.556	6.797	96.04	4787	2303	3251	0.2927	750.2	996.0
100	4627.1	1743.9	4.963	12.517	6.784	95.31	4730	2284	3207	0.2920	733.2	995.5
101	4661.7	1709.3	4.942	12.477	6.772	94.53	4671	2266	3160	0.2912	716.2	995.0
102	4696.3	1674.7	4.920	12.437	6.760	93.76	4612	2248	3113	0.2903	699.3	994.6
103	4730.9	1640.1	4.899	12.398	6.746	93.03	4557	2229	3071	0.2887	682.5	994.2
104	4765.5	1605.5	4.882	12.357	6.727	92.35	4508	2209	3035	0.2894	665.7	993.9
105	4800.2	1570.8	4.868	12.313	6.706	91.65	4461	2188	3002	0.2892	649.0	993.7
106	4834.8	1536.2	4.854	12.266	6.687	90.83	4408	2170	2961	0.2885	632.4	993.5
107	4869.4	1501.6	4.837	12.215	6.672	89.84	4345	2153	2909	0.2873	615.8	993.4
108	4904.0	1467.0	4.820	12.159	6.654	88.79	4279	2134	2856	0.2862	599.2	993.3
109	4938.6	1432.4	4.805	12.099	6.630	87.77	4216	2111	2808	0.2854	582.7	993.3
110	4973.2	1397.8	4.791	12.039	6.605	86.77	4156	2090	2762	0.2846	566.3	993.4
111	5007.8	1363.2	4.777	11.984	6.586	85.78	4098	2072	2716	0.2836	549.9	993.5
112	5042.4	1328.6	4.763	11.929	6.568	84.78	4037	2054	2667	0.2825	533.5	993.6
113	5077.0	1294.0	4.744	11.868	6.545	83.73	3972	2032	2617	0.2815	517.2	993.8
114	5111.6	1259.4	4.724	11.804	6.520	82.64	3903	2008	2564	0.2804	501.0	994.0

TABLE 6 (*cont.*)

level	radius km	depth km	ρ g cm^{-3}	V_p km s^{-1}	V_s km s^{-1}	ϕ km^2 s^{-2}	κ kbar	μ kbar	λ kbar	σ	pressure kbar	g cm s^{-2}
115	5146.2	1224.7	4.705	11.741	6.500	81.52	3835	1987	2510	0.2791	484.8	994.3
116	5180.9	1190.1	4.689	11.681	6.484	80.40	3770	1971	2456	0.2774	468.7	994.6
117	5215.5	1155.5	4.673	11.625	6.468	79.36	3708	1954	2405	0.2759	452.7	994.9
118	5250.1	1120.9	4.655	11.570	6.449	78.42	3650	1936	2359	0.2746	436.7	995.3
119	5284.7	1086.3	4.634	11.518	6.426	77.60	3595	1913	2319	0.2740	420.7	995.7
120	5319.3	1051.7	4.609	11.466	6.398	76.89	3543	1886	2285	0.2739	404.9	996.1
121	5353.9	1017.1	4.586	11.414	6.366	76.25	3497	1858	2258	0.2734	389.1	996.5
122	5388.5	982.5	4.567	11.365	6.334	75.66	3455	1832	2233	0.2747	373.4	996.9
123	5423.1	947.9	4.548	11.317	6.304	75.10	3415	1807	2210	0.2751	357.7	997.4
124	5457.7	913.3	4.526	11.274	6.279	74.54	3373	1784	2183	0.2751	342.1	997.8
125	5492.3	878.7	4.503	11.235	6.259	73.98	3330	1764	2154	0.2749	326.6	998.3
126	5526.9	844.1	4.482	11.197	6.244	73.39	3289	1747	2124	0.2743	311.1	998.8
127	5561.6	809.4	4.462	11.159	6.227	72.82	3249	1730	2095	0.2739	295.7	999.3
128	5596.2	774.8	4.442	11.118	6.205	72.27	3209	1710	2069	0.2737	280.4	999.8
129	5630.8	740.2	4.420	11.078	6.183	71.75	3171	1689	2045	0.2738	265.1	1000.3
130	5665.4	705.6	4.397	11.043	6.155	71.43	3140	1665	2030	0.2747	249.9	1000.9
131	5700.0	671.0	4.372	11.013	6.117	71.39	3121	1635	2031	0.2770	235.2	1001.4
132	5700.0	671.0	4.100	9.945	5.475	58.94	2416	1229	1596	0.2825	235.2	1001.4
133	5731.4	639.6	4.049	9.900	5.415	58.91	2385	1187	1593	0.2865	222.6	1001.1
134	5762.7	608.2	4.003	9.859	5.363	58.86	2356	1151	1588	0.2899	210.1	1000.8
135	5794.1	576.9	3.958	9.805	5.306	58.61	2319	1114	1576	0.2929	197.8	1000.4
136	5825.5	545.5	3.906	9.762	5.259	58.41	2281	1080	1561	0.2955	185.6	999.9
137	5856.9	514.1	3.865	9.703	5.203	58.05	2243	1046	1545	0.2981	173.5	999.4
138	5888.3	482.7	3.821	9.639	5.161	57.40	2193	1017	1515	0.2992	161.6	998.8
139	5919.6	451.4	3.779	9.581	5.112	56.95	2151	987	1493	0.3010	149.9	998.2
140	5951.0	420.0	3.746	9.515	5.052	56.49	2116	956	1478	0.3036	138.3	997.5
141	5951.0	420.0	3.605	8.893	4.796	48.42	1745	829	1192	0.2949	138.3	997.5
142	5975.9	395.1	3.593	8.832	4.765	47.72	1714	815	1170	0.2947	129.5	996.7
143	6000.9	370.1	3.562	8.761	4.748	46.70	1663	802	1128	0.2922	120.6	995.9
144	6025.8	345.2	3.535	8.688	4.710	45.90	1622	784	1099	0.2918	111.9	995.1
145	6050.8	320.2	3.512	8.616	4.657	45.32	1591	761	1083	0.2937	103.2	994.2
146	6075.7	295.3	3.488	8.544	4.599	44.79	1562	737	1070	0.2961	94.6	993.4
147	6100.6	270.4	3.461	8.470	4.532	44.34	1534	711	1060	0.2993	86.1	992.5
148	6125.6	245.4	3.434	8.392	4.453	43.98	1510	681	1056	0.3040	77.6	991.6
149	6150.5	220.5	3.409	8.315	4.382	43.54	1484	654	1048	0.3079	69.3	990.7
150	6175.4	195.6	3.387	8.245	4.343	42.83	1450	638	1024	0.3081	60.9	989.8
151	6200.4	170.6	3.364	8.176	4.344	41.68	1402	634	979	0.3035	52.7	988.9
152	6225.3	145.7	3.351	8.098	4.355	40.28	1349	635	925	0.2965	44.4	987.9
153	6250.3	120.7	3.338	8.021	4.416	38.34	1279	650	845	0.2826	36.2	987.0
154	6275.2	95.8	3.323	7.947	4.514	35.99	1195	677	743	0.2616	28.1	986.1
155	6300.1	70.9	3.321	7.881	4.624	33.61	1116	710	642	0.2374	19.9	985.3
156	6325.1	45.9	3.309	7.808	4.725	31.21	1032	738	540	0.2113	11.8	984.4
157	6350.0	21.0	3.293	7.742	4.759	29.74	979	745	482	0.1964	4.3	983.6
158	6350.0	21.0	2.802	6.200	3.400	23.03	645	323	429	0.2852	4.3	983.6
159	6360.5	10.5	2.802	6.200	3.400	23.03	645	323	429	0.2852	1.4	982.8
160	6371.0	0.0	2.803	6.200	3.400	23.03	645	323	429	0.2852	0.0	982.0

uniform coverage corresponding to rays that turn in the lower mantle and there are 34 modes that are ScS equivalent. By ScS equivalent is meant a mode whose radial eigenfunction has no turning point between the core-mantle boundary and the surface. A discussion of the ray-mode duality, including the effect of interface waves, such as the Stoneley waves on the core-mantle boundary and on the inner -outer core boundary has been given in Alaska I (pp. 410–411) and Alaska II (§ 3).

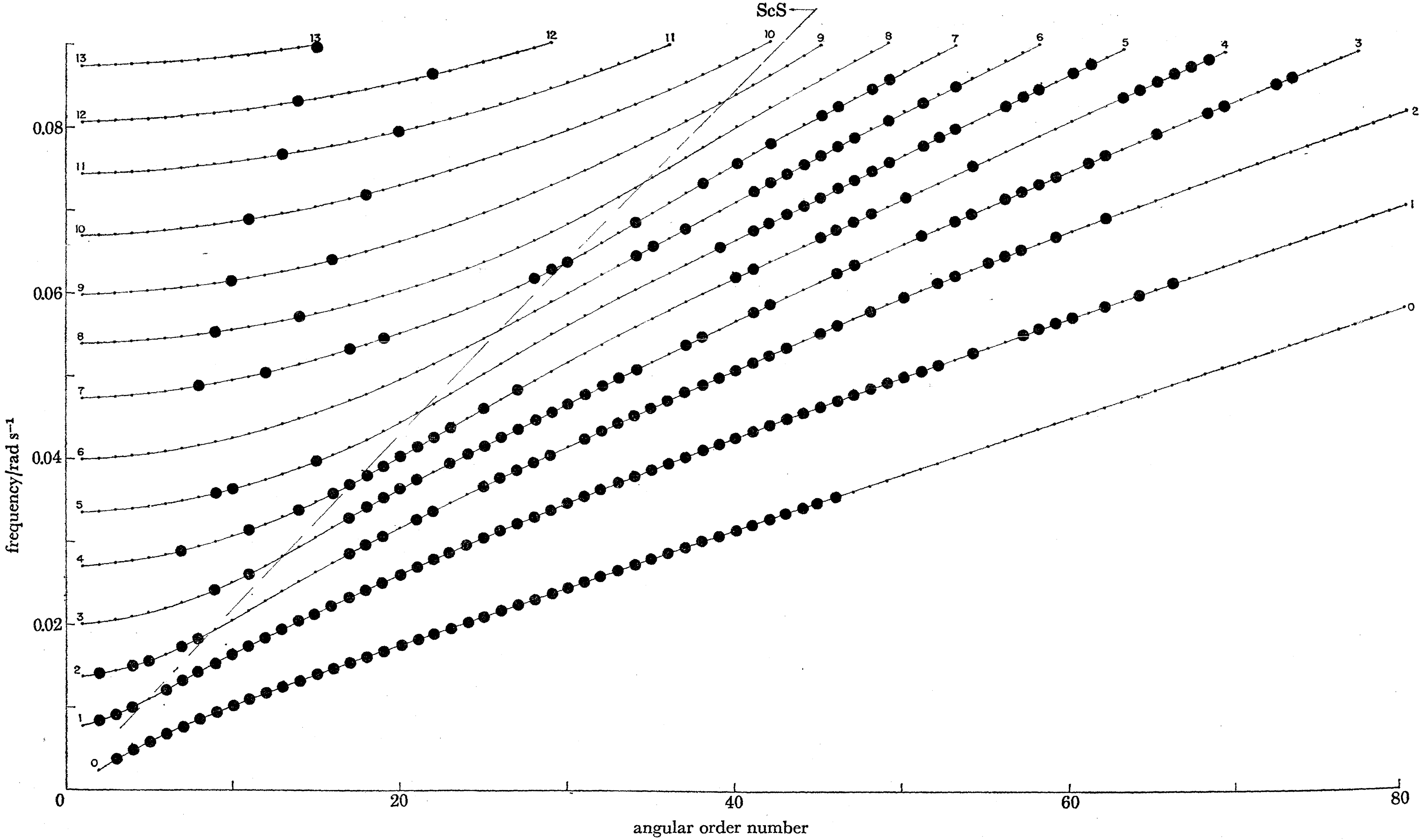

FIGURE 16. Toroidal normal modes in the (ω, l) plane. The large dots indicate observed modes used in the inversions. Most of the toroidal overtones identified by Brune & Gilbert (1964) fall outside the range of the figure. The dashed line designated 'ScS' divides the modes into two groups according to the normal mode–body wave analogy: modes to the left of this line correspond to $(ScS)_H$ reflexions, those to the right correspond to mantle S_H waves.

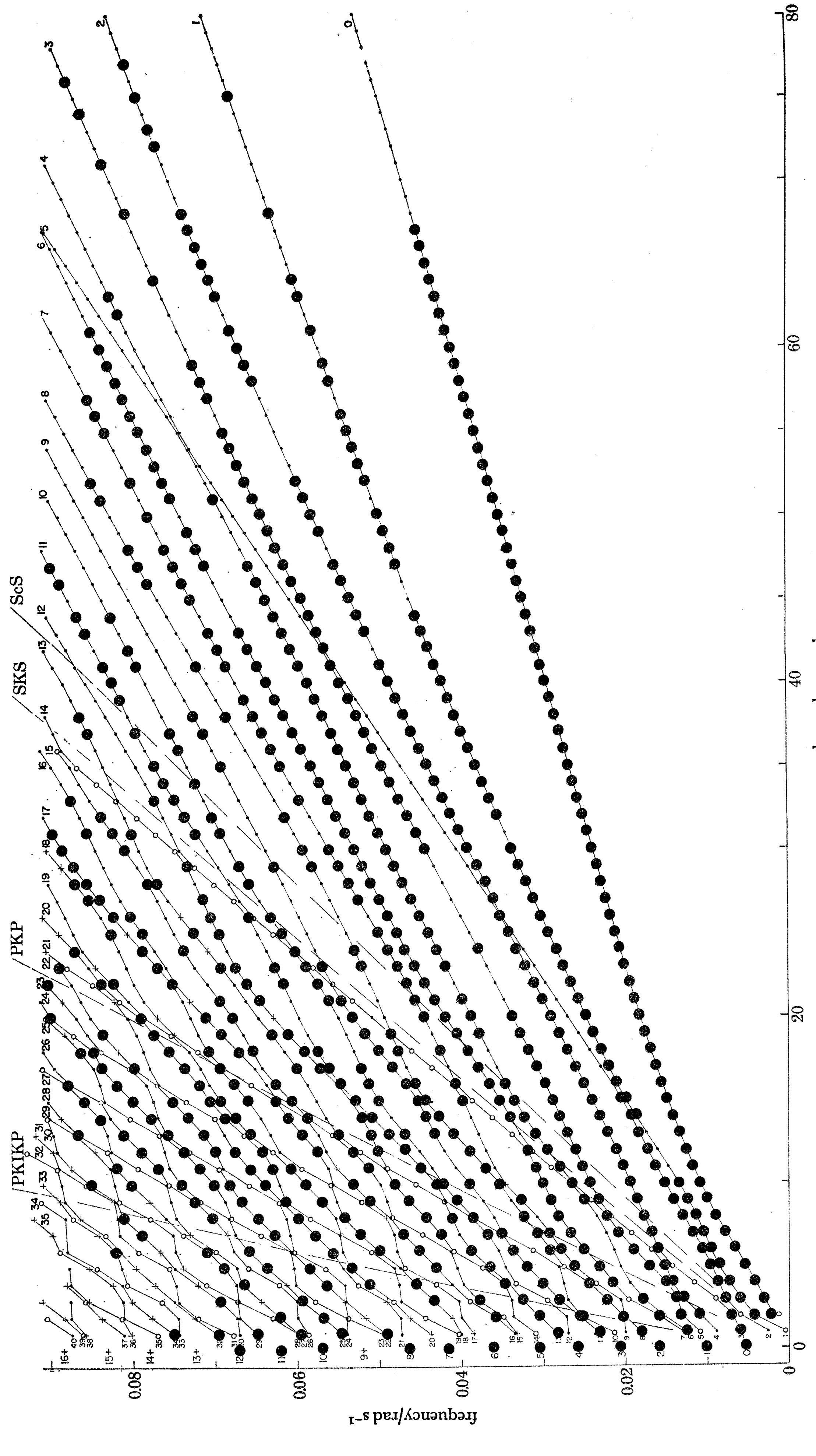

FIGURE 17. Spheroidal normal modes in the (ω, l) plane. The large dots indicate observed modes used in the inversions. For further details we refer the reader to §3 of Alaska II. •, $CE < 0.5$; +, $CE \geqslant 0.5$; ∘ core modes.

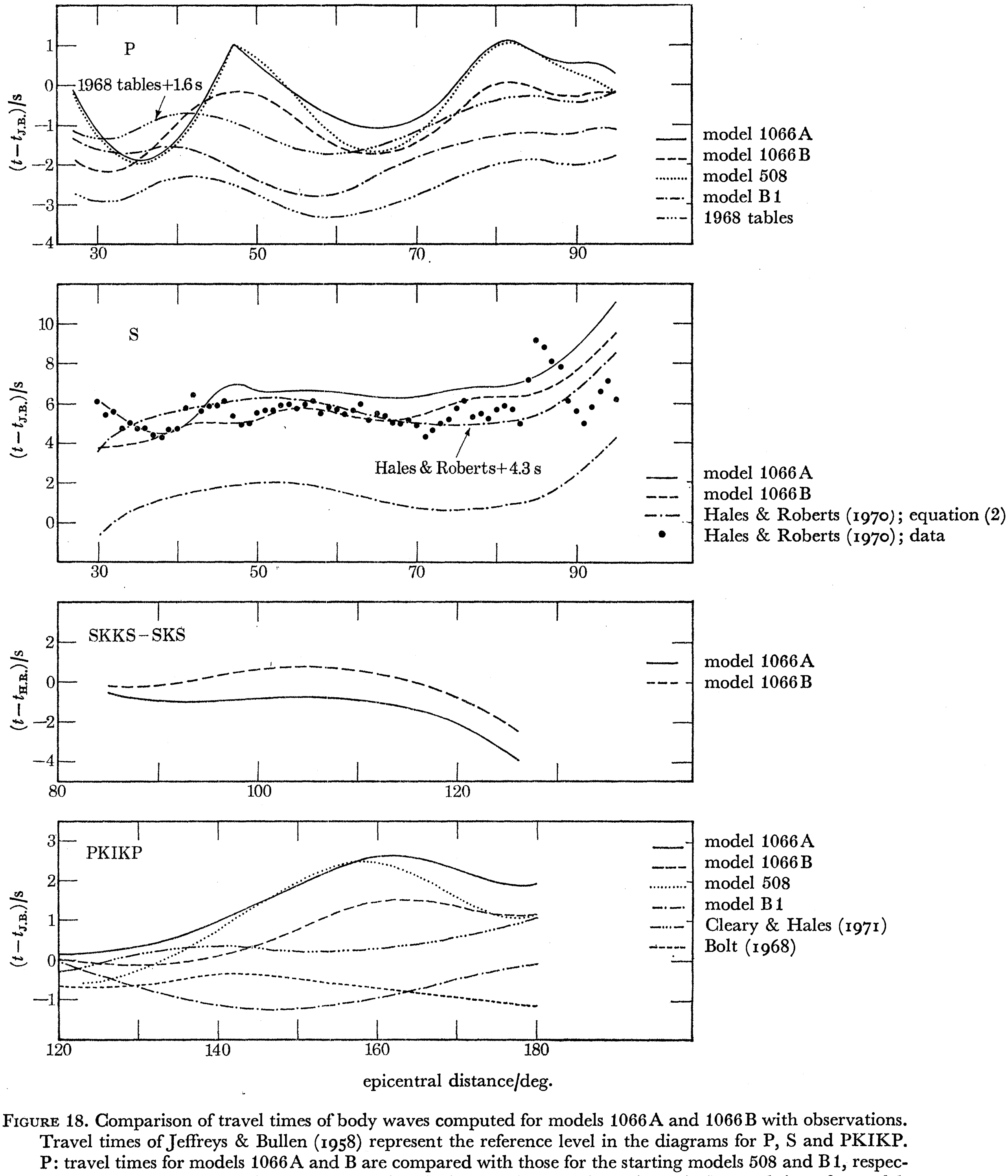

FIGURE 18. Comparison of travel times of body waves computed for models 1066A and 1066B with observations. Travel times of Jeffreys & Bullen (1958) represent the reference level in the diagrams for P, S and PKIKP. P: travel times for models 1066A and B are compared with those for the starting models 508 and B1, respectively, as well as the times from the 1968 Seismological Tables (Herrin *et al.* 1968). S: travel times for models 1066A and B are compared with the results of Hales & Roberts (1970). The chain line corresponds to their equation (2), the dots to their observations (table 3, column 4) with a base-line correction of +4.3 s. SKKS – SKS: residuals of the differential travel time $t_{SKKS}-t_{SKS}$ for models 1066 A and B with respect to the values predicted by equation (3) of Hales & Roberts (1971). PKIKP: travel times for models 1066 A and B compared with those for the respective starting models and observations of Bolt (1968, Table 8) and Cleary & Hales (1971, Table 3).

The asymptotic behaviour, for large n, of the ScS equivalent ${}_nT_l$ modes has been discussed by Anderssen, Cleary & Osborne (1974). They have used asymptotic Sturm–Liouville theory, which shows that the behaviour for large n is governed by the travel time of ScS at vertical incidence, to show that the data of Brune & Gilbert (1974) provide a tight constraint on that travel time. The asymptotic behaviour, for large n, of the ${}_nS_l$ modes has not been completely developed, but the decoupling of the normal mode equations into P and S factors as $l \to 0$ suggests decoupling as $n \to \infty$. Also, the partition of potential energy shows that the suggested decoupling does occur (Alaska I and II). Consequently, the very large number of overtone modes, both ${}_nS_l$ and ${}_nT_l$, should provide tight constraints on the P and S travel times whose ray parameters are embraced by the modes.

Although travel time data have not been used to derive the two final models, it is very important to present the calculated values. Both Gilbert *et al.* (1973) and Jordan & Anderson (1974) have discussed the problem of baselines for the travel time data. The differential travel times of Jordan & Anderson (1974) are compatible with the modal data that they used, and the ${}_nT_l$ modes derived from the phase spectra of SH pulses (Brune & Gilbert 1974) are compatible with the other modal data. Yet the travel time data themselves are not compatible unless significant baseline corrections are made.

That this feature persists is made evident by figure 18 where the calculated travel times for both models 1066A and 1066B are presented. It has been shown that the amount of information contained in the travel time data, but not contained in the modal data, is small (Gilbert *et al.* 1973). Now that the number of s.e.d. in the modal data set has risen from 43 to 57 it has become obvious that the baseline corrections implied in figure 16 are absolutely necessary.

A more detailed discussion of the compatibility of the modal data and ray data is motivated by an examination of the residuals of the P and S travel times. The two initial models have quite different P residuals (with respect to standard tables) but the two final models have P residuals that are nearly identical in shape and that differ by less than 1 s in most places.

The shapes of the distributions of P residuals of the two final models are remarkably similar to those presented by Johnson (1969, Figure 11) in his study of array measurements of P velocities in the lower mantle. There is good agreement with his models CIT 206 and CIT 208. The results of Johnson (1969) have been supported by the independent work of Vinnick & Nikolayev (1970). The two studies show virtually identical distributions of the ray parameter $\mathrm{d}T/\mathrm{d}\Delta$ as a function of range Δ. The models CIT 206 and CIT 208 of Johnson (1969) show detailed variations in V_p at depths of 2200–2300 km that agree in shape with models 1066A and 1066B. It is difficult to escape the conclusion that these detailed variations are real. They are required to fit the array measurements of $\mathrm{d}T/\mathrm{d}\Delta$ and the network measurements of the normal mode eigenperiods. The only question not fully answered is the exact value of the baseline correction for the P travel times.

A similar situation exists for the S residuals. In figure 18 the two final models have residuals that are nearly identical in shape while the two initial models do not. In fact, the two final models are in equal agreement with the data of Hales & Roberts (1970), after a suitable baseline correction is made, as are the low order polynomials given by those authors. This result lends credibility to the details of $V_\mathrm{s}(r)$ in the lower mantle of the two final models. Again, the only question outstanding is the exact value of the baseline correction for the S travel times.

The differential times, SKKS–SKS, are in very acceptable agreement with the data of Hales & Roberts (1971).

The residuals for PKIKP also show that the two final models are in better agreement than the two initial models. Because of the divergence of observations reported by different authors (Bolt 1968; Cleary & Hales 1971) it is difficult to make a meaningful comparison between computed and observed values, but the trend of the residuals does appear to favour Cleary & Hales (1971). Perhaps this is as good a place as any to raise a concern about travel time studies in critical regions.

Only recently have a few seismologists begun to use an adequate dynamical theory of wave propagation to study multiplicities, diffraction, tunnelling, wide angle reflexions and other phenomena where geometrical ray theory is either of doubtful value or known to be useless. All of the travel time data that we have discussed in this section have been interpreted (inverted) by using geometrical ray theory. The major discontinuities in the Earth are those places where classical ray theory and normal mode theory diverge. If a more resolute application of adequate dynamical (generalized) ray theory were made to the travel time (body wave) problems, perhaps the relatively minor disagreements between models derived from ray data and models derived from modal data would become diminished to an acceptable level.

4.2. *A standard set of gross Earth data*

For those data that are common to two or more of the studies listed in §4.1 we have chosen a 'best value'. If there are K values of an observed datum $\gamma(\gamma_k, k = 1, 2, \ldots, K)$ and if the difference with respect to model 1066A (1066B) is $a_k(b_k)$ then that value for which $a_k^2 + b_k^2$ is least is chosen as the 'best value'. In this manner we derive 1066 distinct g.e.d. from the set of 1463 g.e.d. used in the inversions in §4.1.

Now that we have performed the inversions we can re-examine the errors assigned in §3.4 and we find that by increasing the errors assigned in table 4 by a factor of 1.3 we obtain a better approximation to a normal distribution. With the reassigned errors we present a standard set of 1064 gross Earth data (normal mode eigenperiods) in table 7. It is our very firm opinion that the establishment of a standardized dataset should precede the establishment of a standardized model.

The distribution of relative errors between the data in table 7 and the two final models is presented in the form of histograms in figure 19. For both models a nearly normal distribution is obtained, but a slight skewness for model 1066B is apparent. The skewness is approximately $\frac{1}{3}\sigma$, where σ is the standard error of the distribution. Perhaps more iterative inversions of model 1066B would reduce the skewness but these calculations have been omitted as being of minor interest at the present time.

In appendix A of Alaska I we discussed the problem of potentially systematic errors in the eigenperiods, especially when two or more modes are nearly coincident. Near coincidence is the probable explanation of those errors in table 7 that appear to be excessively large. Most such errors occur for the data of Alaska I and II. To these remarks we must add that stacking and stripping will produce biased results for a variety of reasons. Multiplets will interfere because the network of stations is not uniformly distributed, some components are absent from some stations, real multiplets are not completely degenerate, and nearly coincident multiplets may be strongly coupled (quasi degenerate coupling). Also, errors in the source mechanism or in those parameters that are model-dependent, can introduce bias.

At this stage we are forced to rely on the internal consistency of the modal data in table 7 and the apparently small bias in the distribution of errors in figure 19. As in Alaska I (p. 397)

Table 7. Eigenperiods and relative errors of a standard set of 1064 normal modes compared with the theoretical values computed for the models 1066A and 1066B†

(The code to sources of data is as follows: DERR, Derr (1969); A1/2, Alaska I or II; MEND, Mendiguren (1973); B & G, Brune & Gilbert (1974); T.R., this report (table 4).)

mode			observation period (s)	observation error (%)	observation source	model 1066A period (s)	model 1066A diff. (%)	model 1066B period (s)	model 1066B diff. (%)
0	S	0	1227.64	0.06	A1/2	1230.48	−0.23	1230.12	−0.20
1	S	0	613.59	0.05	A1/2	613.77	−0.03	613.69	−0.02
2	S	0	398.55	0.05	A1/2	398.52	0.01	398.60	−0.01
3	S	0	305.84	0.05	A1/2	305.76	0.03	305.68	0.05
4	S	0	243.67	0.06	T.R.	243.71	−0.02	243.61	0.02
5	S	0	204.61	0.05	A1/2	204.86	−0.12	204.82	−0.10
6	S	0	174.25	0.06	T.R.	174.26	−0.00	174.30	−0.02
7	S	0	151.86	0.05	A1/2	151.97	−0.07	152.03	−0.11
8	S	0	134.65	0.05	A1/2	134.58	0.05	134.65	−0.00
10	S	0	110.68	0.26	T.R.	110.38	0.27	110.36	0.29
11	S	0	101.30	0.09	T.R.	101.14	0.16	101.09	0.20
12	S	0	93.54	0.09	T.R.	93.51	0.03	93.46	0.08
0	T	3	1705.95	0.15	A1/2	1703.03	0.17	1701.75	0.25
0	T	4	1305.46	0.07	A1/2	1304.09	0.10	1303.12	0.18
0	T	5	1075.98	0.08	A1/2	1075.85	0.01	1075.08	0.08
0	T	6	925.84	0.06	A1/2	925.79	0.01	925.15	0.07
0	T	7	819.31	0.08	A1/2	818.27	0.13	817.75	0.19
0	T	8	736.86	0.05	A1/2	736.63	0.03	736.21	0.09
0	T	9	671.80	0.05	A1/2	672.01	−0.03	671.67	0.02
0	T	10	618.97	0.05	A1/2	619.26	−0.05	618.99	−0.00
0	T	11	574.59	0.08	A1/2	575.20	−0.10	574.98	−0.07
0	T	12	536.84	0.06	A1/2	537.72	−0.16	537.55	−0.13
0	T	13	504.96	0.08	A1/2	505.36	−0.08	505.22	−0.05
0	T	14	477.52	0.06	MEND	477.06	0.10	476.95	0.12
0	T	15	451.83	0.13	T.R.	542.06	−0.05	451.96	−0.03
0	T	16	429.18	0.06	A1/2	429.75	−0.13	429.67	−0.11
0	T	17	410.24	0.13	T.R.	409.70	0.13	409.63	0.15
0	T	18	390.94	0.07	A1/2	391.56	−0.16	391.50	−0.14
0	T	19	374.76	0.05	A1/2	375.04	−0.08	375.00	−0.06
0	T	20	359.59	0.08	A1/2	359.93	−0.09	359.90	−0.09
0	T	21	346.07	0.13	T.R.	346.05	0.01	346.02	0.01
0	T	22	333.15	0.13	T.R.	333.23	−0.03	333.21	−0.02

mode			observation period (s)	observation error (%)	observation source	model 1066A period (s)	model 1066A diff. (%)	model 1066B period (s)	model 1066B diff. (%)
0	T	23	321.21	0.09	A1/2	321.36	−0.05	321.35	−0.04
0	T	24	310.36	0.10	MEND	310.33	0.01	310.32	0.01
0	T	25	300.19	0.09	MEND	300.04	0.05	300.05	0.04
0	T	26	290.26	0.05	A1/2	290.44	−0.06	290.45	−0.07
0	T	27	281.35	0.13	T.R.	281.44	−0.03	281.45	−0.04
0	T	28	272.91	0.13	T.R.	272.98	−0.03	273.00	−0.03
0	T	29	264.93	0.07	MEND	265.03	−0.04	265.05	−0.04
0	T	30	257.29	0.15	A1/2	257.53	−0.09	257.56	−0.10
0	T	31	250.29	0.13	T.R.	250.44	−0.06	250.47	−0.08
0	T	32	244.26	0.13	T.R.	243.74	0.21	243.78	0.20
0	T	33	237.37	0.13	T.R.	237.38	−0.01	237.43	−0.02
0	T	34	231.29	0.10	A1/2	231.36	−0.03	231.40	−0.05
0	T	35	224.93	0.15	A1/2	225.63	−0.31	225.67	−0.33
0	T	36	220.70	0.13	T.R.	220.18	0.24	220.22	0.22
0	T	37	213.89	0.10	A1/2	214.98	−0.51	215.03	−0.53
0	T	38	209.83	0.28	A1/2	210.02	−0.09	210.07	−0.11
0	T	39	204.27	0.05	A1/2	205.29	−0.50	205.34	−0.52
0	T	40	199.96	0.19	A1/2	200.76	−0.40	200.82	−0.43
0	T	41	195.88	0.22	A1/2	196.43	−0.28	196.49	−0.31
0	T	42	191.26	0.13	A1/2	192.29	−0.54	192.34	−0.56
0	T	43	187.40	0.26	A1/2	188.31	−0.48	188.36	−0.51
0	T	44	183.78	0.15	A1/2	184.49	−0.39	184.55	−0.42
0	T	45	180.25	0.05	A1/2	180.82	−0.32	180.88	−0.35
0	T	46	176.85	0.05	A1/2	177.30	−0.25	177.36	−0.29
1	T	2	756.57	0.08	A1/2	756.40	0.02	756.18	0.05
1	T	3	695.18	0.07	A1/2	693.93	0.18	693.81	0.20
1	T	4	629.98	0.10	A1/2	629.91	0.01	629.88	0.02
1	T	6	519.10	0.06	A1/2	518.65	0.09	518.74	0.07
1	T	7	475.17	0.13	MEND	474.71	0.10	474.82	0.07
1	T	8	438.49	0.05	A1/2	437.98	0.12	438.10	0.09
1	T	9	407.73	0.09	T.R.	407.24	0.12	407.36	0.09
1	T	10	381.24	0.13	MEND	381.24	−0.00	381.35	−0.03

† We have pointed out in Alaska II (p. 405) that assignment of the radial order number spheroidal overtones must be made with respect to a particular model of the Earth. The assignments in table 7 are made with respect to model 1066A. The following are the modes that have different identifications for model 1066B; the first symbol represents the identification used in table 7, the second is the identification proper for model 1066B:

${}_{5}S_{10} \rightarrow {}_{6}S_{10}$; ${}_{7}S_{16} \rightarrow {}_{8}S_{16}$; ${}_{9}S_{23} \rightarrow {}_{10}S_{23}$; ${}_{10}S_{25} \rightarrow {}_{11}S_{25}$; ${}_{11}S_{8} \rightarrow {}_{12}S_{8}$; ${}_{15}S_{14} \rightarrow {}_{16}S_{14}$; ${}_{17}S_{18} \rightarrow {}_{18}S_{18}$; ${}_{20}S_{14} \rightarrow {}_{21}S_{14}$; ${}_{20}S_{22} \rightarrow {}_{21}S_{22}$; ${}_{22}S_{17} \rightarrow {}_{21}S_{17}$; ${}_{24}S_{20} \rightarrow {}_{23}S_{20}$; ${}_{28}S_{13} \rightarrow {}_{29}S_{13}$; ${}_{30}S_{10} \rightarrow {}_{31}S_{10}$.

mode			observation period (s)	observation error (%)	observation source	model 1066A period (s)	model 1066A diff. (%)	model 1066B period (s)	model 1066B diff. (%)
1	T	11	359.08	0.14	MEND	358.93	0.04	359.01	0.02
1	T	12	339.54	0.06	T.R.	339.50	0.01	339.56	−0.00
1	T	13	322.12	0.06	T.R.	322.34	−0.07	322.38	−0.08
1	T	14	307.02	0.06	T.R.	307.04	−0.01	307.05	−0.01
1	T	15	293.33	0.06	T.R.	293.28	0.02	293.28	0.02
1	T	16	280.59	0.06	T.R.	280.83	−0.09	280.80	−0.08
1	T	17	269.68	0.06	T.R.	269.49	0.07	269.46	0.08
1	T	18	259.09	0.13	MEND	259.14	−0.02	259.09	−0.00
1	T	19	249.61	0.06	T.R.	249.63	−0.01	249.58	0.01
1	T	20	240.82	0.06	T.R.	240.89	−0.03	240.83	−0.01
1	T	21	232.53	0.05	MEND	232.81	−0.12	232.75	−0.10
1	T	22	225.24	0.06	T.R.	225.33	−0.04	225.27	−0.01
1	T	23	218.38	0.06	MEND	218.39	−0.00	218.33	0.02
1	T	24	211.87	0.06	T.R.	211.93	−0.03	211.88	−0.00
1	T	25	205.85	0.05	MEND	205.90	−0.02	205.85	−0.00
1	T	26	200.27	0.05	MEND	200.27	0.00	200.22	0.02
1	T	27	194.94	0.05	MEND	194.99	−0.02	194.95	−0.00
1	T	28	190.09	0.06	MEND	190.03	0.03	190.00	0.05
1	T	29	185.34	0.05	MEND	185.37	−0.02	185.34	−0.00
1	T	30	180.80	0.06	T.R.	180.98	−0.10	180.95	−0.08
1	T	31	176.85	0.07	MEND	176.83	0.01	176.81	0.02
1	T	32	172.96	0.06	T.R.	172.90	0.04	172.89	0.04
1	T	33	169.16	0.05	MEND	169.17	−0.01	169.17	−0.01
1	T	34	165.72	0.05	MEND	165.64	0.05	165.64	0.05
1	T	35	162.31	0.06	T.R.	162.28	0.02	162.29	0.01
1	T	36	159.08	0.06	T.R.	159.08	0.00	159.09	−0.01
1	T	37	155.98	0.05	MEND	156.02	−0.03	156.04	−0.04
1	T	38	153.11	0.06	T.R.	153.10	0.01	153.12	−0.01
1	T	39	150.28	0.06	T.R.	150.31	−0.02	150.33	−0.03
1	T	40	147.68	0.05	MEND	147.63	0.03	147.66	0.02
1	T	41	145.12	0.05	MEND	145.06	0.04	145.09	0.02
1	T	42	142.66	0.05	MEND	142.60	0.04	142.63	0.02
1	T	43	140.23	0.08	MEND	140.22	0.00	140.26	−0.02
1	T	44	137.96	0.06	MEND	137.94	0.02	137.97	−0.01
1	T	45	135.64	0.24	MEND	135.74	−0.07	135.77	−0.10
1	T	46	133.63	0.06	T.R.	133.61	0.01	133.65	−0.01
1	T	47	131.59	0.17	MEND	131.56	0.02	131.60	−0.01
1	T	48	129.56	0.06	T.R.	129.58	−0.01	129.62	−0.04
1	T	49	127.65	0.05	MEND	127.66	−0.01	127.70	−0.04
1	T	50	125.92	0.13	T.R.	125.81	0.09	125.84	0.06
1	T	51	124.13	0.43	MEND	124.01	0.10	124.04	0.07
1	T	52	122.26	0.13	T.R.	122.26	−0.00	122.30	−0.03
1	T	54	118.96	0.13	T.R.	118.93	0.02	118.97	−0.01
1	T	57	114.41	0.13	T.R.	114.28	0.11	114.32	0.08
1	T	58	112.92	0.13	T.R.	112.82	0.09	112.85	0.06
1	T	59	111.40	0.13	T.R.	111.39	0.01	111.42	−0.02
1	T	60	110.24	0.13	T.R.	110.00	0.22	110.04	0.19
1	T	62	107.44	0.13	T.R.	107.33	0.10	107.36	0.07
1	T	64	104.94	0.13	T.R.	104.79	0.14	104.82	0.11
1	T	66	102.59	0.13	T.R.	102.38	0.21	102.41	0.18
2	T	2	447.30	0.09	T.R.	447.58	−0.06	447.60	−0.07
2	T	4	419.38	0.09	T.R.	419.79	−0.10	419.77	−0.09
2	T	5	401.82	0.09	T.R.	402.16	−0.09	402.11	−0.07
2	T	7	363.65	0.07	A1/2	363.18	0.13	363.08	0.16
2	T	8	343.34	0.06	A1/2	343.28	0.02	343.18	0.05
2	T	17	219.95	0.06	T.R.	219.91	0.02	219.94	0.00
2	T	18	211.90	0.06	T.R.	211.98	−0.04	212.02	−0.06
2	T	19	204.63	0.06	T.R.	204.71	−0.04	204.76	−0.06
2	T	21	191.91	0.06	T.R.	191.81	0.05	191.87	0.02
2	T	22	186.19	0.06	T.R.	186.05	0.08	186.11	0.04
2	T	25	170.90	0.06	T.R.	170.93	−0.02	171.00	−0.05
2	T	26	166.50	0.06	T.R.	166.50	0.00	166.56	−0.04
2	T	27	162.34	0.06	T.R.	162.32	0.01	162.38	−0.02
2	T	28	158.41	0.09	MEND	158.37	0.03	158.43	−0.01
2	T	29	154.70	0.06	T.R.	154.63	0.04	154.69	0.01
2	T	31	147.71	0.06	T.R.	147.73	−0.01	147.77	−0.04
2	T	32	144.59	0.06	T.R.	144.52	0.05	144.56	0.02
2	T	33	141.54	0.06	T.R.	141.47	0.05	141.51	0.02
2	T	34	138.62	0.06	T.R.	138.56	0.04	138.59	0.02
2	T	35	135.73	0.06	T.R.	135.78	−0.04	135.80	−0.06
2	T	36	133.14	0.06	T.R.	133.12	0.01	133.14	−0.00
2	T	37	130.51	0.06	T.R.	130.58	−0.05	130.60	−0.07
2	T	38	128.17	0.08	MEND	128.15	0.02	128.16	0.01
2	T	39	125.71	0.06	T.R.	125.81	−0.08	125.82	−0.09
2	T	40	123.56	0.06	T.R.	123.57	−0.01	123.58	−0.02
2	T	41	121.30	0.06	T.R.	121.34	−0.10	121.43	−0.11
2	T	42	119.33	0.14	MEND	119.36	−0.03	119.37	−0.03
2	T	44	115.49	0.06	T.R.	115.48	0.01	115.49	0.00
2	T	45	113.57	0.06	T.R.	113.65	−0.07	113.66	−0.08
2	T	47	110.22	0.06	T.R.	110.20	0.02	110.21	0.01
2	T	49	106.98	0.06	T.R.	106.99	−0.01	107.02	−0.03
2	T	51	104.01	0.06	T.R.	104.02	−0.00	104.05	−0.04
2	T	52	102.60	0.06	T.R.	102.61	−0.01	102.65	−0.05
2	T	54	99.93	0.06	T.R.	99.93	0.00	99.99	−0.06
2	T	55	98.61	0.06	T.R.	98.66	−0.05	98.72	−0.11
2	T	56	97.40	0.06	T.R.	97.43	−0.03	97.50	−0.10
2	T	58	95.08	0.06	T.R.	95.08	0.00	95.17	−0.09
2	T	61	91.85	0.06	T.R.	91.82	0.03	91.94	−0.09
3	T	9	259.26	0.09	T.R.	259.49	−0.09	259.35	−0.03
3	T	11	240.50	0.09	T.R.	240.98	−0.20	240.86	−0.15
3	T	17	189.97	0.13	MEND	190.87	−0.47	190.89	−0.49
3	T	18	184.09	0.09	T.R.	184.33	−0.13	184.38	−0.15
3	T	19	178.17	0.09	T.R.	178.34	−0.09	178.40	−0.13
3	T	20	172.74	0.06	T.R.	172.84	−0.06	172.92	−0.11

TABLE 7 (*cont.*)

mode			observation period (s)	observation error (%)	observation source	model 1066A period (s)	model 1066A diff. (%)	model 1066B period (s)	model 1066B diff. (%)
3	T	21	167.69	0.06	T.R.	167.78	−0.05	167.87	−0.11
3	T	23	158.54	0.06	T.R.	158.72	−0.11	158.80	−0.17
3	T	24	154.61	0.06	T.R.	154.62	−0.01	154.70	−0.06
3	T	25	150.66	0.05	MEND	150.76	−0.07	150.83	−0.11
3	T	26	147.15	0.06	T.R.	147.12	0.02	147.18	−0.02
3	T	27	143.67	0.06	T.R.	143.66	0.00	143.72	−0.03
3	T	28	140.41	0.06	T.R.	140.38	0.02	140.42	−0.01
3	T	29	137.24	0.06	T.R.	137.25	−0.01	137.29	−0.04
3	T	30	134.23	0.06	T.R.	134.27	−0.03	134.31	−0.06
3	T	31	131.37	0.06	T.R.	131.43	−0.05	131.46	−0.07
3	T	32	128.68	0.06	T.R.	128.71	−0.03	128.75	−0.05
3	T	33	126.16	0.06	T.R.	126.11	0.04	126.15	0.01
3	T	34	123.75	0.06	T.R.	123.63	0.10	123.66	0.07
3	T	37	116.89	0.06	T.R.	116.78	0.10	116.82	0.06
3	T	38	114.66	0.06	T.R.	114.68	−0.01	114.72	−0.05
3	T	41	108.87	0.06	T.R.	108.86	0.01	108.92	−0.05
3	T	42	107.04	0.06	T.R.	107.07	−0.02	107.13	−0.08
3	T	46	100.56	0.06	T.R.	100.53	0.03	100.61	−0.05
3	T	47	99.08	0.06	T.R.	99.03	0.05	99.12	−0.04
3	T	51	93.67	0.09	T.R.	93.52	0.16	93.62	0.05
3	T	53	91.15	0.09	T.R.	91.02	0.14	91.12	0.04
3	T	54	89.90	0.09	T.R.	89.82	0.08	89.92	−0.02
3	T	56	87.67	0.09	T.R.	87.53	0.15	87.63	0.05
3	T	57	86.41	0.09	T.R.	86.44	−0.03	86.53	−0.13
3	T	58	85.33	0.09	T.R.	85.37	−0.05	85.45	−0.15
3	T	59	84.35	0.09	T.R.	84.33	0.02	84.41	−0.07
3	T	61	82.44	0.09	T.R.	82.34	0.12	82.41	0.04
3	T	62	81.44	0.09	T.R.	81.39	0.06	81.44	−0.00
3	T	65	78.69	0.09	T.R.	78.68	0.02	78.70	−0.02
3	T	68	76.19	0.09	T.R.	76.17	0.02	76.17	0.02
3	T	69	75.42	0.09	T.R.	75.38	0.05	75.37	0.06
3	T	72	73.16	0.09	T.R.	73.13	0.04	73.10	0.09
3	T	73	72.36	0.09	T.R.	72.42	−0.08	72.38	−0.02
4	T	7	216.81	0.19	T.R.	217.29	−0.22	217.34	−0.24
4	T	11	199.74	0.19	T.R.	200.02	−0.14	200.09	−0.17
4	T	14	184.86	0.19	T.R.	185.37	−0.28	185.41	−0.30
4	T	16	174.72	0.19	T.R.	175.31	−0.33	175.31	−0.34
4	T	17	169.68	0.19	T.R.	170.29	−0.36	170.28	−0.35
4	T	18	164.71	0.19	T.R.	165.35	−0.38	165.32	−0.37
4	T	19	160.11	0.19	T.R.	160.52	−0.26	160.48	−0.23
4	T	20	155.64	0.19	T.R.	155.88	−0.15	155.84	−0.13
4	T	21	151.15	0.19	T.R.	151.46	−0.20	151.42	−0.18
4	T	22	147.47	0.19	T.R.	147.28	0.13	147.26	0.15
4	T	23	143.67	0.19	T.R.	143.35	0.22	143.35	0.22
4	T	25	136.30	0.19	T.R.	136.22	0.06	136.25	0.04
4	T	27	130.03	0.19	T.R.	129.91	0.10	129.96	0.05

mode			observation period (s)	observation error (%)	observation source	model 1066A period (s)	model 1066A diff. (%)	model 1066B period (s)	model 1066B diff. (%)
4	T	41	99.71	0.09	T.R.	99.65	0.06	99.75	−0.04
4	T	45	93.79	0.09	T.R.	93.77	0.02	93.87	−0.08
4	T	46	92.29	0.09	T.R.	92.42	−0.14	92.52	−0.25
4	T	47	91.11	0.09	T.R.	91.11	−0.01	91.21	−0.11
4	T	48	89.82	0.09	T.R.	89.85	−0.03	89.94	−0.13
4	T	50	87.46	0.09	T.R.	87.43	0.03	87.51	−0.05
4	T	54	82.95	0.09	T.R.	83.00	−0.06	83.03	−0.10
4	T	62	75.46	0.45	B & G	75.45	0.01	75.41	0.07
4	T	63	74.72	0.09	T.R.	74.62	0.14	74.57	0.20
4	T	64	73.79	0.09	T.R.	73.80	−0.01	73.75	0.06
4	T	65	72.94	0.09	T.R.	73.00	−0.08	72.95	−0.01
4	T	66	72.28	0.09	T.R.	72.22	0.08	72.16	0.16
4	T	67	71.07	0.47	B & G	71.46	−0.54	71.40	−0.46
4	T	80	63.06	0.45	B & G	62.94	0.19	62.95	0.17
4	T	84	60.85	0.45	B & G	60.74	0.19	60.78	0.12
4	T	90	57.69	0.45	B & G	57.76	−0.13	57.81	−0.21
4	T	95	55.43	0.45	B & G	55.55	−0.22	55.58	−0.27
4	T	97	54.95	0.45	B & G	54.73	0.41	54.75	0.37
4	T	98	54.50	0.45	B & G	54.33	0.32	54.34	0.30
4	T	99	53.94	0.45	B & G	53.94	0.00	53.95	−0.02
5	T	9	174.33	0.09	T.R.	174.62	−0.17	174.62	−0.17
5	T	10	171.89	0.09	T.R.	172.14	−0.15	172.14	−0.15
5	T	15	157.57	0.09	T.R.	157.75	−0.11	157.74	−0.11
5	T	38	97.11	0.09	T.R.	97.10	0.01	97.21	−0.10
5	T	40	94.12	0.09	T.R.	94.09	0.03	94.20	−0.09
5	T	41	92.65	0.09	T.R.	92.66	−0.01	92.77	−0.13
5	T	42	91.34	0.09	T.R.	91.27	0.08	91.38	−0.04
5	T	43	89.97	0.09	T.R.	89.93	0.05	90.03	−0.06
5	T	44	88.64	0.09	T.R.	88.62	0.02	88.71	−0.08
5	T	45	87.47	0.09	T.R.	87.36	0.13	87.44	0.04
5	T	46	86.26	0.09	T.R.	86.13	0.15	86.20	0.07
5	T	47	85.08	0.09	T.R.	84.94	0.17	85.00	0.10
5	T	48	83.75	0.09	T.R.	83.78	−0.04	83.83	−0.09
5	T	50	81.60	0.09	T.R.	81.57	0.04	81.59	0.02
5	T	51	80.55	0.09	T.R.	80.51	0.05	80.51	0.05
5	T	52	79.52	0.09	T.R.	79.48	0.05	79.47	6.06
5	T	55	76.52	0.09	T.R.	76.56	−0.05	76.52	−0.01
5	T	56	75.67	0.09	T.R.	75.64	0.04	75.60	0.10
5	T	57	74.75	0.09	T.R.	74.74	0.01	74.70	0.07
5	T	59	72.64	0.42	B & G	73.02	−0.53	72.97	−0.46
5	T	60	72.13	0.42	B & G	72.20	−0.09	72.15	−0.02
5	T	64	68.76	0.42	B & G	69.10	−0.49	69.06	−0.44
5	T	77	60.87	0.42	B & G	60.85	0.03	60.87	−0.01
5	T	79	59.69	0.42	B & G	59.78	−0.14	59.80	−0.17
5	T	99	51.07	0.42	B & G	50.97	0.18	51.00	0.13
5	T	105	48.79	0.42	B & G	48.83	−0.08	48.88	−0.18

mode			observation period (s)	observation error (%)	observation source	model 1066A period (s)	model 1066A diff. (%)	model 1066B period (s)	model 1066B diff. (%)
5	T	109	47.68	0.43	B & G	47.51	0.36	47.57	0.23
5	T	110	47.23	0.42	B & G	47.19	0.09	47.25	−0.03
5	T	111	46.77	0.42	B & G	46.87	−0.23	46.93	−0.35
5	T	118	44.68	0.42	B & G	44.82	−0.32	44.86	−0.40
5	T	121	44.17	0.42	B & G	44.01	0.37	44.03	0.32
6	T	34	79.13	0.09	T.R.	97.06	0.07	97.12	[illegible]
6	T	35	95.46	0.09	T.R.	95.40	0.06	95.48	−0.02
6	T	37	92.29	0.09	T.R.	92.29	0.00	92.38	−0.09
6	T	41	86.70	0.09	T.R.	86.73	−0.04	86.81	−0.13
6	T	42	85.35	0.09	T.R.	85.46	−0.13	85.53	−0.2[illegible]
6	T	43	84.30	0.09	T.R.	84.23	0.08	84.29	0.01
6	T	44	83.13	0.09	T.R.	83.05	0.10	83.09	0.05
6	T	45	81.85	0.09	T.R.	81.89	−0.05	81.92	−0.09
6	T	47	79.71	0.09	T.R.	79.70	0.01	79.69	0.02
6	T	49	77.65	0.09	T.R.	77.64	0.01	77.60	0.06
6	T	51	75.75	0.09	T.R.	75.70	0.07	75.64	0.14
6	T	53	73.89	0.09	T.R.	73.86	0.04	73.80	0.12
6	T	71	60.82	0.40	B & G	60.97	−0.25	61.02	−0.33
6	T	72	60.12	0.40	B & G	60.40	−0.45	60.45	−0.54
6	T	81	56.02	0.40	B & G	55.72	0.54	55.77	0.46
6	T	82	55.51	0.40	B & G	55.25	0.46	55.30	0.38
6	T	89	51.97	0.40	B & G	52.20	−0.43	52.23	−0.49
6	T	91	51.52	0.40	B & G	51.39	0.24	51.42	0.19
6	T	92	51.02	0.40	B & G	51.00	0.04	51.02	−0.00
6	T	98	48.62	0.40	B & G	48.80	−0.37	48.80	−0.37
6	T	117	43.24	0.40	B & G	43.08	0.39	43.06	0.42
6	T	125	40.98	0.40	B & G	41.06	−0.20	41.11	−0.30
6	T	129	40.30	0.40	B & G	40.13	0.44	40.20	0.26
6	T	131	39.67	0.40	B & G	39.67	−0.01	39.75	−0.22
6	T	132	39.43	0.40	B & G	39.45	−0.06	39.53	−0.27
6	T	141	37.36	0.40	B & G	37.57	−0.56	37.66	−0.78
6	T	143	37.36	0.40	B & G	37.19	0.46	37.26	0.26
6	T	145	36.89	0.40	B & G	36.81	0.21	36.88	0.03
6	T	149	35.90	0.40	B & G	36.10	−0.56	36.14	−0.67
6	T	154	35.19	0.40	B & G	35.26	−0.21	35.27	−0.23
6	T	163	33.71	0.40	B & G	33.90	−0.54	33.87	−0.45
6	T	165	33.26	0.40	B & G	33.61	−1.05	33.58	−0.95
7	T	8	129.67	0.39	B & G	129.30	0.29	129.35	0.24
7	T	12	125.95	0.39	B & G	125.16	0.63	125.19	0.61
7	T	17	118.57	0.13	T.R.	118.60	−0.03	118.60	−0.03
7	T	19	115.58	0.13	T.R.	115.69	−0.10	115.69	−0.10
7	T	28	101.15	0.13	T.R.	101.43	−0.28	101.50	−0.35
7	T	29	99.53	0.13	T.R.	99.75	−0.22	99.83	−0.30
7	T	30	97.93	0.13	T.R.	98.07	−0.14	98.15	−0.23
7	T	34	91.46	0.13	T.R.	91.45	0.01	91.51	−0.05
7	T	38	85.45	0.13	T.R.	85.53	−0.10	85.53	−0.09

mode			observation period (s)	observation error (%)	observation source	model 1066A period (s)	model 1066A diff. (%)	model 1066B period (s)	model 1066B diff. (%)
7	T	40	82.84	0.13	T.R.	82.94	−0.12	82.89	0.06
7	T	42	80.51	0.13	T.R.	80.55	−0.05	80.47	0.05
7	T	45	77.23	0.13	T.R.	77.29	−0.08	77.19	0.06
7	T	46	76.18	0.13	T.R.	76.28	−0.13	76.17	0.01
7	T	48	74.28	0.13	T.R.	74.35	−0.09	74.25	0.04
7	T	49	73.36	0.13	T.R.	73.43	−0.09	73.34	0.02
7	T	66	60.54	0.39	B & G	60.89	−0.58	60.96	−0.70
7	T	77	54.70	0.39	B & G	55.00	−0.55	55.00	−0.54
7	T	81	53.04	0.39	B & G	53.17	−0.25	53.16	−0.23
7	T	82	52.79	0.39	B & G	52.74	0.10	52.72	0.12
7	T	83	52.10	0.39	B & G	52.31	−0.40	52.30	−0.37
7	T	94	48.30	0.39	B & G	48.06	0.50	48.07	0.48
7	T	95	47.92	0.39	B & G	47.71	0.45	47.72	0.42
7	T	102	45.31	0.39	B & G	45.41	−0.21	45.44	−0.28
7	T	106	44.29	0.39	B & G	44.20	0.21	44.24	0.12
7	T	109	43.12	0.39	B & G	43.35	−0.52	43.39	−0.62
7	T	130	38.33	0.39	B & G	38.30	0.08	38.29	0.11
7	T	144	35.65	0.39	B & G	35.61	0.12	35.61	0.12
7	T	150	34.67	0.39	B & G	34.56	0.32	34.60	0.22
7	T	151	34.43	0.39	B & G	34.39	0.11	34.43	−0.01
7	T	152	34.23	0.39	B & G	34.23	0.01	34.27	−0.12
7	T	165	32.39	0.39	B & G	32.21	0.58	32.30	0.28
7	T	178	30.45	0.39	B & G	30.48	−0.10	30.53	−0.24
7	T	187	29.37	0.37	B & G	29.45	−0.26	29.45	−0.24
7	T	191	28.75	0.39	B & G	29.03	−0.96	29.01	−0.91
8	T	9	113.82	0.37	B & G	113.55	0.23	113.54	0.24
8	T	14	109.64	0.37	B & G	109.69	−0.04	109.74	−0.09
8	T	75	53.33	0.37	B & G	53.59	−0.49	53.60	−0.50
8	T	88	47.99	0.37	B & G	48.22	−0.48	48.24	−0.52
8	T	92	46.70	0.37	B & G	46.80	−0.22	46.82	−0.25
8	T	93	46.58	0.37	B & G	46.46	0.24	46.48	0.22
8	T	94	46.07	0.37	B & G	46.13	−0.14	46.14	−0.16
8	T	95	45.64	0.37	B & G	45.80	−0.36	45.81	−0.38
8	T	108	42.20	0.37	B & G	41.97	0.55	42.00	0.48
8	T	116	39.88	0.37	B & G	39.94	−0.15	39.98	−0.25
8	T	121	38.79	0.37	B & G	38.79	0.02	38.82	−0.08
8	T	123	38.15	0.37	B & G	38.34	−0.49	38.38	−0.59
8	T	125	37.86	0.37	B & G	37.91	−0.15	37.95	−0.24
8	T	147	33.92	0.37	B & G	33.81	0.33	33.82	0.29
8	T	164	31.29	0.37	B & G	31.29	0.00	31.29	−0.01
8	T	170	30.62	0.37	B & G	30.48	0.45	30.51	0.37
8	T	171	30.42	0.37	B & G	30.35	0.22	30.38	0.13
8	T	173	30.10	0.37	B & G	30.10	0.01	30.13	−0.11
8	T	188	28.45	0.37	B & G	28.30	−0.54	28.39	0.20
8	T	193	27.70	0.37	B & G	27.75	−0.19	27.85	−0.53
8	T	195	27.45	0.37	B & G	27.55	−0.35	27.63	−0.67
8	T	202	26.84	0.37	B & G	26.85	−0.04	26.91	−0.26

TABLE 7 (cont.)

mode	observation period (s)	observation error (%)	observation source	model 1066A period (s)	model 1066A diff. (%)	model 1066B period (s)	model 1066B diff. (%)
8 T 212	25.92	0.37	B & G	25.96	−0.13	25.97	−0.16
8 T 216	25.43	0.37	B & G	25.63	−0.78	25.62	−0.76
8 T 219	25.60	0.37	B & G	25.39	0.83	25.37	0.89
9 T 10	101.29	0.37	B & G	101.23	0.05	101.50	−0.21
9 T 16	97.18	0.37	B & G	97.46	−0.29	97.67	−0.50
9 T 84	47.69	0.37	B & G	47.85	−0.33	47.86	−0.37
9 T 99	42.76	0.37	B & G	42.93	−0.40	42.96	−0.47
9 T 103	41.76	0.37	B & G	41.81	−0.12	41.85	−0.21
9 T 104	41.67	0.37	B & G	41.54	0.33	41.58	0.24
9 T 105	41.23	0.37	B & G	41.27	−0.09	41.31	−0.18
9 T 106	40.86	0.37	B & G	41.01	−0.36	41.05	−0.45
9 T 121	37.67	0.37	B & G	37.46	0.54	37.48	0.51
9 T 130	35.59	0.37	B & G	35.65	−0.15	35.67	−0.22
9 T 135	34.77	0.37	B & G	34.72	0.14	34.76	0.04
9 T 136	34.51	0.37	B & G	34.54	−0.09	34.58	−0.20
9 T 138	34.08	0.37	B & G	34.19	−0.34	34.23	−0.46
9 T 140	33.84	0.37	B & G	33.85	−0.03	33.89	−0.16
9 T 163	30.58	0.37	B & G	30.41	0.58	30.44	0.48
9 T 181	28.36	0.37	B & G	28.23	0.45	28.23	0.44
9 T 183	28.05	0.37	B & G	28.01	0.15	28.01	0.14
9 T 185	27.76	0.37	B & G	27.79	−0.12	27.79	−0.13
9 T 190	27.42	0.37	B & G	27.26	0.56	27.27	0.53
9 T 191	27.24	0.37	B & G	27.16	0.28	27.17	0.24
9 T 194	26.83	0.37	B & G	26.85	−0.10	26.88	−0.18
9 T 211	25.36	0.37	B & G	25.24	0.49	25.33	0.10
9 T 217	24.65	0.37	B & G	24.72	−0.30	24.82	−0.71
9 T 220	24.33	0.37	B & G	24.47	−0.58	24.57	−0.98
9 T 229	23.68	0.37	B & G	23.78	−0.39	23.84	−0.65
9 T 237	23.19	0.37	B & G	23.21	−0.09	23.23	−0.16
9 T 241	22.81	0.37	B & G	22.95	−0.58	22.95	−0.58
9 T 246	22.79	0.37	B & G	22.63	0.72	22.61	0.79
10 T 11	91.24	0.36	B & G	91.06	0.20	90.96	0.31
10 T 18	87.29	0.36	B & G	87.52	−0.26	87.32	−0.03
10 T 109	38.80	0.36	B & G	38.92	−0.33	38.94	−0.36
10 T 113	38.03	0.36	B & G	37.99	0.10	38.00	0.09
10 T 115	37.70	0.36	B & G	37.55	0.41	37.55	0.40
10 T 117	37.11	0.36	B & G	37.11	−0.01	37.12	−0.02
10 T 118	36.78	0.36	B & G	36.90	−0.32	36.31	−0.34
10 T 134	34.01	0.36	B & G	33.84	0.52	33.88	0.39
10 T 144	32.16	0.36	B & G	32.19	−0.10	32.24	−0.23
10 T 149	31.52	0.36	B & G	31.43	0.27	31.48	0.13
10 T 152	30.94	0.36	B & G	31.00	−0.19	31.04	−0.33
10 T 154	30.75	0.36	B & G	30.72	0.10	30.76	−0.03
10 T 199	25.79	0.36	B & G	25.63	0.63	25.66	0.52
10 T 202	25.40	0.36	B & G	25.36	0.19	25.38	0.09

mode	observation period (s)	observation error (%)	observation source	model 1066A period (s)	model 1066A diff. (%)	model 1066B period (s)	model 1066B diff. (%)
10 T 213	24.52	0.36	B & G	24.41	0.45	24.43	0.38
10 T 214	24.34	0.36	B & G	24.33	0.06	24.34	−0.00
10 T 233	22.97	0.36	B & G	22.85	0.50	22.92	0.19
10 T 245	21.85	0.36	B & G	22.02	−0.78	22.11	−1.19
10 T 258	21.02	0.36	B & G	21.22	−0.95	21.27	−1.18
10 T 262	20.98	0.36	B & G	21.00	−0.10	21.03	−0.23
10 T 265	20.75	0.36	B & G	20.83	−0.40	20.85	−0.47
10 T 275	20.39	0.36	B & G	20.32	0.37	20.29	0.49
11 T 13	82.62	0.35	B & G	82.49	0.16	82.18	0.54
11 T 20	79.27	0.35	B & G	79.52	−0.32	79.30	−0.04
12 T 14	75.81	0.35	B & G	75.71	0.13	75.74	0.10
12 T 22	72.62	0.35	B & G	72.85	−0.32	72.94	−0.43
13 T 15	70.04	0.35	B & G	69.93	0.17	70.00	0.06
13 T 24	67.02	0.35	B & G	67.19	−0.27	67.20	−0.27
14 T 16	65.10	0.34	B & G	64.98	0.18	64.89	0.32
14 T 25	62.52	0.34	B & G	62.68	−0.25	62.60	−0.13
15 T 17	60.80	0.34	B & G	60.70	0.16	60.70	0.16
15 T 27	58.33	0.34	B & G	58.46	−0.23	58.49	−0.28
16 T 18	57.03	0.34	B & G	56.93	0.16	56.93	0.16
16 T 29	54.67	0.34	B & G	54.77	−0.18	54.72	−0.09
17 T 20	53.54	0.34	B & G	53.45	0.17	53.36	0.34
17 T 31	51.45	0.34	B & G	51.51	−0.12	51.44	0.01
18 T 21	50.59	0.33	B & G	50.51	0.14	50.52	0.13
18 T 33	48.58	0.33	B & G	48.64	−0.12	48.70	0.25
0 S 2	3233.26	0.06	DERR	3232.35	0.03	3232.51	0.02
0 S 3	2133.58	0.11	DERR	2134.41	−0.04	2134.73	−0.05
0 S 4	1547.32	0.06	A1/2	1545.90	0.09	1546.25	0.07
0 S 5	1190.13	0.05	A1/2	1190.42	−0.02	1190.70	−0.05
0 S 6	963.18	0.05	A1/2	963.74	−0.06	963.92	−0.08
0 S 7	811.45	0.05	A1/2	812.38	−0.11	812.42	−0.12
0 S 8	707.64	0.05	A1/2	708.00	−0.05	707.92	−0.04
0 S 9	633.95	0.05	A1/2	634.13	−0.03	633.94	0.00
0 S 10	580.06	0.05	A1/2	579.72	0.06	579.50	0.10
0 S 11	536.98	0.06	T.R.	537.42	−0.08	537.21	−0.04
0 S 12	502.33	0.06	T.R.	502.87	−0.11	502.69	−0.07
0 S 13	473.17	0.06	T.R.	473.69	−0.11	473.54	−0.08
0 S 14	448.29	0.05	A1/2	448.52	−0.05	448.41	−0.03

mode			observation period (s)	observation error (%)	observation source	model 1066A period (s)	model 1066A diff. (%)	model 1066B period (s)	model 1066B diff. (%)
0	S	16	406.78	0.05	A1/2	407.09	−0.08	407.04	−0.06
0	S	17	389.32	0.05	A1/2	389.80	−0.12	389.77	−0.12
0	S	18	374.02	0.05	MEND	374.29	−0.07	374.29	−0.07
0	S	19	360.23	0.06	T.R.	360.30	−0.02	360.31	−0.02
0	S	20	347.69	0.06	T.R.	347.59	0.03	347.61	0.02
0	S	21	336.00	0.05	A1/2	335.99	0.00	336.01	−0.00
0	S	22	325.30	0.05	A1/2	325.32	−0.01	325.35	−0.02
0	S	23	315.44	0.05	A1/2	315.48	−0.01	315.50	−0.02
0	S	24	306.29	0.05	MEND	306.34	−0.02	306.36	−0.02
0	S	25	297.72	0.06	T.R.	297.82	−0.03	297.84	−0.04
0	S	26	289.69	0.05	A1/2	289.84	−0.05	289.86	0.06
0	S	27	282.34	0.05	A1/2	282.35	−0.00	282.37	−0.01
0	S	28	275.20	0.06	T.R.	275.28	−0.03	275.30	−0.03
0	S	29	268.45	0.06	T.R.	268.60	−0.05	268.61	−0.06
0	S	30	262.15	0.05	A1/2	262.26	−0.04	262.27	−0.05
0	S	31	256.07	0.06	T.R.	256.24	−0.07	256.24	−0.07
0	S	32	250.34	0.06	T.R.	250.50	−0.07	250.50	−0.07
0	S	33	244.95	0.06	T.R.	245.02	−0.03	245.02	−0.03
0	S	34	239.70	0.05	A1/2	239.79	−0.04	239.78	−0.04
0	S	35	234.69	0.05	A1/2	234.77	−0.03	234.77	−0.03
0	S	36	229.86	0.06	T.R.	229.96	−0.04	229.96	−0.04
0	S	37	225.22	0.05	MEND	225.34	−0.05	225.34	−0.05
0	S	38	220.75	0.06	T.R.	220.90	−0.07	220.90	−0.07
0	S	39	216.48	0.05	MEND	216.63	−0.07	216.63	−0.07
0	S	40	212.41	0.06	T.R.	212.51	−0.05	212.52	−0.05
0	S	41	208.39	0.06	T.R.	208.54	−0.07	208.55	−0.08
0	S	42	204.58	0.05	MEND	204.72	−0.07	204.73	−0.07
0	S	43	200.93	0.05	MEND	201.02	−0.04	201.04	−0.05
0	S	44	197.40	0.05	MEND	197.45	−0.03	197.47	−0.04
0	S	45	194.03	0.05	A1/2	194.00	0.02	194.02	0.01
0	S	46	190.62	0.05	MEND	190.66	−0.02	190.68	−0.03
0	S	47	187.43	0.05	A1/2	187.42	0.00	187.46	−0.01
0	S	48	184.29	0.08	MEND	184.29	−0.00	184.33	−0.02
0	S	49	181.30	0.06	A1/2	181.26	0.02	181.30	0.00
0	S	50	178.35	0.06	MEND	178.32	0.02	178.36	−0.01
0	S	51	175.41	0.06	T.R.	175.47	−0.03	175.52	−0.06
0	S	52	172.56	0.06	T.R.	172.70	−0.08	172.75	−0.11
0	S	53	170.07	0.09	T.R.	170.01	0.03	170.07	−0.00
0	S	54	167.37	0.05	MEND	167.40	−0.02	167.47	−0.06
0	S	55	164.84	0.05	MEND	164.87	−0.02	164.93	−0.06
0	S	56	162.41	0.09	T.R.	162.40	0.00	162.47	0.04
0	S	57	160.24	0.09	T.R.	160.01	0.15	160.08	0.10
0	S	58	157.69	0.09	T.R.	157.68	0.01	157.76	−0.04
0	S	59	155.58	0.09	T.R.	155.41	0.11	155.49	0.06
0	S	60	153.39	0.09	T.R.	153.20	0.12	153.29	0.07
0	S	61	151.19	0.09	T.R.	151.06	0.09	151.14	0.03
0	S	62	149.21	0.09	T.R.	148.96	0.16	149.05	0.10
0	S	63	147.12	0.09	T.R.	146.92	0.13	147.02	0.07

mode			observation period (s)	observation error (%)	observation source	model 1066A period (s)	model 1066A diff. (%)	model 1066B period (s)	model 1066B diff. (%)
0	S	64	144.96	0.09	T.R.	144.94	0.02	145.03	−0.05
0	S	65	142.99	0.09	T.R.	143.00	−0.01	143.10	−0.07
0	S	66	141.22	0.09	T.R.	141.11	0.08	141.21	0.01
1	S	2	1470.85	0.08	A1/2	1470.27	0.04	1469.13	0.12
1	S	3	1060.83	0.09	A1/2	1063.45	−0.25	1062.65	−0.17
1	S	4	852.67	0.05	A1/2	852.09	0.07	851.46	0.14
1	S	5	730.56	0.06	A1/2	729.36	0.16	728.89	0.23
1	S	6	657.61	0.05	A1/2	656.98	0.10	656.74	0.13
1	S	7	603.92	0.05	A1/2	604.27	−0.06	604.26	−0.06
1	S	8	556.03	0.09	T.R.	556.14	−0.02	556.32	−0.05
1	S	9	509.96	0.05	A1/2	509.68	0.05	509.99	−0.01
1	S	10	465.46	0.06	A1/2	465.95	−0.11	466.34	−0.19
1	S	14	337.01	0.05	A1/2	336.45	0.17	336.73	0.08
1	S	15	316.06	0.05	A1/2	315.50	0.18	315.59	0.15
1	S	16	299.50	0.09	T.R.	299.42	0.03	299.36	0.05
1	S	17	285.96	0.05	A1/2	286.09	−0.04	286.00	−0.01
1	S	18	274.75	0.10	MEND	274.25	0.18	274.15	0.22
1	S	19	263.63	0.09	T.R.	263.51	0.05	263.41	0.09
1	S	20	253.97	0.09	T.R.	253.66	0.12	253.56	0.16
1	S	21	244.93	0.09	T.R.	244.58	0.14	244.48	0.18
1	S	22	236.21	0.09	T.R.	236.16	0.02	236.07	0.06
1	S	23	228.42	0.09	T.R.	228.34	0.03	228.26	0.07
1	S	24	220.99	0.09	T.R.	221.05	−0.03	220.97	0.01
1	S	25	214.44	0.09	T.R.	214.24	0.10	214.16	0.13
1	S	26	207.71	0.09	T.R.	207.85	−0.07	207.79	−0.04
1	S	27	201.70	0.09	T.R.	201.87	−0.08	201.81	−0.05
1	S	28	196.31	0.09	T.R.	196.24	0.04	196.19	0.06
1	S	29	190.89	0.06	MEND	190.95	−0.03	190.91	−0.01
1	S	30	185.94	0.09	T.R.	185.96	−0.01	185.93	0.01
1	S	32	176.71	0.13	T.R.	176.80	−0.05	176.79	−0.04
1	S	33	172.34	0.13	T.R.	172.59	−0.15	172.59	−0.15
1	S	34	168.30	0.13	T.R.	168.61	−0.18	168.62	−0.19
1	S	35	164.60	0.13	T.R.	164.83	−0.14	164.85	−0.15
1	S	36	161.35	0.05	MEND	161.25	0.07	161.28	0.04
1	S	37	157.67	0.13	T.R.	157.84	−0.11	157.88	−0.14
1	S	38	154.69	0.09	T.R.	154.60	0.06	154.66	0.02
1	S	39	151.48	0.05	MEND	151.52	−0.03	151.58	−0.07
1	S	40	148.61	0.09	T.R.	148.59	0.02	148.65	−0.03
1	S	41	145.83	0.05	MEND	145.79	0.03	145.86	−0.02
1	S	42	143.17	0.09	T.R.	143.11	0.04	143.19	−0.02
1	S	43	140.61	0.09	T.R.	140.55	0.04	140.64	−0.02
1	S	44	138.25	0.09	T.R.	138.11	0.10	138.20	0.03
1	S	47	131.50	0.13	T.R.	131.36	0.11	131.47	0.02
1	S	48	129.18	0.13	T.R.	129.29	−0.08	129.40	−0.17
1	S	49	127.14	0.13	T.R.	127.29	−0.12	127.41	−0.21
1	S	50	125.39	0.23	MEND	125.37	0.01	125.50	−0.08
1	S	52	121.68	0.13	T.R.	121.74	−0.05	121.87	−0.15

TABLE 7 (cont.)

mode			observation period (s)	observation error (%)	observation source	model 1066A period (s)	model 1066A diff. (%)	model 1066B period (s)	model 1066B diff. (%)
1	S	53	120.07	0.05	MEND	120.01	0.05	120.14	−0.06
1	S	54	118.50	0.13	T.R.	118.35	0.13	118.48	0.02
1	S	55	116.81	0.13	T.R.	116.73	0.07	116.87	−0.05
1	S	56	115.32	0.13	T.R.	115.17	0.13	115.31	0.01
1	S	58	112.25	0.13	T.R.	112.19	0.05	112.32	−0.07
1	S	59	110.91	0.13	T.R.	110.76	0.13	110.90	0.01
1	S	61	108.06	0.13	T.R.	108.04	0.02	108.17	−0.10
1	S	63	105.69	0.13	T.R.	105.45	0.23	105.58	0.10
1	S	64	104.41	0.13	T.R.	104.21	0.19	104.34	0.06
1	S	68	99.71	0.13	T.R.	99.56	0.16	99.68	0.03
1	S	75	92.48	0.13	T.R.	92.39	0.09	92.51	−0.03
2	S	3	804.17	0.06	A1/2	805.77	−0.20	805.22	−0.13
2	S	4	724.87	0.05	A1/2	725.85	−0.14	725.49	−0.09
2	S	5	660.41	0.05	A1/2	660.73	−0.05	660.53	−0.02
2	S	6	595.00	0.13	MEND	595.22	−0.04	595.03	−0.01
2	S	7	535.70	0.13	T.R.	536.26	−0.11	536.07	−0.07
2	S	8	488.01	0.05	A1/2	487.95	0.01	487.78	0.05
2	S	9	448.35	0.05	A1/2	448.59	−0.05	448.43	−0.02
2	S	10	415.91	0.18	MEND	416.04	−0.03	415.90	0.00
2	S	11	388.28	0.06	A1/2	388.65	−0.09	388.53	−0.06
2	S	12	365.13	0.05	A1/2	365.20	−0.02	365.10	0.01
2	S	13	344.72	0.09	T.R.	344.76	−0.01	344.69	0.01
2	S	14	326.59	0.09	T.R.	326.46	0.04	326.44	0.04
2	S	15	309.20	0.05	A1/2	308.94	0.08	309.09	0.03
2	S	26	179.24	0.06	T.R.	179.22	0.01	179.25	−0.00
2	S	27	174.03	0.06	T.R.	174.11	−0.04	174.09	−0.03
2	S	28	169.33	0.06	T.R.	169.35	−0.01	169.33	0.00
2	S	29	164.87	0.06	T.R.	164.86	0.00	164.84	0.02
2	S	30	160.55	0.05	MEND	160.63	−0.05	160.61	−0.04
2	S	31	156.62	0.06	MEND	156.62	−0.00	156.60	0.01
2	S	32	152.68	0.24	MEND	152.83	−0.10	152.81	−0.09
2	S	33	149.17	0.10	MEND	149.23	−0.04	149.22	−0.03
2	S	34	145.95	0.06	T.R.	145.82	0.09	145.80	0.10
2	S	35	142.61	0.05	MEND	142.57	0.03	142.56	0.03
2	S	36	139.51	0.05	MEND	139.48	0.02	139.47	0.03
2	S	37	136.65	0.05	MEND	136.54	0.08	136.53	0.09
2	S	38	133.86	0.08	MEND	133.73	0.09	133.73	0.10
2	S	39	131.08	0.06	T.R.	131.06	0.02	131.06	0.02
2	S	40	128.54	0.05	MEND	128.50	0.03	128.50	0.03
2	S	42	123.84	0.06	T.R.	123.71	0.11	123.71	0.10
2	S	43	121.65	0.06	T.R.	121.46	0.16	121.47	0.15
2	S	44	119.49	0.06	T.R.	119.31	0.16	119.32	0.15
2	S	45	117.34	0.06	T.R.	117.24	0.09	117.25	0.08
2	S	46	115.33	0.06	T.R.	115.25	0.07	115.26	0.06
2	S	48	111.87	0.26	T.R.	111.50	0.34	111.52	0.32
2	S	49	110.07	0.26	T.R.	109.72	0.31	109.75	0.29

mode			observation period (s)	observation error (%)	observation source	model 1066A period (s)	model 1066A diff. (%)	model 1066B period (s)	model 1066B diff. (%)
2	S	51	106.71	0.26	T.R.	106.37	0.32	106.39	0.30
2	S	57	98.04	0.26	T.R.	97.60	0.45	97.64	0.41
2	S	58	96.61	0.26	T.R.	96.31	0.31	96.34	0.28
2	S	59	95.29	0.26	T.R.	95.05	0.25	95.09	0.21
2	S	60	94.14	0.26	T.R.	93.84	0.32	93.88	0.28
2	S	62	91.76	0.26	T.R.	91.52	0.26	91.56	0.21
2	S	63	90.59	0.26	T.R.	90.41	0.19	90.46	0.14
2	S	64	89.66	0.26	T.R.	89.34	0.36	89.39	0.30
2	S	65	88.65	0.26	T.R.	88.30	0.39	88.35	0.34
2	S	66	87.66	0.28	T.R.	87.29	0.42	87.35	0.36
2	S	67	86.51	0.26	T.R.	86.31	0.23	86.37	0.16
2	S	71	82.97	0.26	T.R.	82.67	0.37	82.74	0.28
2	S	72	82.02	0.26	T.R.	81.82	0.25	81.89	0.15
2	S	74	80.53	0.26	T.R.	80.18	0.43	80.27	0.32
2	S	76	78.89	0.26	T.R.	78.64	0.32	78.73	0.20
3	S	1	1058.10	0.08	A1/2	1061.19	−0.29	1059.55	−0.14
3	S	2	904.22	0.05	A1/2	903.36	0.10	904.22	0.00
3	S	6	392.33	0.05	A1/2	392.20	0.03	392.14	0.05
3	S	7	372.05	0.05	A1/2	372.21	−0.04	372.18	−0.03
3	S	8	354.56	0.05	A1/2	354.57	−0.00	354.57	−0.00
3	S	9	338.90	0.08	T.R.	338.69	0.06	338.72	0.05
3	S	10	323.94	0.05	MEND	324.06	−0.04	324.11	−0.05
3	S	11	310.27	0.08	T.R.	310.34	−0.02	310.40	−0.04
3	S	12	297.41	0.08	T.R.	297.36	0.02	297.43	−0.00
3	S	13	285.08	0.08	T.R.	285.06	0.01	285.13	−0.02
3	S	14	273.35	0.05	MEND	273.42	−0.03	273.49	−0.05
3	S	15	262.47	0.05	MEND	262.45	0.01	262.50	−0.01
3	S	16	251.98	0.05	MEND	252.12	−0.06	252.17	−0.07
3	S	17	242.43	0.05	MEND	242.45	−0.00	242.48	−0.02
3	S	18	233.29	0.05	MEND	233.39	−0.04	233.42	−0.06
3	S	19	224.91	0.05	MEND	224.92	−0.00	224.94	−0.01
3	S	20	217.04	0.08	T.R.	217.01	0.01	217.03	0.01
3	S	21	209.56	0.05	MEND	209.62	−0.03	209.62	−0.03
3	S	22	202.77	0.08	T.R.	202.70	0.03	202.70	0.03
3	S	23	196.28	0.08	T.R.	196.22	0.03	196.22	0.03
3	S	24	190.07	0.05	MEND	190.15	−0.04	190.14	−0.04
3	S	25	184.32	0.08	T.R.	184.43	−0.06	184.42	0.05
3	S	41	113.38	0.05	MEND	113.41	−0.03	113.38	0.00
3	S	42	111.45	0.05	MEND	111.43	0.02	111.40	0.04
3	S	43	109.48	0.07	MEND	109.53	−0.04	109.49	−0.01
3	S	44	107.75	0.08	T.R.	107.70	0.05	107.66	0.08
3	S	45	105.98	0.09	MEND	105.93	0.05	105.89	0.08
3	S	46	104.20	0.10	MEND	104.23	−0.02	104.19	0.01
3	S	47	102.59	0.07	MEND	102.58	0.01	102.54	0.04
3	S	48	101.00	0.08	T.R.	100.99	0.01	100.96	0.04
3	S	49	99.46	0.08	MEND	99.45	0.01	99.42	0.04

mode	observation period (s)	observation error (%)	observation source	model 1066A period (s)	model 1066A diff. (%)	model 1066B period (s)	model 1066B diff. (%)
3 S 51	96.44	0.07	MEND	96.53	−0.09	96.50	−0.06
3 S 52	94.96	0.05	MEND	95.14	−0.19	95.11	−0.16
3 S 53	93.73	0.08	T.R.	93.79	−0.06	93.76	−0.03
3 S 54	92.39	0.08	T.R.	92.48	−0.10	92.46	−0.07
3 S 56	90.10	0.05	MEND	89.98	0.13	89.97	0.15
3 S 57	88.72	0.13	T.R.	88.79	−0.08	88.78	−0.06
3 S 58	87.65	0.05	MEND	87.64	0.02	87.62	0.03
3 S 63	82.38	0.13	T.R.	82.33	0.06	82.33	0.06
3 S 67	78.76	0.13	T.R.	78.59	0.22	78.59	0.22
3 S 70	76.11	0.13	T.R.	76.03	0.11	76.03	0.11
3 S 73	73.78	0.13	T.R.	73.66	0.17	73.64	0.19
3 S 75	72.12	0.13	T.R.	72.17	−0.07	72.14	−0.03
4 S 2	580.81	0.12	A1/2	580.88	−0.01	580.76	0.01
4 S 3	489.04	0.07	A1/2	488.42	0.13	488.35	0.14
4 S 4	439.17	0.11	A1/2	438.63	0.12	438.52	0.15
4 S 5	414.62	0.06	T.R.	414.68	−0.01	414.60	0.01
4 S 9	269.59	0.06	T.R.	269.54	0.02	269.62	−0.01
4 S 10	258.85	0.05	A1/2	258.73	0.05	258.77	0.03
4 S 11	249.38	0.06	T.R.	249.34	0.02	249.35	0.01
4 S 12	240.78	0.06	T.R.	240.78	−0.00	240.79	−0.00
4 S 13	232.75	0.06	T.R.	232.80	−0.02	232.80	−0.02
4 S 14	225.08	0.06	T.R.	225.25	−0.08	225.25	−0.07
4 S 15	218.17	0.05	A1/2	218.05	0.06	218.04	0.06
4 S 16	211.24	0.06	T.R.	211.14	0.05	211.13	0.05
4 S 17	204.66	0.06	T.R.	204.51	0.07	204.50	0.08
4 S 18	198.16	0.06	T.R.	198.15	0.00	198.14	0.01
4 S 19	191.96	0.06	T.R.	192.07	−0.06	192.05	−0.05
4 S 20	186.33	0.06	T.R.	186.25	0.04	186.24	0.05
4 S 24	165.68	0.06	T.R.	165.71	−0.02	165.69	−0.01
4 S 30	141.97	0.06	T.R.	142.03	−0.04	142.01	−0.03
4 S 31	138.72	0.06	T.R.	138.76	−0.03	138.74	−0.02
4 S 32	135.65	0.05	MEND	135.65	−0.00	135.64	0.01
4 S 33	132.70	0.06	T.R.	132.70	0.00	132.68	0.01
4 S 34	129.93	0.05	MEND	129.88	0.04	129.86	0.05
4 S 35	127.24	0.05	MEND	127.20	0.03	127.18	0.05
4 S 36	124.66	0.06	T.R.	124.64	0.01	124.62	0.03
4 S 37	122.19	0.06	T.R.	122.20	−0.00	122.17	0.02
4 S 38	119.84	0.05	MEND	119.86	−0.01	119.83	0.01
4 S 39	117.61	0.05	MEND	117.62	−0.01	117.59	0.02
4 S 40	115.44	0.06	MEND	115.47	−0.03	115.44	−0.00
4 S 62	77.77	0.13	T.R.	77.66	0.14	77.61	0.21
4 S 63	76.65	0.13	T.R.	76.72	−0.09	76.67	−0.02
5 S 2	479.34	0.05	A1/2	477.98	0.28	477.90	0.30
5 S 3	460.78	0.05	A1/2	460.72	0.01	460.63	0.03
5 S 4	420.36	0.06	T.R.	420.53	−0.04	420.54	−0.04
5 S 5	370.10	0.06	T.R.	370.09	0.00	370.15	−0.01
5 S 6	332.11	0.05	A1/2	332.19	−0.02	332.30	−0.06
5 S 7	303.98	0.05	A1/2	303.78	0.06	303.94	0.01
5 S 8	283.56	0.05	A1/2	283.47	0.03	283.62	−0.02
5 S 10	237.63	0.05	A1/2	237.68	−0.02	237.71	−0.03
5 S 11	224.49	0.06	T.R.	224.53	−0.02	224.59	−0.04
5 S 12	213.03	0.05	A1/2	213.05	−0.01	213.12	−0.04
5 S 13	203.10	0.06	T.R.	203.16	−0.03	203.22	−0.06
5 S 14	194.61	0.05	A1/2	194.77	−0.08	194.80	−0.10
5 S 15	187.75	0.05	A1/2	187.72	0.02	187.72	0.01
5 S 16	181.74	0.06	T.R.	181.70	0.02	181.69	0.03
5 S 19	166.78	0.06	T.R.	166.87	−0.05	166.85	−0.04
5 S 20	162.45	0.06	T.R.	162.51	−0.03	162.49	−0.03
5 S 21	158.47	0.06	T.R.	158.35	0.08	158.35	0.08
5 S 23	150.57	0.06	T.R.	150.57	−0.00	150.59	−0.01
5 S 24	146.92	0.06	T.R.	146.94	−0.02	146.97	−0.03
5 S 25	143.59	0.05	MEND	143.48	0.08	143.51	0.06
5 S 26	140.23	0.06	T.R.	140.18	0.03	140.21	0.01
5 S 27	137.12	0.05	MEND	137.04	0.05	137.07	0.03
5 S 28	134.06	0.05	MEND	134.06	0.00	134.08	−0.02
5 S 29	131.18	0.05	MEND	131.22	−0.03	131.24	−0.04
5 S 30	128.51	0.06	T.R.	128.51	−0.00	128.53	−0.02
5 S 31	125.92	0.06	T.R.	125.93	−0.01	125.95	−0.02
5 S 32	123.43	0.05	MEND	123.47	−0.03	123.48	−0.04
5 S 33	121.03	0.05	MEND	121.12	−0.07	121.12	−0.08
5 S 34	118.77	0.05	MEND	118.86	−0.07	118.86	−0.08
5 S 35	116.66	0.06	T.R.	116.68	−0.02	116.69	−0.03
5 S 36	114.60	0.06	T.R.	114.59	0.01	114.60	0.00
5 S 37	112.57	0.06	T.R.	112.57	−0.00	112.58	−0.01
5 S 38	110.59	0.05	MEND	110.62	−0.02	110.63	−0.04
5 S 39	108.67	0.05	MEND	108.73	−0.05	108.75	−0.07
5 S 40	106.85	0.05	MEND	106.89	−0.04	106.92	−0.06
5 S 41	105.07	0.06	T.R.	105.11	−0.04	105.14	−0.07
5 S 42	103.37	0.06	T.R.	103.39	−0.02	103.42	−0.05
5 S 43	101.71	0.05	MEND	101.71	0.00	101.75	−0.03
5 S 44	100.10	0.06	T.R.	100.08	0.02	100.12	−0.02
5 S 45	98.45	0.06	T.R.	98.50	−0.05	98.54	−0.09
5 S 46	96.98	0.06	T.R.	96.96	0.02	97.00	−0.03
5 S 47	95.51	0.06	T.R.	95.47	0.04	95.51	−0.00
5 S 51	89.91	0.06	T.R.	89.93	−0.02	89.95	−0.05
6 S 1	505.81	0.05	A1/2	505.50	0.06	505.28	0.10
6 S 3	353.52	0.05	A1/2	354.60	−0.30	354.64	−0.32
6 S 9	252.63	0.09	T.R.	252.48	0.06	252.45	0.07
6 S 14	185.15	0.05	A1/2	184.95	0.10	184.98	0.09
6 S 15	178.76	0.09	T.R.	178.56	0.11	178.62	0.08
6 S 16	172.34	0.06	MEND	172.19	0.08	172.28	0.04
6 S 17	166.16	0.06	MEND	166.07	0.05	166.17	−0.01
6 S 18	160.39	0.09	T.R.	160.33	0.04	160.44	−0.03

TABLE 7 (cont.)

mode			observation period (s)	observation error (%)	observation source	model 1066A period (s)	model 1066A diff. (%)	model 1066B period (s)	model 1066B diff. (%)
6	S	19	154.97	0.05	MEND	155.04	−0.04	155.15	−0.11
6	S	20	150.17	0.06	T.R.	150.20	−0.02	150.30	−0.09
6	S	21	145.76	0.05	MEND	145.79	−0.02	145.89	−0.09
6	S	22	141.82	0.06	T.R.	141.80	0.02	141.88	−0.04
6	S	23	138.13	0.06	T.R.	138.16	−0.02	138.23	−0.07
6	S	24	134.85	0.06	T.R.	134.83	0.01	134.89	−0.03
6	S	25	131.78	0.05	MEND	131.75	0.02	131.80	−0.01
6	S	26	128.85	0.06	T.R.	128.86	−0.01	128.91	−0.05
6	S	27	125.98	0.06	T.R.	126.13	−0.12	126.18	−0.16
6	S	28	123.51	0.06	MEND	123.53	−0.02	123.58	−0.06
6	S	29	121.04	0.05	MEND	121.04	0.00	121.10	−0.05
6	S	30	118.75	0.09	T.R.	118.64	0.09	118.71	0.03
6	S	31	116.40	0.09	T.R.	116.33	0.06	116.41	−0.01
6	S	32	114.10	0.09	T.R.	114.10	−0.00	114.19	−0.08
6	S	33	112.06	0.09	T.R.	111.95	0.09	112.05	0.01
6	S	34	109.90	0.09	T.R.	109.88	0.02	109.98	−0.07
6	S	35	107.96	0.09	T.R.	107.88	0.07	107.98	−0.01
6	S	36	106.06	0.09	T.R.	105.95	0.10	106.04	0.01
6	S	37	104.18	0.09	T.R.	104.09	0.08	104.18	0.00
6	S	38	102.38	0.09	T.R.	102.30	0.08	102.38	0.00
6	S	39	100.68	0.09	T.R.	100.58	0.10	100.64	0.04
6	S	40	98.97	0.09	T.R.	98.92	0.05	98.96	0.01
6	S	41	97.47	0.09	T.R.	97.32	0.16	97.35	0.13
6	S	42	95.80	0.09	T.R.	95.78	0.03	95.79	0.01
6	S	43	94.32	0.09	T.R.	94.29	0.03	94.29	0.03
6	S	47	89.02	0.09	T.R.	88.87	0.17	88.81	0.24
6	S	48	87.62	0.09	T.R.	87.63	−0.01	87.56	0.07
6	S	49	86.41	0.09	T.R.	86.44	−0.03	86.36	0.06
6	S	51	84.07	0.09	T.R.	84.15	−0.10	84.08	−0.01
6	S	52	82.99	0.09	T.R.	83.06	−0.09	83.00	−0.01
6	S	53	81.93	0.09	T.R.	82.00	−0.09	81.95	−0.03
6	S	54	81.05	0.09	T.R.	80.97	0.10	80.94	0.14
6	S	55	79.95	0.09	T.R.	79.97	−0.02	79.95	−0.00
6	S	56	78.92	0.09	T.R.	78.99	−0.09	78.99	−0.09
6	S	57	77.97	0.09	T.R.	78.04	−0.09	78.06	−0.12
6	S	58	77.11	0.09	T.R.	77.11	0.00	77.15	−0.06
6	S	59	76.20	0.09	T.R.	76.20	−0.00	76.27	−0.09
6	S	60	75.33	0.09	T.R.	75.31	0.02	75.40	−0.09
6	S	61	74.46	0.09	T.R.	74.44	0.03	74.55	−0.12
7	S	2	397.37	0.05	A1/2	397.01	0.09	397.39	−0.00
7	S	4	293.20	0.05	A1/2	292.91	0.10	292.89	0.10
7	S	5	273.51	0.05	A1/2	273.38	0.05	273.43	0.03
7	S	6	252.71	0.13	T.R.	252.79	−0.03	252.87	−0.06
7	S	7	236.12	0.13	T.R.	236.10	0.01	236.17	−0.02
7	S	8	224.36	0.13	T.R.	224.65	−0.13	224.70	−0.15

mode			observation period (s)	observation error (%)	observation source	model 1066A period (s)	model 1066A diff. (%)	model 1066B period (s)	model 1066B diff. (%)
7	S	11	203.09	0.13	T.R.	203.50	−0.20	203.49	−0.20
7	S	12	197.12	0.13	T.R.	197.34	−0.11	197.33	−0.11
7	S	16	154.52	0.09	T.R.	154.78	−0.17	154.79	−0.17
7	S	18	147.82	0.09	T.R.	147.88	−0.04	147.90	−0.06
7	S	20	141.23	0.09	T.R.	141.28	−0.03	141.31	−0.06
7	S	21	138.06	0.09	T.R.	138.03	0.02	138.08	−0.02
7	S	22	134.81	0.09	T.R.	134.82	−0.01	134.88	−0.05
7	S	23	131.81	0.09	T.R.	131.64	0.13	131.71	0.08
7	S	24	128.57	0.09	T.R.	128.52	0.04	128.60	−0.02
7	S	25	125.48	0.09	T.R.	125.49	−0.01	125.57	−0.07
7	S	27	119.96	0.09	T.R.	119.77	0.16	119.85	0.10
7	S	28	117.21	0.09	T.R.	117.10	0.09	117.17	0.03
7	S	29	114.65	0.09	T.R.	114.57	0.07	114.63	0.02
7	S	30	112.16	0.09	T.R.	112.15	0.01	112.20	−0.04
7	S	33	105.75	0.09	T.R.	105.59	0.15	105.61	0.14
7	S	35	101.74	0.09	T.R.	101.71	0.03	101.70	0.04
7	S	36	99.98	0.09	T.R.	99.89	0.09	99.87	0.11
7	S	37	98.19	0.09	T.R.	98.15	0.04	98.12	0.07
7	S	38	96.51	0.09	T.R.	96.48	0.03	96.45	0.07
7	S	39	94.89	0.09	T.R.	94.88	0.01	94.84	0.05
7	S	41	91.72	0.09	T.R.	91.85	−0.14	91.82	−0.11
7	S	42	90.30	0.09	T.R.	90.42	−0.13	90.40	−0.11
7	S	43	88.99	0.09	T.R.	89.04	−0.05	89.03	−0.05
7	S	45	86.37	0.09	T.R.	86.41	−0.05	86.44	−0.08
7	S	46	85.13	0.09	T.R.	85.16	−0.04	85.21	−0.09
7	S	47	84.09	0.09	T.R.	83.95	0.17	84.01	0.09
7	S	48	82.76	0.09	T.R.	82.77	−0.02	82.86	−0.12
7	S	50	80.42	0.09	T.R.	80.53	−0.13	80.64	−0.28
7	S	52	78.34	0.09	T.R.	78.41	−0.08	78.55	−0.27
7	S	55	75.53	0.09	T.R.	75.45	0.11	75.60	−0.09
7	S	56	74.59	0.09	T.R.	74.52	0.10	74.66	−0.09
7	S	57	73.68	0.09	T.R.	73.61	0.09	73.74	−0.09
8	S	1	348.41	0.05	A1/2	348.33	0.02	348.31	0.03
8	S	5	239.96	0.05	A1/2	240.08	−0.05	240.12	−0.07
8	S	6	225.40	0.05	A1/2	225.53	−0.06	225.52	−0.05
8	S	7	215.13	0.05	A1/2	215.14	−0.01	215.13	−0.00
8	S	9	191.89	0.09	T.R.	192.03	−0.07	192.04	−0.08
8	S	15	158.50	0.09	T.R.	158.39	0.07	158.39	0.07
8	S	23	120.87	0.09	T.R.	120.76	0.09	120.77	0.09
8	S	24	118.67	0.09	T.R.	118.57	0.08	118.59	0.07
8	S	29	108.08	0.09	T.R.	108.07	0.01	108.15	−0.06
8	S	30	106.04	0.09	T.R.	106.06	−0.02	106.15	−0.10
8	S	32	102.20	0.09	T.R.	102.16	0.04	102.28	−0.07
8	S	38	91.81	0.09	T.R.	91.71	0.11	91.85	−0.04
8	S	41	87.28	0.09	T.R.	87.23	0.05	87.36	−0.10

mode			observation period (s)	observation error (%)	observation source	model 1066A period (s)	model 1066A diff. (%)	model 1066B period (s)	model 1066B diff. (%)
8	S	48	78.57	0.09	T.R.	78.53	0.05	78.57	−0.00
8	S	51	75.51	0.09	T.R.	75.42	0.12	75.41	0.13
8	S	52	74.60	0.09	T.R.	74.45	0.20	74.43	0.23
9	S	2	310.04	0.09	T.R.	309.20	0.27	309.18	0.28
9	S	3	281.42	0.09	T.R.	281.37	0.02	281.48	−0.02
9	S	4	258.10	0.09	T.R.	257.65	0.18	258.03	0.03
9	S	6	216.45	0.05	A1/2	216.42	0.02	216.39	0.03
9	S	7	205.26	0.05	A1/2	205.28	−0.01	205.24	0.01
9	S	8	194.22	0.09	T.R.	194.46	−0.12	194.42	−0.10
9	S	10	178.72	0.09	T.R.	178.37	0.19	178.41	0.17
9	S	11	170.05	0.09	T.R.	170.02	0.02	170.09	−0.03
9	S	12	161.64	0.05	A1/2	161.69	−0.03	161.75	−0.07
9	S	13	154.30	0.09	T.R.	154.26	0.02	154.32	−0.02
9	S	14	147.81	0.05	A1/2	147.75	0.04	147.81	0.00
9	S	15	142.25	0.05	A1/2	142.25	−0.00	142.29	−0.03
9	S	16	137.91	0.09	T.R.	138.14	−0.17	138.16	−0.18
9	S	18	132.47	0.09	T.R.	132.44	0.03	132.44	0.02
9	S	19	129.87	0.09	T.R.	129.95	−0.06	129.95	−0.06
9	S	23	110.56	0.09	T.R.	110.62	−0.05	110.65	−0.08
9	S	29	100.32	0.09	T.R.	100.25	0.07	100.29	0.03
9	S	35	91.16	0.09	T.R.	91.17	−0.01	91.17	−0.01
9	S	37	88.49	0.09	T.R.	88.38	0.13	88.37	0.13
9	S	38	87.07	0.09	T.R.	87.03	0.05	87.03	0.05
10	S	2	247.74	0.05	A1/2	247.86	−0.05	248.44	−0.28
10	S	10	161.65	0.05	A1/2	161.63	0.01	161.62	0.02
10	S	13	145.46	0.09	T.R.	145.48	−0.01	145.52	−0.04
10	S	14	142.06	0.06	T.R.	142.07	−0.00	142.11	−0.03
10	S	15	138.77	0.06	T.R.	138.69	0.05	138.74	0.02
10	S	16	134.95	0.05	A1/2	134.69	0.19	134.74	0.15
10	S	17	130.31	0.05	A1/2	130.25	0.05	130.29	0.02
10	S	18	125.94	0.05	A1/2	125.93	0.01	125.97	−0.02
10	S	19	121.95	0.06	T.R.	121.95	0.00	121.97	−0.02
10	S	20	118.35	0.06	T.R.	118.32	0.03	118.33	0.01
10	S	21	115.20	0.06	T.R.	115.24	−0.03	115.25	−0.04
10	S	25	101.73	0.09	T.R.	101.85	−0.12	101.86	−0.12
10	S	26	99.63	0.09	T.R.	99.55	0.08	99.53	0.10
10	S	28	95.58	0.09	T.R.	95.61	−0.03	95.57	0.01
10	S	29	93.90	0.09	T.R.	93.95	−0.05	93.90	−0.00
10	S	31	91.14	0.09	T.R.	91.03	0.13	90.98	0.17
10	S	32	89.78	0.09	T.R.	89.69	0.11	89.65	0.14
10	S	34	87.21	0.09	T.R.	87.15	0.07	87.14	0.07
10	S	36	84.86	0.09	T.R.	84.75	0.13	84.78	0.10
10	S	37	83.58	0.09	T.R.	83.58	−0.00	83.63	−0.06
10	S	41	79.18	0.09	T.R.	79.15	0.04	79.28	−0.13
10	S	42	78.04	0.09	T.R.	78.10	−0.07	78.24	−0.26
10	S	44	76.05	0.09	T.R.	76.05	−0.00	76.22	−0.22

mode			observation period (s)	observation error (%)	observation source	model 1066A period (s)	model 1066A diff. (%)	model 1066B period (s)	model 1066B diff. (%)
11	S	1	271.36	0.09	T.R.	271.30	0.02	271.58	−0.08
11	S	2	246.89	0.05	A1/2	244.68	0.90	247.03	−0.06
11	S	3	224.01	0.09	T.R.	224.06	−0.02	224.13	−0.05
11	S	4	209.62	0.05	A1/2	209.81	−0.09	209.89	−0.13
11	S	5	197.19	0.09	T.R.	197.13	0.03	197.17	0.01
11	S	6	186.88	0.05	A1/2	186.95	−0.03	186.93	−0.02
11	S	7	179.70	0.13	T.R.	179.54	0.09	179.77	−0.04
11	S	8	163.26	0.13	T.R.	163.40	−0.09	163.01	0.15
11	S	9	155.44	0.05	A1/2	155.38	0.04	155.42	0.01
11	S	10	149.03	0.05	A1/2	148.98	0.04	149.01	0.02
11	S	13	134.99	0.09	T.R.	134.90	0.07	134.90	0.07
11	S	15	126.44	0.09	T.R.	126.30	0.11	126.33	0.09
11	S	16	123.22	0.09	T.R.	123.33	−0.09	123.37	−0.12
11	S	17	120.89	0.09	T.R.	120.91	−0.02	120.95	−0.05
11	S	21	112.16	0.09	T.R.	112.26	−0.09	112.33	−0.15
11	S	22	109.66	0.09	T.R.	109.70	−0.03	109.75	−0.08
11	S	23	107.15	0.09	T.R.	107.00	0.14	107.04	0.11
11	S	24	104.31	0.05	A1/2	104.35	−0.04	104.37	−0.06
11	S	31	87.29	0.09	T.R.	87.34	−0.05	87.38	−0.11
11	S	32	85.78	0.09	T.R.	85.75	0.03	85.78	0.00
11	S	33	84.11	0.09	T.R.	84.26	−0.18	84.28	−0.20
11	S	34	82.87	0.09	T.R.	82.88	−0.01	82.89	−0.02
11	S	35	81.45	0.09	T.R.	81.60	−0.19	81.61	−0.19
11	S	37	79.15	0.09	T.R.	79.30	−0.19	79.31	−0.20
11	S	39	77.24	0.09	T.R.	77.22	0.02	77.25	−0.01
11	S	40	76.21	0.09	T.R.	76.24	−0.04	76.26	−0.07
11	S	41	75.21	0.09	T.R.	75.29	−0.10	75.31	−0.13
11	S	43	73.39	0.09	T.R.	73.44	−0.07	73.46	−0.09
11	S	44	72.53	0.09	T.R.	73.54	−0.02	72.56	−0.04
11	S	46	70.68	0.09	T.R.	70.80	−0.17	70.81	−0.19
11	S	47	69.99	0.09	T.R.	69.95	0.06	69.96	0.04
12	S	7	170.69	0.05	A1/2	170.70	−0.01	170.81	−0.07
12	S	10	145.67	0.06	T.R.	145.81	−0.10	145.80	−0.09
12	S	11	140.17	0.05	A1/2	140.21	−0.03	140.19	−0.01
12	S	12	134.25	0.06	T.R.	134.27	−0.01	134.26	−0.00
12	S	13	128.70	0.06	T.R.	128.70	−0.00	128.70	0.00
12	S	14	123.64	0.05	A1/2	123.59	0.04	123.59	0.04
12	S	15	118.93	0.05	A1/2	118.87	0.05	118.88	0.04
12	S	16	115.07	0.09	T.R.	114.99	0.07	115.00	0.06
12	S	17	111.79	0.09	T.R.	111.88	−0.08	111.91	−0.11
12	S	18	109.39	0.09	T.R.	109.28	0.11	109.33	0.05
12	S	22	102.08	0.09	T.R.	101.96	0.11	102.05	0.03
12	S	23	100.48	0.09	T.R.	100.41	0.07	100.50	−0.02
12	S	26	95.80	0.09	T.R.	95.76	0.04	95.85	−0.05
12	S	33	81.43	0.09	T.R.	81.32	0.13	81.38	0.06
13	S	1	222.69	0.09	T.R.	222.48	0.09	222.57	0.06

TABLE 7 (*cont.*)

mode			observation period (s)	observation error (%)	observation source	model 1066A period (s)	model 1066A diff. (%)	model 1066B period (s)	model 1066B diff. (%)
13	S	2	206.42	0.05	A1/2	206.50	−0.04	206.53	−0.05
13	S	3	192.55	0.05	A1/2	192.67	−0.06	192.63	−0.04
13	S	5	170.74	0.13	T.R.	171.22	−0.28	171.74	−0.58
13	S	6	162.45	0.05	A1/2	162.40	0.03	162.41	0.02
13	S	8	152.39	0.13	T.R.	152.59	−0.13	152.58	−0.13
13	S	12	125.76	0.13	T.R.	125.58	0.14	125.58	0.14
13	S	13	123.21	0.13	T.R.	123.48	−0.22	123.47	−0.21
13	S	14	120.96	0.13	T.R.	121.02	−0.05	121.01	−0.04
13	S	17	110.19	0.05	A1/2	110.30	−0.10	110.33	−0.12
13	S	18	106.77	0.13	T.R.	106.63	0.13	106.66	0.10
13	S	19	103.36	0.13	T.R.	103.29	0.07	103.32	0.04
13	S	21	97.65	0.13	T.R.	97.61	0.04	97.63	0.02
13	S	22	95.32	0.13	T.R.	95.34	−0.02	95.35	−0.03
13	S	23	93.62	0.13	T.R.	93.48	0.15	93.50	0.13
13	S	25	90.52	0.13	T.R.	90.61	−0.10	90.63	−0.12
13	S	26	89.31	0.13	T.R.	89.36	−0.06	89.38	−0.08
13	S	27	88.02	0.13	T.R.	88.17	−0.17	88.19	−0.20
13	S	29	85.94	0.13	T.R.	85.88	0.07	85.91	0.04
13	S	37	73.52	0.13	T.R.	73.48	0.06	73.52	0.01
13	S	38	72.74	0.13	T.R.	72.60	0.19	72.64	0.14
14	S	4	180.81	0.13	T.R.	180.47	0.19	180.54	0.15
14	S	7	147.79	0.05	A1/2	147.71	0.05	147.73	0.04
14	S	8	141.97	0.05	A1/2	142.01	−0.03	142.02	−0.03
14	S	9	136.09	0.05	A1/2	136.10	−0.01	136.10	−0.01
14	S	10	131.27	0.13	T.R.	131.01	0.20	131.02	0.19
14	S	13	114.53	0.05	A1/2	114.42	0.10	114.41	0.11
14	S	17	104.97	0.09	T.R.	104.82	0.14	104.88	0.08
14	S	19	99.97	0.09	T.R.	99.94	0.03	100.03	−0.06
14	S	23	91.18	0.09	T.R.	91.19	−0.01	91.27	−0.10
14	S	25	87.15	0.09	T.R.	87.14	0.01	87.16	−0.01
14	S	28	82.07	0.09	T.R.	82.12	−0.06	82.05	0.02
14	S	31	78.89	0.09	T.R.	78.83	0.08	78.80	0.11
15	S	3	165.83	0.05	A1/2	165.87	−0.02	165.80	0.02
15	S	11	122.85	0.09	T.R.	122.93	−0.06	122.92	−0.06
15	S	12	118.58	0.05	A1/2	118.50	0.07	118.50	0.07
15	S	14	107.15	0.09	T.R.	107.18	−0.02	107.30	−0.14
15	S	15	103.97	0.09	T.R.	103.99	−0.02	104.09	−0.11
15	S	16	100.57	0.09	T.R.	100.64	−0.07	100.70	−0.12
15	S	18	96.03	0.09	T.R.	95.99	0.04	96.05	−0.02
15	S	20	92.69	0.09	T.R.	92.83	−0.16	92.87	−0.19
15	S	21	91.13	0.09	T.R.	91.01	0.13	91.03	0.10
15	S	24	85.73	0.09	T.R.	85.58	0.18	85.58	0.18
15	S	28	80.39	0.09	T.R.	80.39	−0.01	80.39	−0.01
15	S	30	77.63	0.09	T.R.	77.61	0.02	77.58	0.06
16	S	2	175.29	0.05	A1/2	175.25	0.02	175.81	−0.30
16	S	5	146.34	0.05	A1/2	146.40	−0.04	146.36	−0.02
16	S	6	139.87	0.05	A1/2	139.86	0.01	139.86	0.01
16	S	7	133.90	0.09	T.R.	133.79	0.08	133.82	0.06
16	S	9	123.05	0.09	T.R.	123.13	−0.06	123.20	−0.12
16	S	10	118.53	0.09	T.R.	118.37	0.14	118.43	0.08
16	S	18	94.00	0.09	T.R.	94.02	−0.02	94.02	−0.02
16	S	19	91.18	0.09	T.R.	91.28	−0.11	91.23	−0.05
16	S	20	88.61	0.09	T.R.	88.75	−0.16	88.66	−0.06
16	S	25	80.23	0.09	T.R.	80.33	−0.13	80.29	−0.08
16	S	26	78.81	0.09	T.R.	78.87	−0.07	78.85	−0.05
16	S	31	73.61	0.09	T.R.	73.56	0.07	73.59	0.02
16	S	33	71.86	0.09	T.R.	71.75	0.16	71.74	0.17
17	S	12	109.11	0.09	T.R.	109.23	−0.11	109.24	−0.12
17	S	13	105.93	0.09	T.R.	105.97	−0.03	105.99	−0.05
17	S	14	102.96	0.09	T.R.	102.97	−0.01	103.01	−0.05
17	S	15	100.48	0.09	T.R.	100.55	−0.07	100.62	−0.13
17	S	18	88.85	0.09	T.R.	88.84	0.01	88.79	0.07
17	S	22	83.54	0.09	T.R.	83.52	0.02	83.47	0.08
17	S	23	81.61	0.09	T.R.	81.67	−0.07	81.59	0.02
17	S	24	79.76	0.09	T.R.	79.81	−0.06	79.72	0.05
17	S	26	76.47	0.09	T.R.	76.41	0.08	76.37	0.13
17	S	27	75.01	0.09	T.R.	74.89	0.16	74.92	0.12
17	S	28	73.56	0.09	T.R.	73.48	0.10	73.56	0.00
17	S	29	72.26	0.09	T.R.	72.18	0.11	72.29	−0.04
17	S	30	71.11	0.09	T.R.	71.02	0.12	71.15	−0.06
17	S	31	69.98	0.09	T.R.	70.01	−0.05	70.14	−0.23
18	S	3	145.28	0.05	A1/2	145.19	0.06	145.18	0.07
18	S	4	138.11	0.05	A1/2	138.14	−0.02	138.11	0.00
18	S	6	125.40	0.05	A1/2	125.59	−0.15	125.81	−0.33
18	S	7	120.40	0.05	A1/2	120.42	−0.01	120.46	−0.05
18	S	8	115.62	0.05	A1/2	116.11	−0.42	116.15	−0.46
18	S	15	95.68	0.09	T.R.	95.55	0.13	95.60	0.09
18	S	16	93.28	0.09	T.R.	93.26	0.02	93.26	0.03
18	S	17	90.84	0.09	T.R.	90.87	−0.04	90.84	−0.01
18	S	25	76.19	0.09	T.R.	76.16	0.04	76.14	0.07
18	S	27	73.62	0.09	T.R.	73.72	−0.14	73.68	−0.08
18	S	28	72.37	0.09	T.R.	72.33	0.05	72.28	0.13
19	S	9	110.55	0.05	A1/2	110.50	0.05	110.52	0.03
19	S	10	106.88	0.05	A1/2	106.86	0.02	106.89	−0.01
19	S	11	103.63	0.09	T.R.	103.56	0.06	103.62	0.01
19	S	13	95.86	0.09	T.R.	95.87	−0.01	95.87	−0.01
19	S	14	93.36	0.09	T.R.	93.36	0.00	93.31	0.05

mode			observation period (s)	observation error (%)	observation source	model 1066A period (s)	model 1066A diff. (%)	model 1066B period (s)	model 1066B diff. (%)
20	S	4	123.18	0.05	A1/2	123.17	0.01	123.20	−0.02
20	S	5	118.06	0.05	A1/2	117.94	0.10	117.97	0.08
20	S	9	102.09	0.06	T.R.	102.05	0.04	102.47	−0.37
20	S	11	99.66	0.06	T.R.	99.64	0.02	99.79	−0.13
20	S	12	98.18	0.06	T.R.	98.12	0.06	98.19	−0.01
20	S	14	90.38	0.06	T.R.	90.30	0.09	90.21	0.19
20	S	15	89.12	0.06	T.R.	89.14	−0.02	89.06	0.07
20	S	16	87.39	0.09	T.R.	87.47	−0.09	87.42	−0.03
20	S	17	85.30	0.09	T.R.	85.34	−0.05	85.28	0.02
20	S	18	83.16	0.09	T.R.	83.18	−0.02	83.12	0.05
20	S	19	81.12	0.09	T.R.	81.14	−0.03	81.08	0.05
20	S	20	79.46	0.09	T.R.	79.37	0.11	79.32	0.18
20	S	22	75.24	0.09	T.R.	75.34	−0.13	75.35	−0.15
20	S	25	70.75	0.09	T.R.	70.71	0.06	70.65	0.15
21	S	6	112.96	0.05	A1/2	112.94	0.02	112.94	0.01
21	S	7	108.94	0.06	T.R.	108.97	−0.03	108.98	−0.04
21	S	8	105.36	0.05	A1/2	105.24	0.11	105.29	0.07
21	S	10	98.70	0.06	T.R.	98.72	−0.02	98.71	−0.01
21	S	11	95.84	0.06	T.R.	95.79	0.05	95.76	0.08
21	S	12	93.32	0.06	T.R.	93.30	0.02	93.25	0.07
22	S	1	127.88	0.09	T.R.	127.82	0.04	127.94	−0.05
22	S	12	89.88	0.09	T.R.	89.87	0.01	89.80	0.09
22	S	13	88.23	0.09	T.R.	88.19	0.04	88.13	0.12
22	S	14	86.08	0.09	T.R.	86.07	0.01	86.01	0.08
22	S	15	83.98	0.09	T.R.	83.90	0.09	83.83	0.18
22	S	17	78.92	0.09	T.R.	79.11	−0.24	79.04	−0.15
22	S	19	75.35	0.09	T.R.	75.44	−0.12	75.47	−0.16
22	S	23	70.88	0.09	T.R.	71.01	−0.18	70.97	−0.13
23	S	4	111.80	0.09	T.R.	111.80	0.00	111.82	−0.02
23	S	5	107.65	0.05	A1/2	107.59	0.06	107.60	0.05
23	S	7	100.14	0.09	T.R.	100.14	0.00	100.18	−0.04
23	S	8	97.06	0.09	T.R.	96.96	0.11	96.92	0.14
23	S	9	94.16	0.09	T.R.	94.20	−0.04	94.13	0.03
23	S	10	92.14	0.09	T.R.	92.24	−0.11	92.17	−0.04
23	S	13	83.03	0.09	T.R.	83.13	−0.12	83.00	0.03
23	S	22	69.59	0.09	T.R.	69.51	0.12	69.51	0.11
24	S	10	89.52	0.13	T.R.	89.66	−0.16	89.57	−0.06
24	S	11	87.33	0.13	T.R.	87.51	−0.20	87.42	−0.10
24	S	12	85.06	0.13	T.R.	85.21	−0.18	85.14	−0.09
24	S	14	80.65	0.13	T.R.	80.78	−0.16	80.73	−0.10
24	S	15	78.63	0.13	T.R.	78.76	−0.16	78.71	−0.10
24	S	16	76.71	0.13	T.R.	76.83	−0.15	76.78	−0.09
24	S	17	75.20	0.13	T.R.	75.16	0.06	75.08	0.16
24	S	18	74.26	0.13	T.R.	74.22	0.05	74.17	0.12
24	S	20	70.05	0.13	T.R.	70.10	−0.07	70.18	−0.18
25	S	1	115.46	0.09	T.R.	115.46	0.00	115.51	−0.05
25	S	2	110.88	0.05	A1/2	110.82	0.05	110.81	0.06
25	S	3	106.05	0.05	A1/2	106.01	0.04	106.16	−0.10
25	S	5	98.65	0.13	T.R.	98.73	−0.08	98.68	−0.03
25	S	6	95.32	0.13	T.R.	95.46	−0.15	95.39	−0.08
25	S	10	84.78	0.13	T.R.	84.95	−0.21	84.80	−0.02
25	S	18	72.99	0.13	T.R.	72.96	0.04	73.02	−0.04
26	S	1	105.40	0.09	T.R.	105.50	−0.09	105.86	−0.44
26	S	8	89.19	0.09	T.R.	89.33	−0.16	89.25	−0.07
26	S	9	86.82	0.09	T.R.	86.69	0.15	86.83	−0.01
26	S	11	81.77	0.09	T.R.	81.80	−0.04	81.69	0.10
26	S	12	79.66	0.09	T.R.	79.72	−0.08	79.63	0.04
26	S	13	77.58	0.09	T.R.	77.70	−0.15	77.62	−0.05
27	S	2	101.44	0.09	T.R.	101.39	0.05	101.36	0.08
27	S	4	94.37	0.09	T.R.	94.47	−0.10	94.40	−0.03
27	S	14	75.18	0.19	T.R.	75.00	0.24	75.07	0.14
27	S	15	73.43	0.19	T.R.	73.42	0.02	73.47	−0.06
27	S	16	71.60	0.19	T.R.	71.77	−0.24	71.86	−0.36
28	S	5	91.39	0.09	T.R.	91.29	0.11	91.22	0.18
28	S	6	88.61	0.09	T.R.	88.58	0.03	88.50	0.13
28	S	10	78.59	0.09	T.R.	78.53	0.08	78.47	0.16
28	S	11	76.75	0.09	T.R.	76.82	−0.09	76.78	−0.04
28	S	13	72.77	0.09	T.R.	72.74	0.05	72.68	0.13
29	S	1	97.04	0.13	T.R.	97.05	−0.01	96.98	0.06
30	S	3	90.61	0.09	T.R.	90.60	0.01	90.53	0.09
30	S	7	79.69	0.09	T.R.	79.75	−0.07	79.68	0.01
30	S	8	77.52	0.09	T.R.	77.58	−0.08	77.52	−0.00
30	S	10	73.78	0.09	T.R.	73.83	−0.07	73.59	0.26
32	S	1	90.03	0.09	T.R.	90.07	−0.04	90.09	−0.07
33	S	6	77.00	0.13	T.R.	76.85	0.20	76.83	0.22
34	S	1	83.83	0.13	T.R.	83.84	−0.01	83.75	0.09

we conclude that whatever bias exists in the data in table 7, it is small. Only when the seismic spectra of more earthquakes are processed simultaneously, as in § 3.4, can we eliminate some of the sources of bias.

There are only three groups of modes that exhibit systematic differences between computed and observed values. They are ${}_0\mathrm{T}_l\,(l \geqslant 35)$, ${}_4\mathrm{T}_l\,(l \leqslant 21)$ and ${}_2\mathrm{S}_l\,(l \geqslant 48)$. The ${}_0\mathrm{T}_l$ modes are sensitive to V_s in the upper mantle, the ${}_4\mathrm{T}_l$ modes are sensitive to V_s in the neighbourhood of the core–mantle boundary (these modes are ScS, or grazing S, equivalent modes as can be seen in

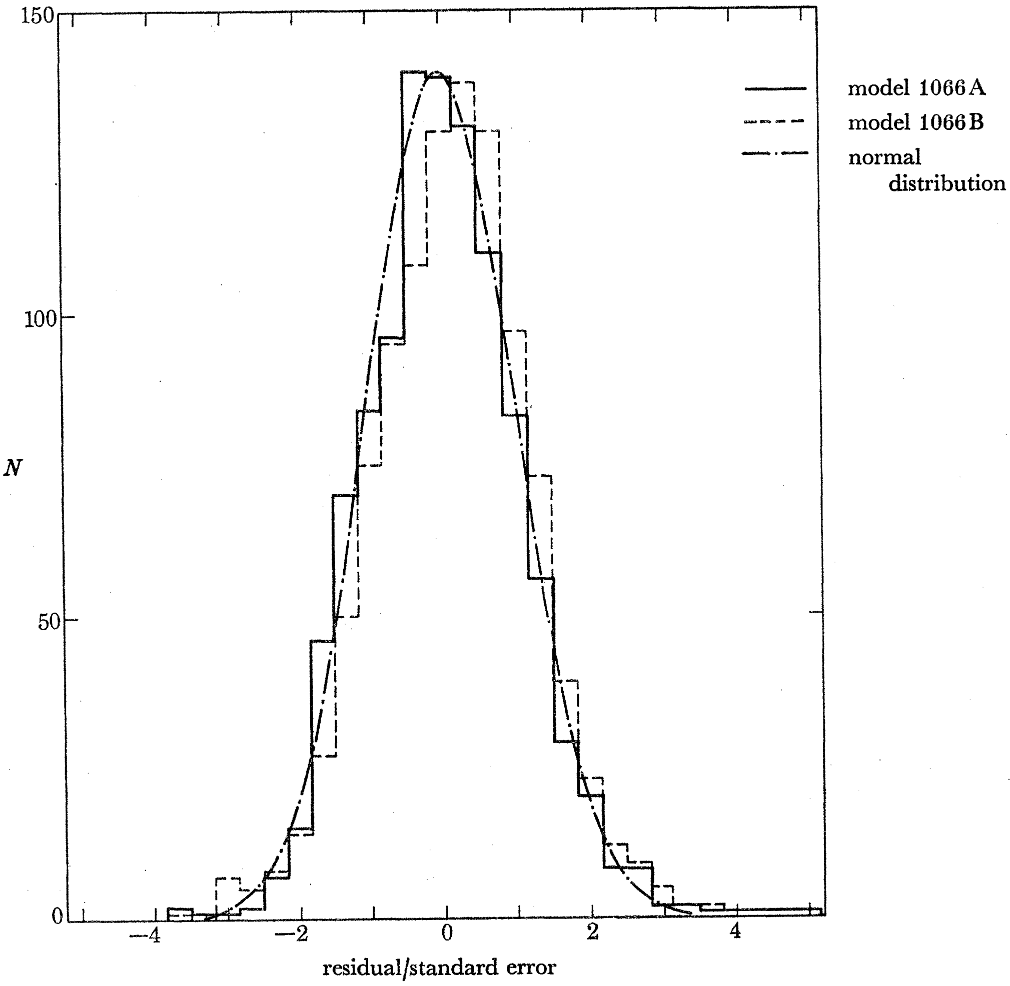

FIGURE 19. Histograms showing the distribution of relative residuals of the eigenfrequencies of 1064 modes (table 7) computed for model 1066A (solid line) and 1066B (broken line), and the error curve for the normal distribution.

figure 16) and the ${}_2\mathrm{S}_l$ modes are sensitive to V_s below the large gradient (1966A) or discontinuity (1066B) at a depth of 671 km. The ${}_2\mathrm{S}_l$ modes have shear potential energies between 96 %, for $l = 48$, and 99 %, for $l = 76$. In support of the remark about ${}_4\mathrm{T}_l$, we remark that ${}_7\mathrm{T}_{28-30}$, also grazing S-equivalent modes, exhibit virtually the same differences as ${}_4\mathrm{T}_l\,(l \leqslant 21)$. While the implications in terms of structure are rather obvious we postpone further speculation to a later date.

The two final models are equally good fits to the 1064 g.e.d. Model 1066A has an r.m.s. error of 0.177 %, and model 1066B has 0.186 %. If we exclude the 155 ${}_nT_l$ of Brune & Gilbert (1974 and personal communication), with an estimated standard error of 0.4 %, the r.m.s. errors are 0.115 % for model 1066A and 0.117 % for model 1066B.

4.3. *Temporal variation of the moment tensor*

If the moment tensor is very nearly a step function in time, the moment rate tensor is very nearly a delta function, whose Fourier cosine transform is constant and whose Fourier sine transform is zero. We have assumed this time behaviour, and that the moment tensor is a double-couple, in our initial resolution of multiplets (§ 3.2).

The actual time behaviour is different. Figures 6 and 7 show conclusively that the stress release is not instantaneous, but is spread over a finite time, some tens of seconds. That the source mechanisms in figures 6 and 7 are better than a double-couple/step-function is made evident by the fact that the latter enabled us to resolve some 500 multiplets while the former increased the number to more than 1000, of which 812 have been presented in § 3.4.

Inasmuch as the pattern of stress release in earthquakes is of very great interest, not only to seismologists but also to petrologists, tectonophysicists and engineers, we explore, in this section, the temporal variation of the moment rate tensor and the moment tensor. We hope to gain some insight into the mechanism of stress release for deep earthquakes. To evaluate the inverse Fourier transform, and find the time functions whose spectra are shown in figures 6 and 7, we must have spectral information at low frequencies $-0.0125 \leqslant \omega \leqslant 0.0125\,\mathrm{s}^{-1}$. Normal modes with periods longer than 1 h have not been detected (we neglect the Chandler wobble in this paper) so we cannot provide siesmic observations to extend the spectra in figures 6 and 7 to longer periods. It is very likely that the long period component of stress release is smooth (Aki 1967) in which case we can interpolate to low frequencies. Without complete information about the Fourier spectrum we must state quite explicitly that a unique time function cannot be found. There is an infinite number of time functions belonging to the spectra in figures 6 and 7. This is a very obvious point. We emphasize it here because we are forced to interpolate to low frequencies in order to learn anything about the temporal behaviour of the moment rate tensor.

Another very obvious point is that we have no information for frequencies $|\omega| > 0.0825\,\mathrm{s}^{-1}$. If we think of the spectra as belonging to discretized functions of time, then the replication interval in frequency is $0.165\,\mathrm{s}^{-1}$ and the temporal sampling interval in 38 s. If we think of the spectra as having been low passed with a cut-off of $0.0825\,\mathrm{s}^{-1}$ and as belonging to continuous functions of time, then details less than 38 s in duration are unresolvable. Sampling the continuous functions every 38 s gives us the discretized functions, both of which have the same low frequency spectra. In particular, any continuous time function beginning at $t = 0$ will exhibit a precursory forerunner of about 38 s duration after it has been low passed with a cut-off of $0.0825\,\mathrm{s}^{-1}$. Sampling the low passed time function every 38 s yields a discretized function with no precursory forerunner.

We dwell at length upon this very obvious and very fundamental point because we present in this section considerable evidence that the isotropic part of the moment rate tensor is precursive. The precursive behaviour of the isotropic part of the moment rate tensor is quite evident even after allowance has been made for low passing the source spectra with a cut-off of $0.0825\,\mathrm{s}^{-1}$. Making the same allowance for the deviatoric part of the moment rate tensor leads us to the conclusion that it is co-seismic; deviatoric stress release begins effectively at the origin time of the earthquake.

We show, then, that the onset of isotropic stress release precedes the onset of deviatoric stress release by over 80 s. The only assumption we make is that the source spectra are smooth for $|\omega| < 0.0125\,\mathrm{s}^{-1}$ which is tantamount to the assumption that stress release is concentrated around the origin time of the earthquake.

In our preliminary discussion of the temporal behaviour of the moment rate tensor (Dziewonski & Gilbert 1974) we interpolated to low frequencies by assuming a model of the time behaviour, a solitary square wave for the moment rate tensor, and by adjusting its parameters to give the best mean square fit to the observations. The interpolated values and the observed values were then inverted to the time domain. Separating the moment rate tensor $\boldsymbol{M}$ into its isotropic and deviatoric parts

$$\boldsymbol{M} = \boldsymbol{I}\mathbf{m} + \boldsymbol{D}, \quad \mathbf{m} = \tfrac{1}{3}\mathit{Tr}\,\boldsymbol{M} \tag{1}$$

we found $\mathbf{m}(t)$ to be precursive by over 80 s for the Colombian earthquake. In fact $\mathbf{m}(t)$ was found to be a nearly symmetrical function of time with a duration of 300–400 s.

To see why this result arises we consider some very elementary properties of Fourier transform pairs

$$\left.\begin{aligned} g(\omega) &= \int_{-\infty}^{\infty} f(t)\,\mathrm{e}^{-\mathrm{i}\omega t}\,\mathrm{d}t, \\ f(t) &= \frac{1}{2\pi}\int_{-\infty}^{\infty} g(\omega)\,\mathrm{e}^{\mathrm{i}\omega t}\,\mathrm{d}\omega. \end{aligned}\right\} \tag{2}$$

If $g(\omega)$ is the transform of $f(t)$, then $g(-\omega)$ is the transform of $f(-t)$, and $2\pi f(\pm\omega)$ is the transform of $g(\mp t)$. In particular, if $g(\omega)$ is an even function, then $f(t)$ is even also.

In figure 1 of Dziewonski & Gilbert (1974) (the sign in figure 1*b* should be changed to be compatible with (2)) it is seen that the sine transform, the odd part of the Fourier spectrum, is very nearly zero for $\mathbf{m}$, while the cosine transform, the even part, is not. Any smooth interpolation to low frequencies that leaves the sine transform small will cause the Fourier spectrum of $\mathbf{m}$ to be an even function of ω. It is then inescapable that $\mathbf{m}(t)$ is an even function of time.

We have no data for $|\omega| < 0.0125\,\mathrm{s}^{-1}$; therefore we cannot prove that the sine transform of $\mathbf{m}(t)$ is small there. It is zero at $\omega = 0$ and it is nearly zero for $|\omega| > 0.0125\,\mathrm{s}^{-1}$ so it seems reasonable that it is nearly zero between these values. If it is, $\mathbf{m}(t)$ is precursive.

To demonstrate the insensitivity of our results to the details of smooth interpolation to low frequencies we select a method where no particular model is forced to fit the data.

We have used Reinsch's (1967) method of smoothing by spline functions to interpolate to low frequencies. The virtue of this method is that assigned errors in the ordinates are taken into account. The interpolating function has the smallest mean square second derivative for a given value of S; $N-(2N)^{\frac{1}{2}} \leqslant \mathrm{S} \leqslant N+(2N)^{\frac{1}{2}}$ for N ordinates. The interpolating function thus meets the chi-squared criterion. We have $N = 28$, counting both positive and negative frequencies.

The amplitude spectrum $|M_{rr}(\omega)|$ for the Colombian earthquake, interpolated by Reinsch's method with $\mathrm{S} = N$, is shown in figure 20. It has been chosen as a representative example of the procedure that we have adopted. The solid curve represents the range of our observations in figure 6. The five dots are interpolated values. Given $|M_{rr}(\omega)|$ in figure 20 we can find the temporal variation, $M_{rr}(t)$, in at least two ways. First, we can interpolate the phase $\phi(\omega)$ (to which we add π to be consistent with the spectrum of M_{rr} in figure 6), and perform the Fourier inversion to the time domain. Alternatively, we can calculate the minimum phase shift spectrum $\phi_c(\omega)$ to ensure that $M_{rr}(t)$ begins at $t = 0$ (Bode 1945, ch. 14; Titchmarsh 1948, ch. 5; Robinson 1962, ch. 7).

$$\phi_c(\omega) = \frac{1}{\pi}\int_{-\infty}^{\infty} \frac{a(\sigma)-a(\omega)}{\sigma-\omega}\,\mathrm{d}\sigma, \tag{3}$$

$$\phi_c(\omega) = \frac{2\omega}{\pi}\int_{0}^{\infty} \frac{a(\sigma)-a(\omega)}{\sigma^2-\omega^2}\,\mathrm{d}\sigma, \tag{4}$$

where

$$a(\omega) = \lg|M_{rr}(\omega)|; \quad M_{rr}(\omega) = \exp[a(\omega)+\mathrm{i}\phi_c(\omega)] \tag{5}$$

and both (3) and (4) are principal value integrals. They can be evaluated quite easily with the Reinsch spline representation of $M_{rr}(\omega)$. We have

$$\left.\begin{aligned} \lim_{\sigma\to\omega}\frac{a(\sigma)-a(\omega)}{\sigma-\omega} &= a'(\omega), \\ a'(\omega) &= |M_{rr}(\omega)|'/|M_{rr}(\omega)|. \end{aligned}\right\} \tag{6}$$

Rather than numerically differentiate the observed data, always to be avoided if possible, we take the second spline coefficient for $|M_{rr}(\omega)|'$. In this way we differentiate a function that has a continuous second derivative that is as small as possible in a mean square sense, and that provides a credible fit to the data.

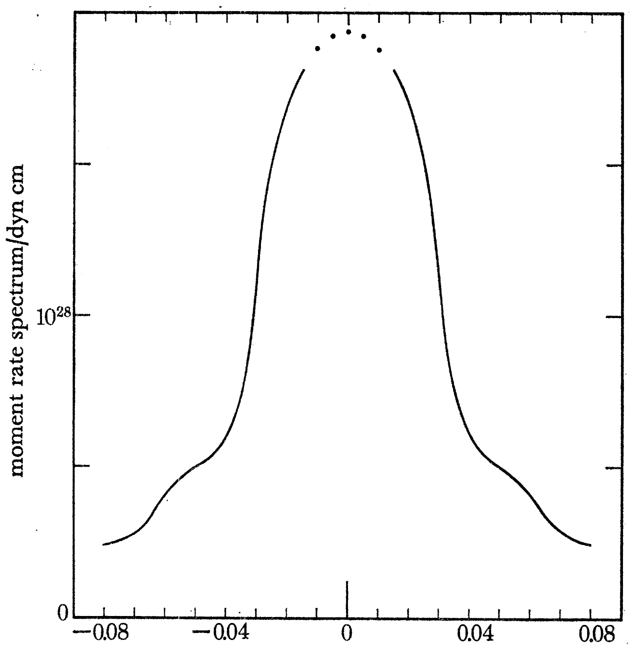

FIGURE 20. The amplitude spectrum $|M_{rr}(\omega)|$ for the Colombian earthquake interpolated by Reinsch's (1967) method of smoothing by spline functions. The solid curve represents the range of our observations in figure 6; the five dots are interpolated values.

The minimum phase shift spectrum and the observed phase spectrum are presented in figure 21. The numerical approximation, Romberg's integration method (Ralston 1965), gives identical results for (3) and (4). The smoothness of the minimum phase shift spectrum $\phi_c(\omega)$, to which π has been added for consistency with the observations in figure 6, indicates the stability of the procedure of numerical quadrature.

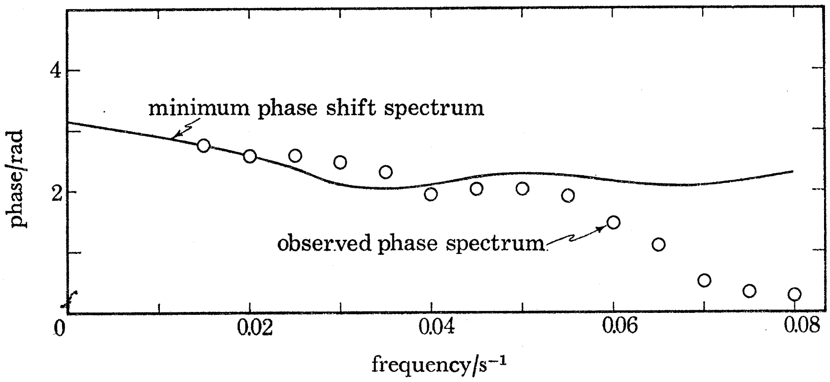

FIGURE 21. Comparison of the minimum phase spectrum computed according to equations (4.4.2) and (4.4.3) using the spline representation of $|M_{rr}(\omega)|$ of figure 20 and the observed phase spectrum inferred from the results in figure 6.

The two phase spectra differ significantly only at high frequencies, $|\omega| > 0.055\,\mathrm{s}^{-1}$. This may be caused by the requirement that we truncate the range of integration in (3) and (4) at

$$|\omega| = 0.0825\,\mathrm{s}^{-1}$$

beyond which we have no data. As there is no conservative method for extrapolating to large frequencies, $|\omega| > 0.0825\,\mathrm{s}^{-1}$, we make the approximation that $M_{rr}(\omega) = 0$ for $|\omega| > 0.0825\,\mathrm{s}^{-1}$.

This approximation violates the Paley–Wiener criterion (Paley & Wiener 1934; Doob 1953, p. 584, theorem 5.1)

$$\int_{-\infty}^{\infty} \frac{\lg |M_{rr}(\omega)|}{1+\omega^2}\,\mathrm{d}\omega > -\infty, \tag{7}$$

another constraint to be met if $M_{rr}(t)$ is to begin at $t = 0$. Violating the Paley–Wiener criterion means that $M_{rr}(t)$, calculated with the minimum phase shift spectrum $\phi_c(\omega)$ in figure 21, will

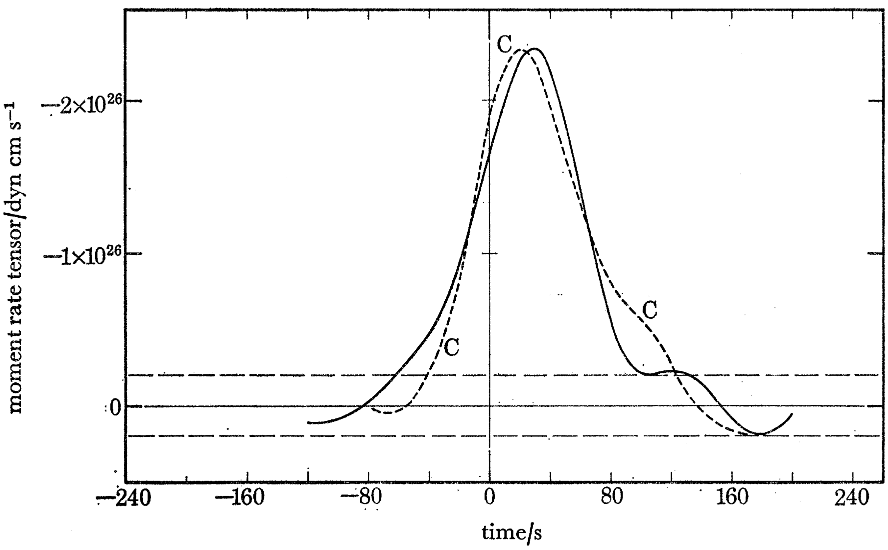

FIGURE 22. Comparison of the time functions $M_{rr}(t)$ derived from the inverse Fourier transform of the Reinsch interpolation of the real and imaginary components of the spectrum of M_{rr} in figure 6 (solid line) and the amplitude spectrum $|M_{rr}(\omega)|$ in figure 20 and the minimum phase spectrum in figure 21 (broken line). The latter is 'co-seismic' and is labelled C.

exist for all time, but, since the shortest period used in the analysis is 76 s, it will be very small for times $t < -38$ s.

This feature is borne out by figure 22 where we present $M_{rr}(t)$ for both phase spectra in figure 21. There are other effects that cause $M_{rr}(t)$ in figure 22 to begin before $t = 0$. In § 3.1 we stated that the observed seismograms were filtered with a low-pass filter with a zero phase shift and a cut-off frequency of 0.0505 Hz ($0.3173\,\mathrm{s}^{-1}$). This will cause time functions to be sensibly precursive (exist for $t < 0$) for about 9 s. Errors in time kept at different stations could make a contribution to precursive behaviour. Also, variations in instrumental response could be important. However, lack of spectral data in figure 6 for $|\omega| > 0.0825\,\mathrm{s}^{-1}$ appears to be the dominant cause of the precursive behaviour of $M_{rr}(t)$ in figure 22.

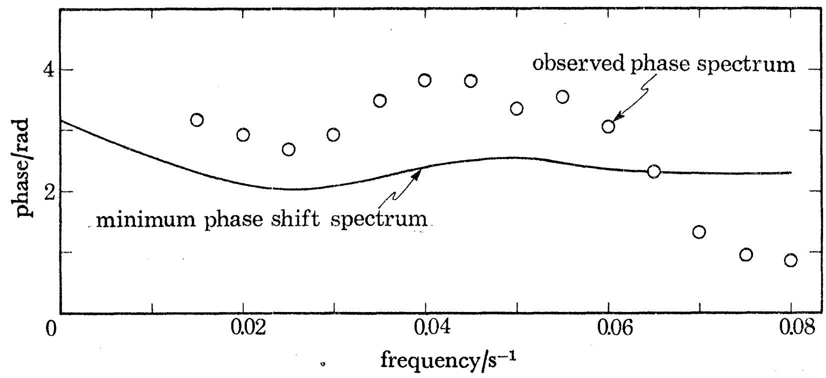

FIGURE 23. Comparison of the observed and minimum phase spectra of the isotropic part of the moment rate tensor of figure 6.

We conclude that $M_{rr}(t)$ is effectively co-seismic in that it appears to begin at $t = 0$. Moreover, we conclude that our assumption that the spectrum is smooth for $|\omega| < 0.007\,\mathrm{s}^{-1}$ is not violated and that our method of interpolating to low frequencies is not demonstrably incorrect. In fact, the similarity of the two time functions in figure 22 convinces us that our assumption and method are essentially correct.

We turn our attention to the Fourier spectrum for $\mathbf{m} = \frac{1}{3}\mathit{Tr}\boldsymbol{M}$ which is shown in figure 1 of Dziewonski & Gilbert (1974) (as mentioned in § 3.3, we have changed to the more prevalent convention for Fourier transforms and the imaginary part in figure 1 (b) should have its sign changed). We have interpolated the amplitude spectrum of $\mathbf{m}$. The minimum phase shift spectrum, calculated from (3) and (4) with

$$a(\omega) = \tfrac{1}{3}\lg|\mathit{Tr}\,\boldsymbol{M}(\omega)| = \lg|\mathbf{m}(\omega)|, \tag{8}$$

and the observed phase spectrum are shown in figure 23. To both phases π has been added because the cosine spectrum is negative at low frequencies.

Unlike figure 21 for $M_{rr}(\omega)$, the two phase spectra in figure 23 differ significantly, even at low frequencies. The minimum phase shift spectrum has minimum group delay $(-\mathrm{d}\phi_c(\omega)/\mathrm{d}\omega)$ over the entire frequency range for a co-seismic time function. Any function whose phase has a group delay less than the minimum (co-seismic) group delay, at any frequency, cannot be co-seismic; it must be precursive or preseismic. In addition, it must lead the co-seismic time function even in the presence of truncating the frequency spectrum (violating the Paley–Wiener criterion (7)).

At low frequencies the observed phase spectrum has group delays smaller than are allowed for a co-seismic function. This explains the behaviour depicted in figure 24 for $\mathbf{m}(t)$. The 'observed' time function leads the co-seismic function by times between 40 and 120 s. The average lead time is over 80 s after allowance has been made for truncating (low-passing) the spectrum of the moment rate tensor. This conclusion can be escaped only either by casting doubt on the validity of the data in figure 6 or by challenging the assumption that the spectrum is smooth at low frequencies.

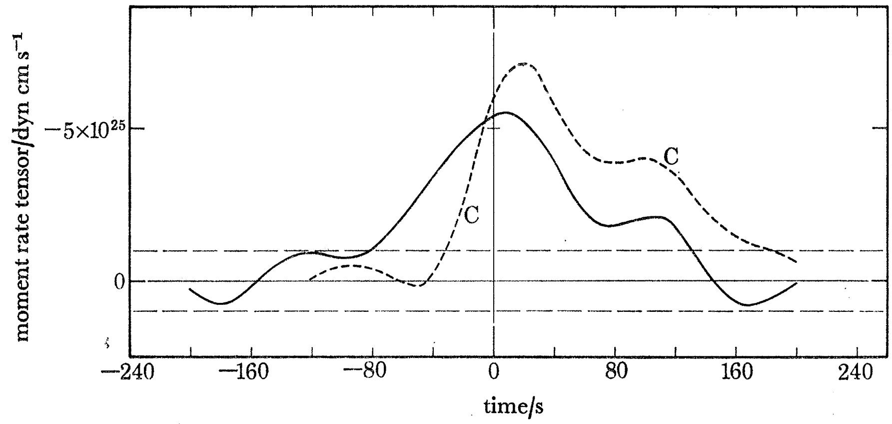

FIGURE 24. Comparison of the time functions $\frac{1}{3}\,\mathrm{Tr}\,\boldsymbol{M}(t)$ derived from the interpolated observed spectra (solid line) and the minimum phase shift spectrum (broken line). The latter is 'co-seismic' and is labelled C.

As we have previously stated, the validity of the data is supported by our results in § 3.4. Using the source spectra in § 3.3, figures 6 and 7, we have resolved more than 800 normal mode multiplets, and the quality of the modal data is supported by the very consistent solutions to the inverse normal mode problem in § 4.1. Attention is thus focused on the assumption that the source spectra are smooth at low frequencies.

If the source spectra are smooth then the details of the method of interpolation are of only minor importance. The 'observed' time function in figure 24 is nearly symmetrical and, therefore, precursive, as is its counterpart in figure 2 of Dziewonski & Gilbert (1974). To remove the symmetry of the time function and make it co-seismic requires the odd part of the Fourier spectrum, the sine transform, to be sensibly different from zero.

Applying the classical Tauberian theorem (Paley & Wiener 1934) to (2) shows that the behaviour of $\mathrm{i}\omega g(\omega)$ as $\omega \to 0$ is the same as $f(t)$ as $t \to \infty$. Consequently, if we cause the sine transform to have fluctuations at low frequencies, say $0.005\,\mathrm{s}^{-1}$, we cause the time function to have fluctuations at long times, say 1200 s. If stress release is concentrated near $t = 0$, as shown in figures 22 and 24, then fluctuations at long times are ruled out, the sine transform is nearly zero and $\mathbf{m}(t)$ is precursive. Until we have evidence to the contrary we adopt the position that stress release is concentrated near the origin time of the earthquake.

To learn more about $\boldsymbol{M}(t)$ we maintain our assumption that spectra are smooth at low frequencies and we interpolate the spectra of the moment rate tensor in figures 6 and 7. The temporal behaviour is shown in figure 25, and the integrated behaviour for the moment tensors is shown in figure 26. In figure 25 we see that the deviatoric part of both sources is effectively co-seismic; that is, the precursive part is a result of truncating the spectra at a period of 76 s. Also the deviatoric components are strongly skewed toward positive times, and stress release is concentrated near the origin.

The isotropic parts are more nearly even functions of time with maximum stress release near the origin. This result is the same whether the trace is formed before or after Fourier inversion. In figure 24 the trace was formed in the frequency domain and in figure 25 the traces were formed in the time domain. The consistency of the results is a support for the numerical methods and the quality of the spectral data. That both earthquakes have a precursive, isotropic mechanism is a consequence of the spectral smoothness at low frequencies and the very small values of the sine transform of the isotropic part.

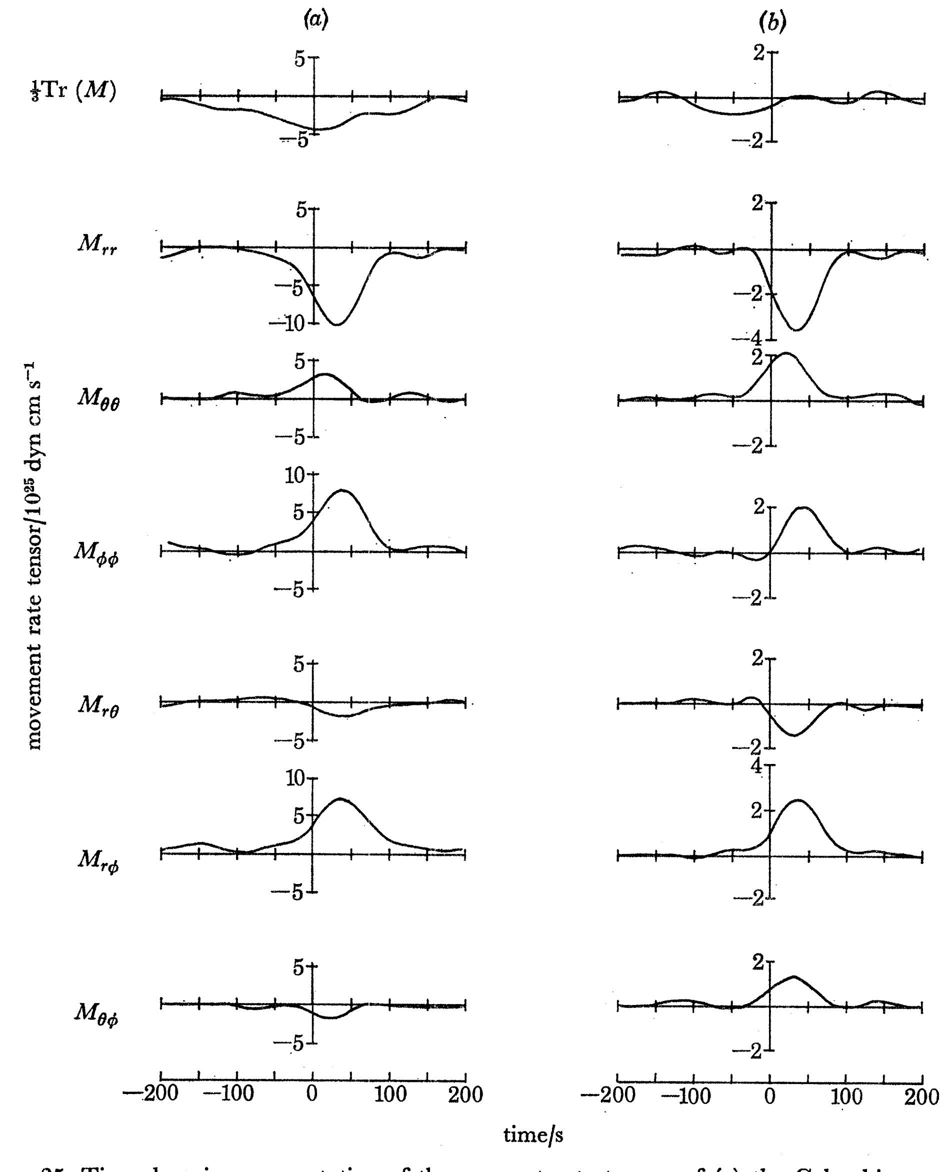

FIGURE 25. Time domain representation of the moment rate tensors of (a) the Colombian and (b) the Peru–Bolivian earthquakes. The time functions are the inverse Fourier transforms of the observed spectra (figures 6 and 7) interpolated to low frequencies according to the method described in the text. The isotropic part of the moment rate tensor has been removed from the diagonal elements M_{rr}, $M_{\theta\theta}$ and $M_{\phi\phi}$.

It is clear from figure 1 of Dziewonski & Gilbert (1974) that the spectrum of the isotropic part is different from the deviatoric spectra, and that, as a consequence, their temporal behaviour must be different. The symmetry in time of $\mathbf{m}(t)$ is a direct consequence of the symmetry in frequency of $\mathbf{m}(\omega)$. Furthermore, the isotropic spectra decay more rapidly with frequency than do the deviatoric spectra and, accordingly, in figure 25 the isotropic time functions are smoother than the deviatoric ones. As a result the deviatoric mechanism should be dominant at high frequencies and this is in accord with the nodal plane solution of Mendiguren (1973).

By applying a principal axis transformation to the moment rate tensors we can study the temporal variation of each principal value and the migration of its axes in space. The results are

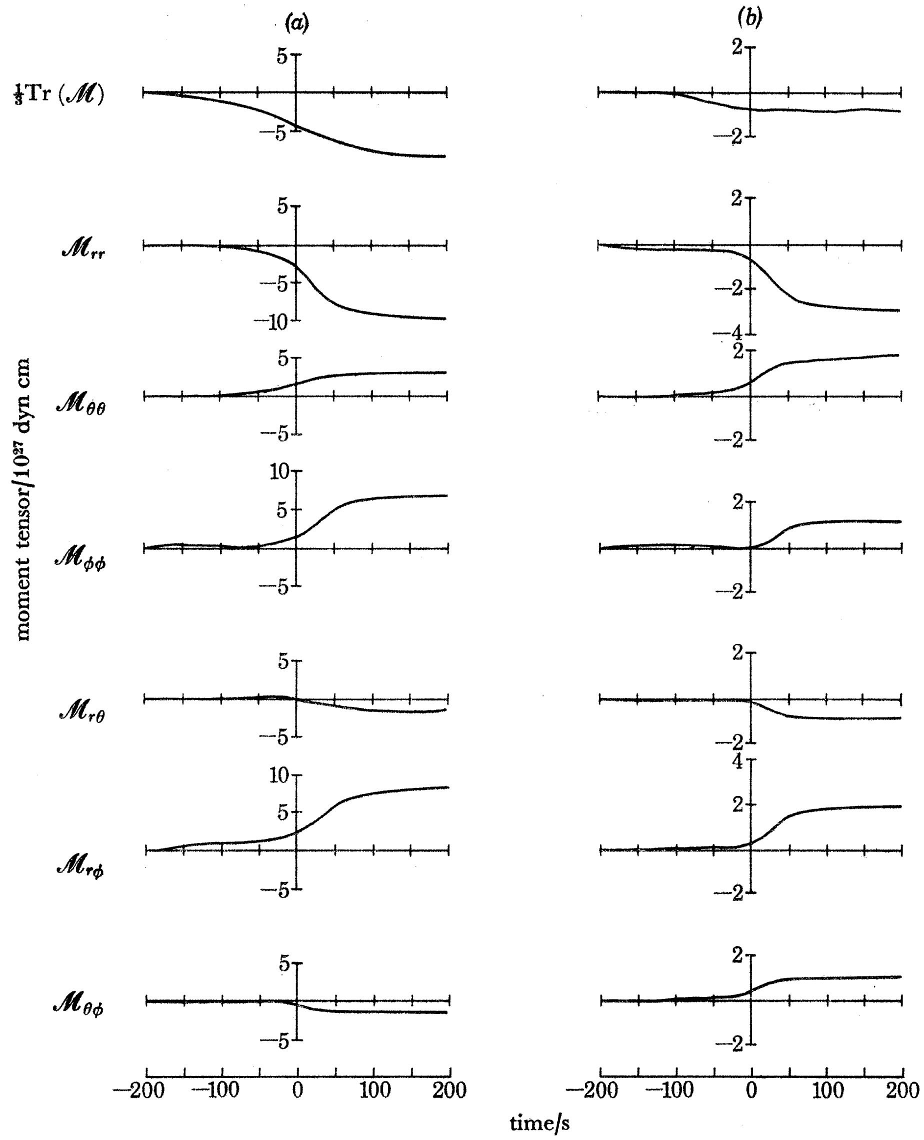

FIGURE 26. Time domain representation of the moment tensor of (a) the Colombian and (b) the Peru–Bolivian earthquakes. $\mathcal{M}(t)$ is obtained by integrating $M(t)$ shown in figure 25:

$$\mathcal{M}(t) = \int_{-200}^{t} M(\tau)\,\mathrm{d}\tau.$$

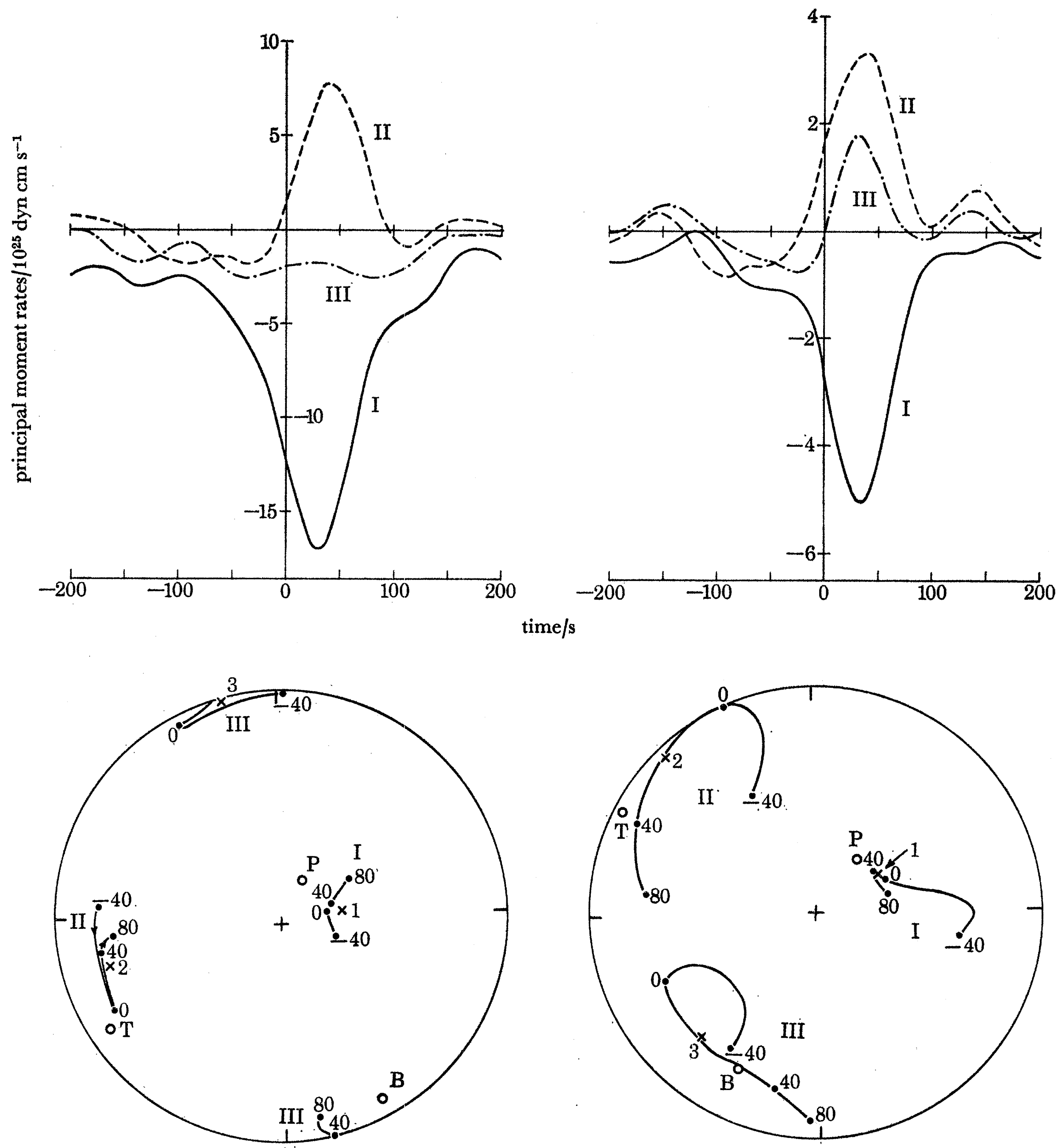

o, P, T, B: directions of compression, tension and null axes from nodal plane solutions;
×, I, II, III: directions of principal axes of the moment tensor

FIGURE 27. Temporal variation of the moment rate tensor in the principal axes system. The upper part of the figure shows variations of the principal values of the moment rate tensor for (*a*) the Columbian and (*b*) the Peru–Bolivian events. The principal values include the isotropic part. The large circles in the lower part of the figure represent equal area projections of the lower focal hemisphere. The continuous lines show instantaneous directions of the principal axes. Crosses indicate the results obtained for the moment $\mathcal{M}$ (200) in figure 26. Open circles indicate the positions of P, T and B axes from the nodal plane solutions of Mendiguren (1973) and Chandra (1970). The principal values are labelled I, II, III, respectively, in order of decreasing magnitude at the origin.

shown in figure 27 and are to be compared with the nodal plane solutions of Mendiguren (1973) for the Colombian earthquake and of Chandra (1970) for the Peru–Bolivian earthquake. Our solution is consistent with that of Mendiguren (1973) with the addition that we show a slight horizontal rotation of the axes and a slow decrease of the plunge of the compression axis. The agreement between our results and those of Chandra (1970) is quite good, in contrast to our earlier finding (Dziewonski & Gilbert 1974). This has been traced to an error (now corrected, of course) in sign in our computer programs for ϵ_6 (2.1.22). The component f_6 for the Colombian earthquake is sufficiently small that the error went undetected, but it was serious for the Peru–Bolivian earthquake where f_6 is larger. Our previous criticisms of the work of Dr Chandra are withdrawn and he has our apologies.

The migration in space of the principal axes of the moment rate tensor for both events is a feature that more traditional methods have failed to detect. It is more profound for the Peru–Bolivian event, where the tension axes rotate about 70°.

It has been shown by Isacks *et al.* (1968) that focal mechanisms of deep earthquakes have compression axes parallel to the local dip of the seismic zone and that the other two axes are less stable in direction and, from event to event, show rotation about the stable compression axis. From our results, this feature appears to apply to the temporal history of a single event. The compression axis is stable; the other two axes rotate about it and a conical zone of maximum shearing develops as stress release occurs.

Isacks *et al.* (1968) interpret their results to indicate that $|\tau_2|-|\tau_3| < |\tau_1|-|\tau_2|$, where $|\tau_1| > |\tau_2| > |\tau_3|$ and the principal moments are τ_i with compression dominant. Our results in figure 27 support their interpretation for the pattern of stress release in both earthquakes, but we cannot resolve whether there is a sequence of events with progressively different mechanisms, or only one event with a temporally and spatially varying mechanism. As we have seen, the quality of the data available to us restricts our temporal resolution to more than 38 s.

More insight into the operative mechanism can be gained by examining the final (t = 200 s) principal values of the moment tensors in figure 26. In the notation of (2.1.29) we have for the final values (the deviatoric principal values are D_i)

Columbia

i	$\dfrac{\tau_i}{10^{27}\,\text{dyn cm}}$	η_i	ζ_i	$\dfrac{D_i}{10^{27}\,\text{dyn cm}}$
1	−22.0	67°	83°	−15.3
1	2.5	22°	255°	9.2
3	−0.6	2.3°	346°	6.1

(9)

Peru–Bolivia

i	$\dfrac{\tau_i}{10^{27}\,\text{dyn cm}}$	η_i	ζ_i	$\dfrac{D_i}{10^{27}\,\text{dyn cm}}$
1	−4.8	63°	68°	−4.0
2	1.9	6°	318°	2.7
3	0.5	26°	225°	1.3

(10)

It is quite clear from (9) and (10) that $|\tau_2|-|\tau_3| < |\tau_1|-|\tau_2|$ for both events and these results support the interpretation given by Isacks *et al.* (1968) of their own results.

For the Colombian earthquake the deviatoric principal values have the approximate pattern $(-5, 3, 2)$ and satisfy $|D_2|-|D_3| < |D_1|-|D_2|$. Consequently, a deviatoric mechanism can satisfy the inequality, but a double-couple deviatoric mechanism cannot (because $D_3 \equiv 0$). Seismologists who support the very plausible interpretation of Isacks *et al.* (1968) must give up the double-couple mechanism for deep earthquakes. They can adopt a deviatoric mechanism more complex than a double-couple, a double-couple *plus* isotropic compression, or a more complex deviatoric mechanism plus isotropic compression. The latter is in better agreement with the data and we favour it.

The simplest approximation to the final moment of the Colombian earthquake is a uniaxial compression (τ_1) often called a linear vector dipole (uncompensated). Such a source mechanism is not in disagreement with the nodal plane solution found by Mendiguren (1973) if we recognize that the former is the final moment at long times while the latter is caused by the moment rate at the origin. Although it is traditional in seismology to equate the two, we have seen how the presence of isotropic stress release at low frequencies, and the migration of the principal axes, negates the traditional equation. Benioff (1963) used strain seismograms at Ñaña of two deep Peruvian earthquakes to show that a dipole source fits the very long period observations. He hypothesized a sudden volume contraction at the source which could be the result of a sudden change of state. An analysis of the mechanisms of deep-focus earthquakes, which makes use of amplitude information rather than just the direction of initial motion, has been presented by Randall (1972), in an attempt to discriminate between the classical dislocation source model and a phase transition model. From the evidence that we have presented, it appears that a dipolar model, with isotropic stress release, can be valid at low frequencies, and a classical dislocation model can be valid at high frequencies. The work of Benioff (1963), Mendiguren (1973), Randall (1972) and many others is made compatible if we take into account the temporal and spatial variation of the seismic moment tensor. This we have attempted to do.

The logical consistency between our findings and the interpretation of Isacks *et al.* (1968) makes it plausible that stability of the compressive principal axes for deep earthquakes is direct evidence for isotropic, compressive stress release. This implies that deep earthquakes, occurring in descending lithospheric slabs, are *not* essentially sudden shearing movements, but do exhibit implosive changes in volume.

It appears, then, for the Colombian earthquake, that $\boldsymbol{M}(t)$ in (1) has both a deviatoric component $\boldsymbol{D}(t)$ and an isotropic component $\mathbf{m}(t)$, that $\boldsymbol{D}(t)$ is effectively co-seismic, that $\mathbf{m}(t)$ leads $\boldsymbol{D}(t)$ by over 80 s, and that $\mathbf{m}(t)$ is compressive. A similar result is found for the Peru–Bolivian earthquake, although the lower signal level (about three times less) requires that less confidence be attached to it. However, that both events have a precursive, isotropic, compressive moment rate substantially improves the credibility of our findings.

Pedantic persons can argue that isotropic, compressive stress release is not proved to be precursive *unless* one cannot find a very low frequency phase that both fluctuates enough to render the isotropic moment rate co-seismic, and remains in agreement with the observed spectral data.

Leaving pedantry aside, we think it is not unwarranted to speculate on the consequence of a source mechanism having a precursive, isotropic, compressive component. It immediately springs to mind that compressive stress release may be caused by a transition of the material in the mantle into a denser phase. Perhaps this is the mechanism whereby light material in a descending lithospheric slab becomes denser as it reaches great depth. If the light material is far within the region of stability of the denser phase it could be sufficiently metastable to undergo the phase change in an abrupt manner.

If such a phase change is associated with a release of thermal energy, the increase in temperature might be sufficient to initiate a shear melting instability, which has been suggested by Griggs & Baker (1969) as a possible cause of deep earthquakes. The theory of Griggs & Baker predicts a slow release of shear stress before the onset of shear melting. In figures 25 and 26 the evidence certainly does not contradict their theory, but there is only the most marginal support that deviatoric stress release is precursive.

Many shallow, strike-slip, earthquakes exhibit spectra in which high-Q overtones appear to be absent. These events appear to have almost perfectly deviatoric (double-couple) mechanisms, in which case it is understandable that the high-Q modes are weak or absent. Deep earthquakes exhibit spectra in which high-Q overtones appear to be prominantly excited. For a single station it can be argued that one is observing the effect of the radiation pattern of the source, but global observations make it more likely that such events have a partly isotropic mechanism. An isotropic mechanism is efficient in exciting modes rich in compressional energy (Gilbert 1973*b*) and such modes have high-Q.

These points motivate us to speculate that low frequency 'silent earthquakes' may occur at depth. If the phase change accompanying the release of isotropic stress were insufficient to trigger the shear melting instability, perhaps there would be no release of deviatoric stress. Such a 'silent earthquake' would almost certainly remain unreported. Only very sensitive instruments could possibly detect the low frequency high-Q oscillations excited by it.

In a descending lithospheric plate, in the region of high metastability of the low density phase, numerous 'silent earthquakes' may occur; the material becomes structurally incompetent. (Analogs such as swiss cheese, termite infested timbers, or pre-Karst topography suggest themselves.) Successive volume changes create the increasing need for a change in shape; finally, a silent earthquake begins and is accompanied by sudden deviatoric stress release. The event is observed and reported. Perhaps that is what happened deep beneath Colombia on 1970 July 31.

The seismograms of the Colombian earthquake were digitized by Mrs Maniatis to whom we are very grateful. This research was supported by grants from the U.S. National Science Foundation and the U.S. Air Force Office of Scientific Research, and by the Committee on Experimental Geology and Geophysics, Harvard University.

References

Aki, K. 1967 *J. geophys. Res.* **72**, 1217–1231.
Alsop, L. E. & Brune, J. N. 1965 *J. geophys. Res.* **70**, 6165–6174.
Anderssen, R. S., Cleary, J. R. & Osborne, M. R. 1974 *Nature, Lond.* **250**, 400–401.
Anderson, D. L. & Archambeau, C. B. 1964 *J. geophys. Res.* **69**, 2071–2084.
Backus, G. & Gilbert, F. 1967 *Geophys. J. R. astron. Soc.* **13**, 247–276.
Backus, G. & Gilbert, F. 1968 *Geophys. J. R. astron. Soc.* **16**, 169–205.
Backus, G. & Gilbert, F. 1970 *Phil. Trans. R. Soc. Lond.* A **266**, 123–192.
Benioff, H. 1963 *Bull. seismol. Soc. Am.* **53**, 893–903.
Ben-Menahem, A. & Singh, S. J. 1972 *Meth. comp. Phys.* **12**, 299–375.
Bode, H. W. 1945 *Network analysis and feedback amplifier design.* New York: Van Nostrand.
Bolt, B. A. 1968 *Bull. seismot. Soc. Am.* **58**, 1305–1324.
Brune, J. N. & Gilbert, F. 1974 *Bull. seismol. Soc. Am.* **64**, 313–320.
Chandra, U. 1970 *Bull. seismol. Soc. Am.* **60**, 639–646.

Cleary, J. R. & Hales, A. L. 1971 *J. geophys. Res.* **76**, 7249–7259.
Dahlen, F. A. 1968 *Geophys. J. R. astron. Soc.* **16**, 329–367.
Dahlen, F. A. 1972 *Geophys. J. R. astron. Soc.* **28**, 357–383.
Dahlen, F. A. 1973 *Geophys. J. R. astron. Soc.* **31**, 469–484.
Davies, D. & McKenzie, D. P. 1969 *Geophys. J. R. astron. Soc.* **18**, 51–64.
Derr, J. S. 1969 *Bull. seismol. Soc. Am.* **59**, 2079–2099.
Doob, J. L. 1953 *Stochastic processes.* New York: Wiley.
Dratler, J., Farrell, W. E., Block, B. & Gilbert, F. 1971 *Geophys J. R. astron. Soc.* **23**, 399–410.
Dziewonski, A. M. 1971 *Geophys. J. R. astron. Soc.* **22**, 289–326.
Dziewonski, A. M. & Gilbert, F. 1972 *Geophys. J. R. astron. Soc.* **27**, 393–446.
Dziewonski, A. M. & Gilbert, F. 1973*a* *EOS* **54**, 374.
Dziewonski, A. M. & Gilbert, F. 1973*b* *Geophys. J. R. astron. Soc.* **35**, 401–437.
Dziewonski, A. M. & Gilbert, F. 1974 *Nature, Lond.* **247**, 185–188.
Gilbert, F. 1971*a* *Geophys. J. R. astron. Soc.* **22**, 223–226.
Gilbert, F. 1971*b* *Geophys. J. R. astron. Soc.* **23**, 119–123.
Gilbert, F. 1971*c* *Geophys. J. R. astron. Soc.* **23**, 125–128.
Gilbert, F. 1973*a* *Phil. Trans. R. Soc. Lond.* A **274**, 369–371.
Gilbert, F. 1973*b* *Geophys. J. R. astron. Soc.* **33**, 487–488.
Gilbert, F. & Dziewonski, A. M. 1973 *EOS* **54**, 374.
Gilbert, F., Dziewonski, A. & Brune, J. 1973 *Proc. natn. Acad. Sci. U.S.A.* **70**, 1410–1413.
Hagiwara, T. 1957 *Bull. Earthq. Res. Inst.* **36**, 139–164.
Hales, A. L. & Roberts, J. L. 1970 *Bull. seismol. Soc. Am.* **60**, 461–489.
Hales, A. L. & Roberts, J. L. 1971 *Bull. seismol. Soc. Am.* **61**, 1051–1059.
Herrin, E., Tucker, W., Taggart, J. N., Gordon, D. W. & Lobdel, J. L. 1968 *Bull. seismol. Soc. Am.* **58**, 1273–1291.
Isacks, B. & Molnar, P. 1971 *Rev. Geoph.* **9**, 103–174.
Isacks, B., Oliver, J. & Sykes, L. 1968 *J. Geophys. Res.* **73**, 5855–5899.
Jeffreys, H. 1970 *The Earth*, 5th ed. Cambridge University Press.
Jeffreys, H. & Bullen, K. E. 1958 *Seismological tables.* British Association for the Advancement of Science, Gray-Milne Trust.
Jordan, T. H. 1972 Ph.D. Thesis, California Institute of Technology, Pasadena.
Jordan, T. H. & Anderson, D. L. 1974 *Geophys J. R. astron. Soc.* **36**, 411–459.
Kenney, J. F. & Keeping, E. S. 1951 *Mathematics of statistics.* New York: Van Nostrand.
Luh, P. C. 1973 *Geophys. J. R. astron. Soc.* **32**, 187–202.
Luh, P. C. 1974 *Geophys. J. R. astron. Soc.* **38**, 187–224.
Mendiguren, J. A. 1972 Ph.D. Thesis, Massachusetts Institute of Technology, Cambridge.
Mendiguren, J. A. 1973 *Geophys. J. R. astron. Soc.* **33**, 281–321.
Mitchell, B. & Landisman, M. 1969 *Bull. seismol. Soc. Am.* **59**, 1335–1348.
Paley, R. E. A. C. & Wiener, N. 1934 *Fourier transforms in the complex domain.* Am. math. Soc. Colloquium Publication **19**. Providence.
Phinney, R. A. & Burridge, R. 1973 *Geophys. J. R. astron. Soc.* **34**, 451–487.
Ralston, A. 1965 *A first course in numerical analysis.* New York: McGraw-Hill.
Randall, M. J. 1972 *Meth. comp. Phys.* **12**, 267–298 (ed. B. Alder, S. Fernbach & M. Rotenberg). New York: Academic Press.
Rayleigh, Baron 1877 *Theory of sound*, vol. I. London: MacMillan.
Reinsch, C. H. 1967 *Num. Math.* **10**, 177–183.
Robinson, E. A. 1962 *Random wavelets and cybernetic systems.* New York: Hafner.
Sabatier, P. C. 1974 *Proc. R. Soc. Lond.* A **337**, 49–71.
Saito, M. 1967 *J. geophys. Res.* **72**, 3689–3699.
Sokolnikoff, I. S. 1956 *Mathematical theory of elasticity*, 2nd ed. New York: McGraw-Hill.
Stauder, W. & Bollinger, G. A. 1966 *Bull. seismol. Soc. Am.* **56**, 1363–1371.
Titchmarsh, E. C. 1948 *Theory of Fourier integrals*, 2nd ed. Oxford.
Vinnick, L. P. & Nikolayev, A. V. 1970 *Izv. Acad. Sci. U.S.S.R. Phys. Solid. Earth* (Engl. Trans.) **11**, 24–40.
Wang, C. 1972 *J. geophys. Res.* **77**, 4318–4329.
Wilkinson, J. H. & Reinsch, C. R. 1971 *Linear algebra.* Berlin: Springer.